

Wireless Power Transfer for Vehicular Applications: Overview and Challenges

Devendra Patil^{ID}, Student Member, IEEE, Matthew K. McDonough, Member, IEEE,
John M. Miller, Life Fellow, IEEE, Babak Fahimi, Fellow, IEEE,
and Poras T. Balsara, Fellow, IEEE

Abstract—More than a century-old gasoline internal combustion engine is a major contributor to greenhouse gases. Electric vehicles (EVs) have the potential to achieve eco-friendly transportation. However, the major limitation in achieving this vision is the battery technology. It suffers from drawbacks such as high cost, rare material, low energy density, and large weight. The problems related to battery technology can be addressed by dynamically charging the EV while on the move. In-motion charging can reduce the battery storage requirement, which could significantly extend the driving range of an EV. This paper reviews recent advances in stationary and dynamic wireless charging of EVs. A comprehensive review of charging pad, power electronics configurations, compensation networks, controls, and standards is presented.

Index Terms—Coils, compensation, electric vehicle (EV), inductive dynamic charging, shielding, standards, stationary charging, wireless power transfer (WPT).

I. INTRODUCTION

IN THE United States transportation industry consumed nearly 28% of energy in 2014 [1], predominantly using gasoline. Gasoline accounts for 56% of total U.S. transportation energy use in 2014 [1]. Extensive use of gasoline leads to the emission of harmful gases into an environment already suffering from the emission of greenhouse gases. Therefore, to alleviate dependence on conventional energy source and to minimize its harmful effects on the environment, there is a need for alternative solutions such as electric vehicles (EVs or battery EVs) and plug-in hybrid electric vehicles (PHEVs) [1]–[4]. The total number of EVs sold from 1999 to 2015 is approximately ~ 2.1 million [4]–[6], with a projected growth of 6 million by 2020 [5], [6]. The biggest impediment to the commercialization of battery EV (BEV) is the energy storage system, which should be sufficient for the driving range of an EV and possess sufficient power for grading, passing, and maneuvering of EVs [2].

Typically, batteries are bulky, heavy, and low in energy density, require long charging time and have a short

Manuscript received July 16, 2017; revised October 16, 2017; accepted November 19, 2017. Date of publication December 6, 2017; date of current version February 5, 2018. (Corresponding author: Devendra Patil.)

D. Patil, B. Fahimi, and P. T. Balsara are with the Erik Jonsson School of Engineering, The University of Texas at Dallas, Richardson, TX 75080 USA (e-mail: drp140230@utdallas.edu).

M. K. McDonough is with the Sandia National Laboratories, Albuquerque, NM 87185 USA.

J. M. Miller is with J-N-J Miller Design Services PLLC, Longview, TX 75601 USA (e-mail: jmmiller35@aol.com).

Digital Object Identifier 10.1109/TTE.2017.2780627

lifetime [8]. Today, EV batteries rely on lithium-ion chemistry using a scarce and moderately costly material, lithium (U.S. \$20/kg) [9]. In addition, batteries take a long time to charge (slow charger takes 6–8 h). Some researchers reported fast battery charging techniques to reduce the charging time to 20–30 min [8], [10]. However, the peak power and cost of fast charging systems are high even if energy storage with future advanced charging methods are used. Still, the charging time is long compared to refueling a car with gasoline. Another solution proposed by better place is “hot swapping” technique, in which the batteries are replaced at charging station with fully charged batteries, a concept adopted and then dropped by Tesla [10].

The current charging technology for EV consists of plugging the cable from ac utility to charge the onboard batteries using an onboard charger [3]. The problem with the conductive charging of EV is that it requires heavy gauge cables to connect to EV which are difficult to handle, has tripping hazards, and are prone to vandalism [7], [8]. An alternative technology to charge an EV, referred to as wireless power transfer (WPT), or inductive power transfer (IPT) has been investigated [11]–[14]. The advantages of wireless charging are aesthetics, safety, convenience, and fully automated charging process [6]. Wireless charging can be classified into stationary, quasi-stationary, and dynamic: stationary wireless charging is suitable for public charging stations, homes, and workplace. Quasi-stationary charging is an extension of stationary charging, but the primary pads may be located at traffic lights, layby's, and rest areas along highways. The range anxiety problem of a BEV can be solved with dynamic wireless charging (DWC) [7], [13], [15]. Theoretically, DWC does not have any battery on EV instead they have Ultracapacitor; the power required for EV is transferred to it through a power rail in the road [16]–[19].

History of WPT extends from the pioneering work of Hertz to present time. Fig. 1 shows the historical development for WPT. In the late eighteenth century, Prof. Heinrich Hertz demonstrated electromagnetic wave propagation in free space with a spark gap to generate high-frequency power and to detect it at the receiving end [20]. In 1890, Nikola Tesla conducted his experiments on the transmission of power by radio waves. His first effort to transmit power was at Colorado Springs, CO, USA, in 1899 [20]. He built a massive coil in his laboratory having a copper ball positioned on a tower. The Tesla coil was resonated at a frequency of 150 kHz when

2332-7782 © 2017 IEEE. Personal use is permitted, but republication/redistribution requires IEEE permission.
See http://www.ieee.org/publications_standards/publications/rights/index.html for more information.

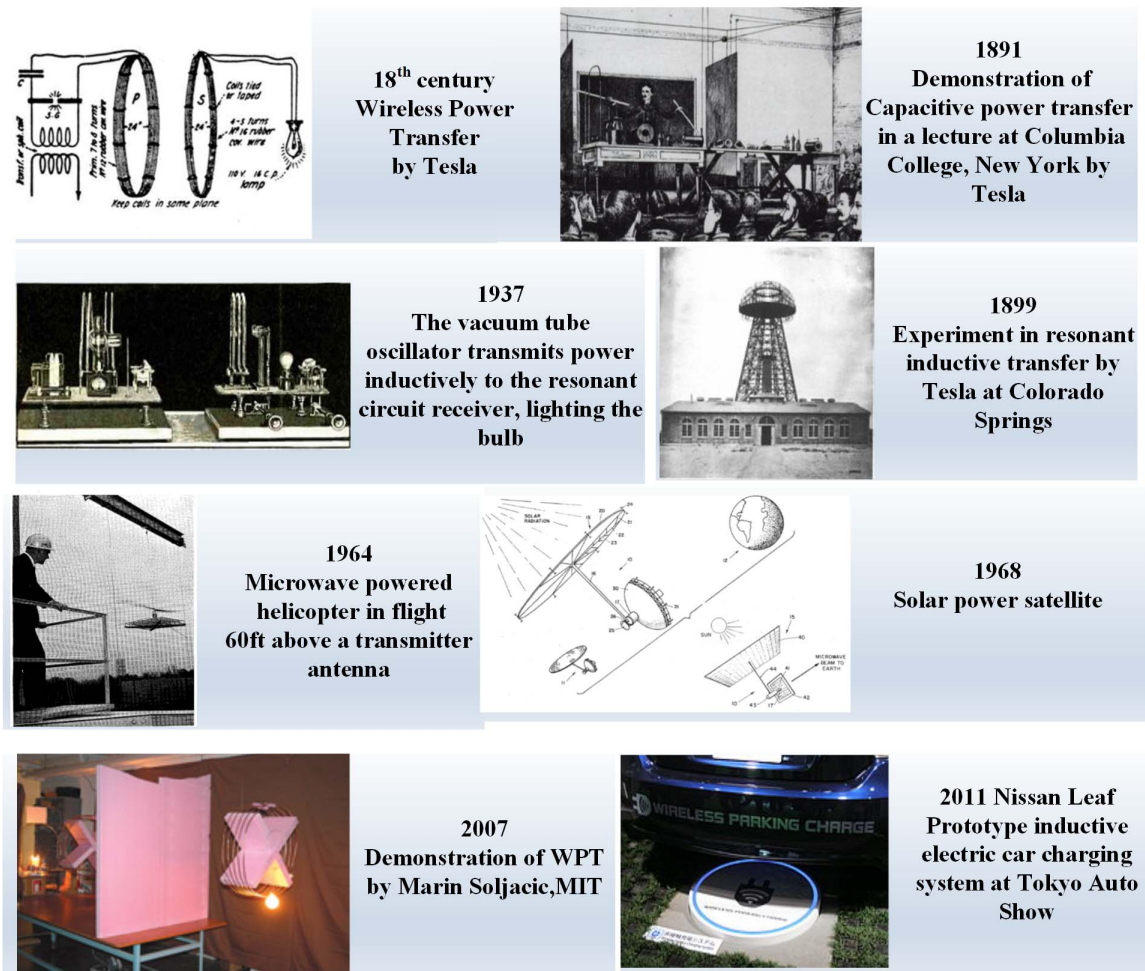


Fig. 1. Timeline diagram of development of the WPT.

supplied with 300 kW [21]. However, there is no evidence of its successful demonstration. In the 1960s, William C. Brown demonstrated a far-field (radiative) method of WPT [22]. The development of klystron and magnetron tubes and parabolic antennas made possible to demonstrate microwave technology [23]. Further, in 1964 using the invention of the rectenna, which could efficiently convert microwaves to dc power, with its demonstration of microwave beaming, a helicopter was powered wirelessly from the ground [22], [23]. In the 1970s, concept of solar power satellite to harvest energy from sunlight using the solar cells in space, then beaming it down to earth using microwaves to rectenna, was conceived by Glaser [24]. Later, in 1975, Brown demonstrated short-range transmission of 475 W of microwaves at 54% dc-to-dc efficiency. Following this, Brown and Robert Dickinson at the NASA's Jet Propulsion Laboratory transmitted 30-kW dc output power over a distance of 1.5 km using 2.38-GHz microwaves from a 26-m dish to a 7.3 m × 3.5 m rectenna array with 80% efficiency [22], [23]. In 2007, a group of researchers from Massachusetts Institute of Technology (MIT) repeated Tesla's experiment based on coupled-mode theory using magnetic resonance with an efficiency of 40% over a distance of 2 m using coupling coils with a radius of 30 cm [25].

Overall WPT can be applied in various applications and the frequency of operation for different methods of power transfer over a wide range. Fig. 2 gives an overview of different techniques for WPT depending on the frequency of operation.

Recent advances in technology have made stationary charging commercially feasible. The history of stationary charging started in 1997/1998 when IPT—Charge Technology—demonstrated an EV with wireless charging at Rotorua Geothermal Park in New Zealand and the first bus charged wirelessly at bus stops in Genoa and Turin in 2002. The major companies working on stationary WPT are WiTricity, Qualcomm, Conductix-Wampfler, Momentum Dynamics, and Bombardier [26]–[31]. WiTricity is a spin-off from the MIT. They have developed transmitter and receiver that operate on strongly coupled magnetic resonance [27]. WiTricity has reported system efficiency of around 90% for 3.3-kW power rating operating at 145 kHz with lateral misalignment of ± 20 - and ± 10 -cm bumper to bumper [27].

Qualcomm's Halo collaborated with the University of Auckland to patent “Double D” polarized magnetic pads capable of delivering twice the power rating with a higher efficiency as compared to circular pads operating at 20-kHz

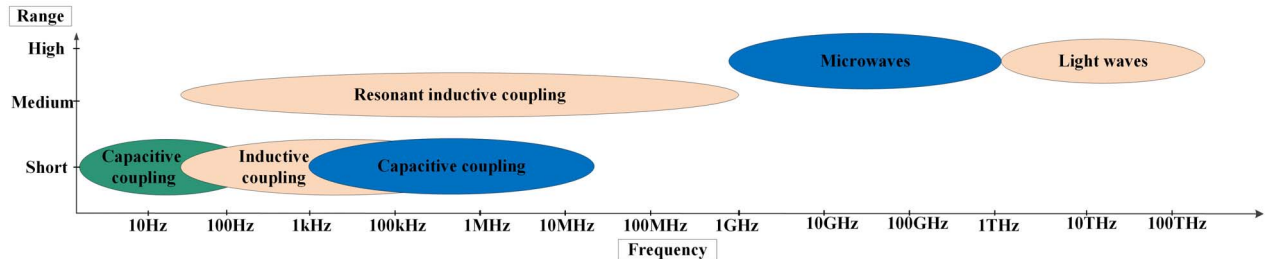


Fig. 2. Review of different technologies in WPT.

TABLE I
COMMERCIALLY AVAILABLE STATIONARY CHARGING

Company	Frequency	Airgap	Power	Efficiency
Witricity [27]	145kHz	180mm	3.3kW	90%
Conductix Wampfler [13]	20kHz	40mm	60-180kW	>90%
Momentum Dynamics [26]	-	610mm	3.3-10kW	92%
HEVO Power [26]	85kHz	~304.8mm	1-10kW	>85%

*-indicates information not available

frequency [28], [29]. Conductix-Wampflers has implemented stationary charging for the electric bus in Turin, Italy. They tune the resonant frequency of each system to achieve 90% efficiency at the separation distance of 40 mm for 60-kW power transfer [13].

Momentum Dynamics has developed stationary WPT system for an air gap of 24 in at 3.3 kW with power transfer efficiency of 92%. Further, the charger can be upgraded to 7.2 and 10 kW, which can charge the Chevy Volt in approximately 1 h [26]. Momentum Dynamics WPT system is currently being implemented in select FedEx trucks from Smith EVs [15], [30]. HEVO Power Company is working on implementing static charging for EV [26]. Table I summarize the commercially available stationary wireless charging systems for EV [26]–[31].

Dynamic WPT (DWPT) application covers passenger cars, taxi, trams, train, trucks, and bus. DWPT is not commercially available due to formidable challenges, including the need for highly efficient transfer of power and extensive infrastructure modification resulting in disruption of current services [14], [31]–[33]. The history of DWPT for EV begins in 1976 at the Lawrence Berkley National Laboratory where the technical feasibility of DWPT was evaluated [30]. In 1979, the Santa Barbara Electric Bus project commenced with a 4.3-m length of track, pickup of 1-m width and using switched capacitor tuning control for power regulation [30]–[32]. In 1992, partners for advanced transit and highway (PATH) installed an IPT station for electric bus with power supply rails constructed along a roadway for evaluation of the environmental and economic impacts it would entail. The PATH team demonstrated 60-kW power transfer with 60% efficiency across a 7.6-cm air gap [30], [32]. However, it was not commercialized due to high cost, heavy coils, low efficiency, insufficient air gap for bus ground clearance and low frequency of operation [30]. Later in 1996,

German IPT Company, Conductix (now IPT Technology) along with the University of Auckland tested the stationary charging of electric buses [13]. The developed technology was capable of charging an EV bus when it is parked or at a stop. The prototype was designed with a power rating of 60 kW, operating frequency of 15–20 kHz, working air gap of 40 mm, and a reported efficiency of 90% [30]. Because the system was designed for such a small air-gap length, the secondary coil was required to be mechanically lowered during charging. Another research team from Korea's Advanced Institute for Science and Technology (KAIST), in 2009 built a 3-kW Online EV (OLEV) with a mechanically controlled pickup, for an air gap of 10 mm, and efficiency of 80% when operating at 20-kHz frequency [30], [33], [34]. Later, in the same year, a 60-kW OLEV for bus was developed. The system was designed for an air gap of 170 mm with a maximum achievable efficiency of 72%, without mechanically moving the pickup. Other researchers have refined these designs and reported on increased power output, reduced weight of the pickup and smaller size of power supply rail with minimized stray electromagnetic field (EMF). In 2016, Oak Ridge National Laboratory (ORNL) extended the power of their earlier 10-kW WPT to 20 kW for demonstration on a passenger car, a Toyota RAV4 with a 10-kWh battery storage [13], [14], [35]. Utah State University startup wireless advanced vehicle electrification developed a 50-kW WPT system for an electric bus. Their system was capable of transferring 50 kW of power over an air gap of 15–30 cm at 20-kHz operating frequency with a reported system efficiency of 90%. Bombardier Primov has developed several IPT systems for stationary and dynamic charging applications. For the dynamic charging application a 250-kW system was developed for Primove Trams in Augsburg, Germany. In their system an E-type power rail is employed with F-type pickup. The air gap between primary and secondary is 60 mm and tolerates a few millimeter of lateral misalignment [30], [36]. Momentum Dynamics has developed the WPT system for powers up to 200 kW, with reported efficiency of 92% for 610-mm air gap [17], [18]. They have successfully implemented WPT system for delivery trucks using dock or roadway embedded-stationary charging installations. Recently, Utah State University has demonstrated 25-kW DWPT with circular primary coil for use in bus in 2016. The system was capable of delivering 25 kW for lateral misalignment of ± 15 cm [37]. A detailed comparison of different IPT technology developments is provided in Table II.

TABLE II
DIFFERENT WPT TECHNOLOGIES FOR DWPT [12]–[38]

Parameters	KAIST				ORNL	Bombardier	Conductix-Wampfler AG	WAVE	Utah State University
Application	Car(2009)	Bus(2009)	Train(2010)	Bus(2016)	Car(2016)	Trams (2010)	Bus (2002)	Bus(2011)	Bus(2016)
Air gap	10mm	170mm	120mm	200mm	162mm	60mm	40mm	~152mm-254mm	
Efficiency	~88%	~72%	~74%	~80%	~93%	~90%	~90%	~90%	~86%
Pickup	E-type	Flat-type	DD coil	DD coil	Rectangular with ferrite bar	-	F-type	-	Circular with ferrite bar
Power rail or primary transmitter	E-type	U-type	W-type	I-type	Rectangular with ferrite core	-	E-type	-	Circular with ferrite bar embedded in concrete
Power level	3kW	6kW	15kW	27kW	~20kW	200kW	120kW	50kW	25kW
Misalignment	~3mm	~230mm	-	240mm	150mm	Low few mm	-	~254mm	150mm
Frequency	20kHz	20kHz	60kHz		~22kHz	20kHz	15-20kHz	20kHz	20kHz

*-indicates information not available

*E-type, F-type or Flat-type, W-type, U-type, I-type classification are based on shapes [12]-[38]

Li and Mi [39] and Musavi and Eberle [40] report the review of WPT for EV in stationary and dynamic WPT. However, the report only provides a brief overview of various topics for the WPT system. The recent topics such as foreign object detection (FOD), recent standards, and power electronics architectures for dynamic and stationary charging are not reported. Choi *et al.* [34] report overview of various subsystems for road-powered EV and its fundamental principles of operation. However, it is predominantly focused on one technology and lacks extensive comparison of various subsystems such as couplers, power electronics architectures, communication methods, and shielding. Mi *et al.* [35] offer an overview of various technologies for DWPT. However, the review is limited in terms of the current status of research and lacks details of implementation issues.

This paper reviews the current status, technology, and implementation issues of WPT charging for EVs. This paper is organized as follows. Section II discusses the fundamental principles of WPT and its architectural elements required for practical implementation. Section III reviews different magnetic couplers needed to transfer power efficiently with minimum leakage flux and high tolerance for misalignment. Section IV presents an overview of various compensation networks. Section V covers the necessary power electronics required to implement high-power stationary and dynamic WPT. In Section VI, enabling control techniques to provide efficient power transfer are investigated. Section VII reviews different impedance matching techniques.

II. FUNDAMENTALS OF WIRELESS POWER TRANSFER

The WPT working principle is governed by Ampere and Faraday's laws. Briefly, the laws are explained as follows:

- 1) **Ampere's Law:** When electric current flows through a conductor in free space, it generates a magnetic field. The resulting magnetic field is proportional to electric

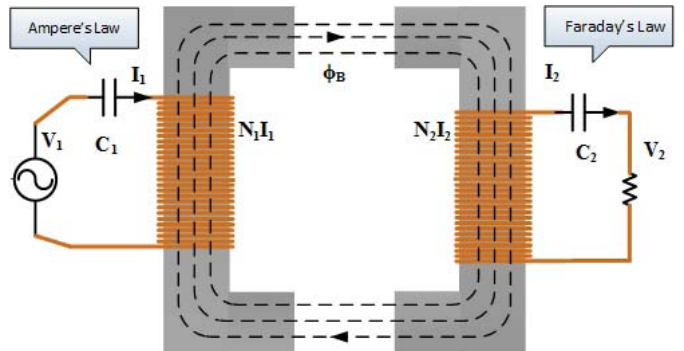


Fig. 3. Fundamental principle of WPT.

current and permeability of free space [41]

$$\sum B_T \Delta l = \mu_0 I N_1. \quad (1)$$

- 2) **Faraday's Law:** If a time-varying magnetic flux links a conductor, it induces a voltage in the conductor. The value is proportional to the rate of change in magnetic flux and the number of turns in the conductor [41]

$$e = -N_2 \frac{d\phi_B}{dt} \quad (2)$$

where B_T is the magnetic flux density in Tesla, Δl is the unit length of the conductor in meters, N_1 is the number of primary turns, N_2 is the number of secondary turns, I is the current in primary conductor in amperes, and ϕ_B is the flux in the magnetic path in weber.

As depicted in Fig. 3, WPT has two coils separated by a large air gap. The coils are placed around a magnetic material to improve coupling and to minimize proximity losses. The primary coil is energized by high-frequency ac current which generates a time-varying magnetic field in accordance with Ampere's law. A portion of the generated time-varying magnetic field is linked with secondary coil depending on the

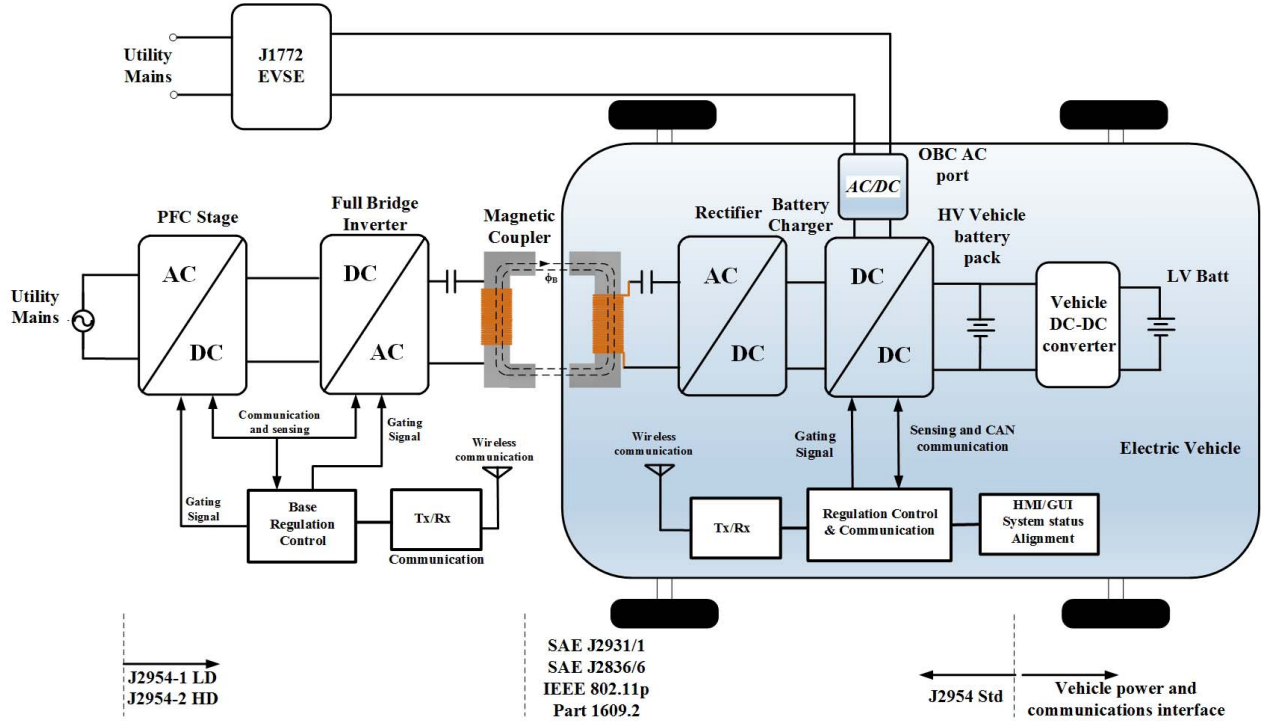


Fig. 4. Block Diagram of a typical wireless charging system for EVs.

coefficient of coupling, k , to induce a voltage according to the Faraday's law in the secondary [42]. Due to the large air gap, the circuit is inductive. Therefore, a large current (i.e., magnetomotive force) is required to produce sufficient magnetic field to link secondary coils. In practical WPT systems, it is necessary to cancel the inductive component in the circuit using a capacitor connected such that it resonates with the primary inductance to reduce the Volt–Amp (VA) rating of the inverter. The secondary side is also tuned to approximately the same resonant frequency to cancel the secondary leakage inductance and to maximize the power transfer efficiency. To provide high-frequency ac current to excite the primary coil, a high-frequency switching inverter is employed. On the secondary side, the induced voltage in the coil is rectified and fed to a load [34], [35], [37].

A WPT system can operate at resonance or above resonance. Typically, if the power transferred is small then the voltage drop of the leakage inductance of the coil will be smaller even with large current. Generally, the switching frequency of the inverter is higher to achieve zero voltage switching and to improve efficiency [34], [43]. At high power, the voltage drop at a higher frequency across leakage inductance will be higher making it difficult to force a large amount of power without increasing the input current. The increase in input current will cause significant conduction losses in the system. In addition, reactive power additionally required will increase the VA rating of the inverter [39], [44], [45].

A. WPT for EV

The overall WPT architecture for EVs is shown in Fig. 4. It consists of front-end ac–dc converter to correct the power factor (PF) and convert ac supply from utility to an adjustable

TABLE III
J2954/1 PROPOSED WPT POWER CLASS [7], [42], [43]

	WPT Power Class			
	WPT1	WPT2	WPT3	WPT4
Maximum input Volt Amps	3.7kVA	7.7kVA	11.1kVA	22kVA
Minimum Target efficiency	>85%	>85%	>85%	TBD
Minimum target efficiency at offset position	>80%	>80%	>80%	TBD
Frequency	85kHz within international frequency band (81.38-90)kHz			

dc level. Various standards for wireless charging of an EV have been published, such as SAE J2954/1 charging standard for light-duty vehicles for which five levels of charging according to power levels are categorized [42], [43]. WPT1 is for a household with a maximum power capacity of 3.7 kVA from single phase 120-V ac supply. WPT2 is for the higher power of 7.7 kW from 240-Vac mains, WPT3 upgrades this to 11.1 kW, and WPT4 to 22 kW input from a 240-V three-phase ac supply outlet. SAE J2954/2 is under development for WPT charging of heavy-duty EVs such as a bus where the power rating is >22–150 kW and higher from a 208-Vac three phase, 480-Vac three phase, or medium voltage supply. At either level of charging, the efficiency of the system must be greater than 85% for a matched system at rated power and >80% for interoperable systems [42], [43]. Table III summarizes the J2594 standard requirements for WPT systems. The second stage in Fig. 4 is a full-bridge inverter which converts dc voltage into high-frequency ac voltage. The high-frequency ac is transferred through the compensating

TABLE IV
J2954 SPECIFICATION OF THE Z-CLASSES [42]

Z-Class	Ground clearance range (mm) between primary and secondary coil
Z1	100-150
Z2	140-210
Z3	170-250

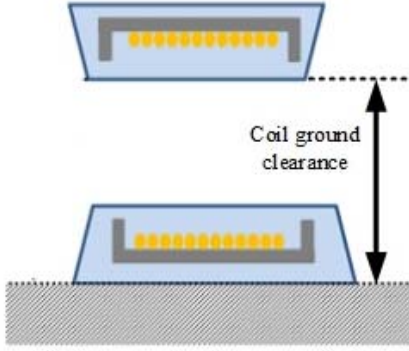


Fig. 5. Definition of ground clearance as specified in [41].

network to compensate the reactive power requirement of the coupler coils. Coupler secondary voltage is passed through the compensation network and rectified by the secondary rectifier. The compensation network is designed to resonate within the allocated frequency band (81.38–90 kHz), generally at its center around 85 kHz and to have coupling coefficient and loading variability adjustment to improve the power transfer efficiency [42]. The control is achieved by primary side control or secondary side control [37].

B. Design Considerations for WPT

The recently published SAE J2954/1 standard reports different requirements of the WPT for EVs [42]. Fig. 4 shows various components of a wireless charging system for an EV and the corresponding standard for each section. The front-end PF correction (PFC) should have PF greater than 0.95 ($\text{PF} > 0.95$), and the total harmonic distortion (THD) should be less than 5% [8], [42]. These levels were formerly specified in SAE J2894/1 Power Quality Requirements for Plug-in EV Chargers but transferred to J2954/1 by agreement with SAE for WPT chargers. The WPT charger should be able to match the battery charging requirement of different EVs such as sedans, SUVs, and pickups. Transmitter and receiver coils should be compatible with various charging power levels through sensing electronics and appropriate controls. The distance between the primary coil and a secondary coil, the magnetic gap, is classified into three Z-classes with values reported in Table IV and the definition of coil ground clearance in Fig. 5 [42]. SAE J2954/1 also reports the misalignment tolerance for various directions and positions, and the details are given in Table V. Vehicle ground clearances are load dependent, and range from 16 cm for small passenger vehicles to >20 cm for SUVs. It is important that the vehicle

TABLE V
J2954 SPECIFICATION OF THE MISALIGNMENT DISTANCE [42]

Offset direction	Misalignment distance (mm)
ΔX	± 75
ΔY	± 100
ΔZ	$Z_{\text{nom}} - \Delta_{\text{low}} \rightarrow Z_{\text{nom}} + \Delta_{\text{high}}$
Rotation, Roll, and Yaw	Testing at +/- 2, 4 and 6 degrees

mounted WPT receiver coil does not reduce the vehicle ground clearance so that obstacles or road debris do not inadvertently damage the coil. The primary or ground assembly coil may be surface mounted as shown in Fig. 5 for residential garages, but should be embedded in public spaces or on highways [42]. SAE J2954/1 system specifies the nominal frequency of 85 kHz. While the system can employ frequency tuning to the range of 81.38–90 kHz, the available spectrum space internationally agreed upon and one having minimal coexistence issues with other services [42]. SAE J2954/1 standard also reports on the interoperability performance requirements such as compatible communication method, FOD, living object detection (LOD), compliance with electromagnetic compatibility (EMC) requirements, and EMF protection requirements [42]. The communication can be dedicated short-range communications (DSRC), or other private and secure communications including near-field communications. Initial positioning of the vehicle may be a magnetic beacon or radio frequency identification. Furthermore, the leakage EMF must comply with International Commission on Non-Ionizing Radiation Protection (ICNIRP) 2010 as stated in SAE J2954/1 while the IEEE C95.1-2345-2014 [42]–[51] offers more insights into physiological effects such as nerve excitation (<100 kHz) and tissue heating (>100 kHz). Practical high PFC circuits for low THD rely on accurate zero-crossing detection methods and high-frequency operation (70–115 kHz). Most commonly used PFC configuration is the interleaved boost PFC circuit for EV chargers [8]. ORNL reported on a silicon carbide-based full bridge ac–dc converter for PFC [48]. Bosshard *et al.* [49] evaluated different coil structures to demonstrate that the main factor necessary for high magnetic coupling is the large coil area [45], [46]. Furthermore, they assessed different coil geometries, concluding that circular coil geometry has higher coupling coefficient k than square or rectangular geometries. For high quality factor Q and coupling coefficient, closely spaced coils with an inner radius of at least half of the outer coil radius is preferred. A η - α -Pareto optimization considering the losses in different components of the system was performed, to achieve efficiency of ~96.5% at 52-mm air gap with 100-kHz switching frequency [49], [50].

C. International Standard

Currently, there exist many standards related to WPT implementation. SAE J2954/1,2 addresses issues related to alignment method, interoperability, the frequency of operation and power level. Aspects of safety, obstacle detection,

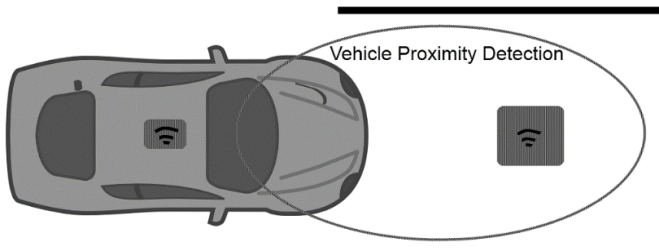


Fig. 6. J2954 Vehicle alignment concept [42].

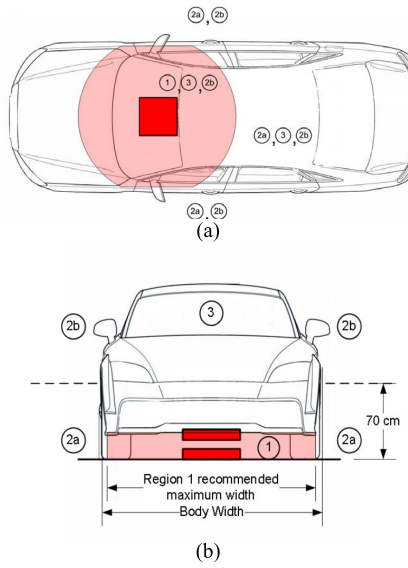


Fig. 7. (a) EMF region top view and (b) EMF region front view [42].

magnetic field levels, contact current, communication, maximum temperature, and electric shock are discussed in [42] and [43].

Fig. 6 shows the vehicle alignment as defined in SAEJ2954/1,2. Further, it reports two alignment methods.

- 1) A small magnetic field is generated by the ground assembly coil. The magnetic field is detected by vehicle assembly coil. However, the range of this method is limited to ~ 1 m.
- 2) Magnetic signal is transmitted from vehicle assembly using the auxiliary coil. The ground assembly coil receives the signal and responds to vehicle assembly the position via the communication interface; the range of this method is around ~ 5 m [42], [43].

Wireless charging of the EV has the presence of high-frequency magnetic field between transmitter and receiver. ICNIRP specifies the guidelines for limiting the time-varying magnetic field, electric field, and EMF [42], [43], [51]. SAE J2954/1,2 reported that electric and magnetic fields and contact current in the regions 2a, 2b, and 3 shown in Fig. 7 have to comply with ICNIRP 2010. Table VI summarizes the EMF exposure limit from ICNIRP 2010 [51]. The contact current limit applies to the current between two conductive sections of a vehicle when a person comes in contact with both these sections. Other standards related to

TABLE VI
EMF EXPOSURE STANDARD LEVEL [42]

	RMS	Peak
Magnetic field	$27\mu\text{T}$ or 21.4A/m	$38.2\mu\text{T}$ or 30.4A/m
Electric field	83V/m	117V/m
Contact current	$0.2 \times f(\text{kHz}) = 17\text{mA}$ $@85\text{kHz}$	$0.283 \times f(\text{kHz}) = 24\text{mA}$ $@85\text{kHz}$

TABLE VII
MAJOR STANDARDS FOR WPT [42], [51]–[54]

Standard	Title
J2954/1,2	Wireless Power Transfer for Light-Duty Plug-In/Electric Vehicles and Alignment Methodology
ICNIRP2010	Guidelines for limiting exposure to time-varying electric and magnetic fields (1 Hz to 100 kHz)
IEEE C95-1234	IEEE Standard for Safety Levels concerning Human Exposure to Radio Frequency Electromagnetic Fields, 3 kHz to 300 GHz
ISO 19363	Electrically propelled road vehicles - Magnetic field wireless power transfer -- Safety and interoperability requirements
ISO 15118-1	Road vehicles -- Vehicle to grid communication interface – Part 1: General information and use-case definition
ISO 15118-2	Road vehicles -- Vehicle-to-Grid Communication Interface – Part 2: Network and application protocol requirements
ISO 15118-8	Road vehicles -- Vehicle to grid communication interface – Part 8: Physical layer and data link layer requirements for wireless communication

communication, safety, and interoperability requirements are reported in Table VII.

D. Generalized Mathematical Analysis for WP

In this section generalized approach to model compensation network is reviewed. An efficient compensation is necessary to transfer the maximum possible power with lowest possible reactive power supplied from the source. Tavakoli and Pantic [38] reported a generalized approach for mathematical analysis based on active and reactive power. The approach can be applied to WPT system operating at any frequency. However, application of this general approach to various compensation networks was not reported. In the literature, many papers have reported maximum efficiency for basic compensation network. Fig. 8 shows the generalized WPT system with compensation network. Primary side is energized by a high frequency supply. To simplify, the analysis semiconductor switches and diodes are not included. The compensation network on the primary and secondary can be connected in series, parallel, or other compensation configurations such as LCC and LCL [39]. In [55], a generalized approach

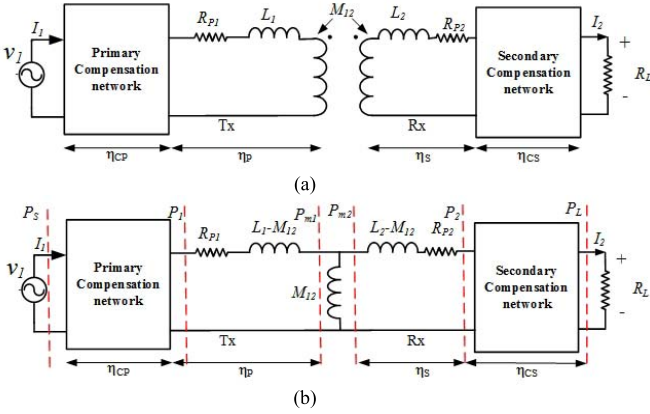


Fig. 8. (a) General WPT system with compensation network. (b) General WPT system with T equivalent circuit.

is reported which will be summarized here. Fig. 8(b) shows the WPT system with T equivalent circuit. The real powers at various stages are illustrated in Fig. 8(b). \$P_S\$, \$P_{1P}\$, \$P_{m1P}\$, \$P_{m2S}\$, \$P_{2S}\$, and \$P_L\$ are the real power at input of compensation, primary input power, medium left power, medium right power, secondary output power, and load power [55].

The efficiency of the WPT system is expressed as

$$\eta = \eta_{cp}\eta_p\eta_s\eta_{cs} \quad (3)$$

where \$\eta_{cp}\$ is the compensation network efficiency, \$\eta_p\$ is the primary-side efficiency, \$\eta_s\$ is the efficiency of the secondary side, and \$\eta_{cs}\$ is the secondary-side compensation network efficiency [55]. The overall efficiency is given by

$$\eta = \frac{P_{m1P}}{P_{1P}} \frac{P_{2S}}{P_{m2S}} = \frac{\text{Re}(Z_{m1})}{R_{P1} + \text{Re}(Z_{m1})} \frac{\text{Re}(Z_2)}{R_2 + \text{Re}(Z_2)} \quad (4)$$

where

$$Z_{m1} = \frac{j\omega M}{j\omega(L_2 - M) + R_2 + Z_2}.$$

\$Z_2\$ is either series impedance \$Z_{2S}\$ or parallel impedance \$Z_{2P}\$ and is given by

$$Z_{2S} = R_L + \frac{1}{j\omega C_2} \quad (5)$$

$$Z_{2P} = R_L // \frac{1}{j\omega C_2}. \quad (6)$$

Substituting (5) and (6) in (4) and simplifying the equation gives the efficiency with secondary series compensation (\$\eta_s\$) and the efficiency of parallel compensation scheme (\$\eta_p\$) [55]

$$\eta_s = \frac{Q_1(Q_2//Q_{LS})k^2\omega_n^2}{1 + Q_1(Q_2//Q_{LS})k^2\omega_n^2 + (Q_2//Q_{LS})^2\left(\omega_n - \frac{1}{\omega_n}\right)^2} \times \frac{1}{1 + \frac{Q_{LS}}{Q_2}} \quad (7a)$$

$$\eta_p = \frac{k^2\omega_n^2Q_1(b_1\omega_n^4 + b_2\omega_n^2 + b_3)}{b_4\omega_n^6 + b_5\omega_n^4 + b_6\omega_n^2 + b_7} \frac{1}{1 + \frac{1}{Q_2Q_{LP}} + \frac{Q_{LP}\omega_n^2}{Q_2}} \quad (7b)$$

where \$\omega_n\$ is the normalized angular frequency, \$\omega_2\$ is the secondary resonant angular frequency, \$Q_1\$ and \$Q_2\$ are the quality factors of coils, and \$Q_{LP}\$ and \$Q_{LS}\$ are the load-side quality factors. These terms are defined as follows [55]:

$$\begin{aligned} \omega_n &= \frac{\omega}{\omega_2}, \quad \omega_2 = \frac{1}{\sqrt{L_2C_2}}, \quad Q_1 = \frac{\omega L_1}{R_{P1}}, \quad Q_2 = \frac{\omega L_2}{R_{P2}} \\ Q_{LS} &= \frac{\omega L_2}{R_L} \quad \text{and} \quad Q_{LP} = \frac{R_L}{\omega L_2} \\ b_1 &= Q_{LP}^4/Q_2, \quad b_2 = Q_{LP}^2(Q_{LP} + 2/Q_2) \\ a_3 &= (Q_{LP} + 1/Q_2), \quad b_4 = \left(1 + \frac{k^2Q_1}{Q_2}\right)Q_{LP}^4 \\ b_5 &= k^2Q_1a_3 + Q_{LP}^2(2 - 2Q_{LP}^2 + Q_{LP}^2/Q_2^2) \\ b_6 &= k^2Q_1a_3 + 2Q_{LP}^2(Q_{LP} + 1/Q_2)/Q_2 + (1 - Q_{LP}^2)^2 \\ \text{and} \quad b_7 &= \left(Q_{LP} + \frac{1}{Q_2}\right)^2. \end{aligned}$$

The maximum efficiency of the WPT system can be found by differentiating (7a) and (7b) with respect to \$\omega_n\$. The maximum efficiency is expressed as [55]

$$\frac{d\eta_s}{d\omega_n} = 0 \quad \omega_{\eta_{Sm}} = \frac{\omega_2}{\sqrt{1 - 1/(2(Q_2//Q_{LS})^2)}} \quad (8)$$

$$\frac{d\eta_p}{d\omega_n} = 0 \quad \omega_{\eta_{Pm}} = \omega_2 \sqrt{\frac{1 + 1/(Q_2Q_{LP})}{\sqrt{1 + k^2Q_1/Q_2}}} \quad (9)$$

III. COUPLING PAD

The coupler is the most important part of WPT system. It consists of transmitter and receiver coils separated by an air gap. The desired characteristics for coupling pads are the high coefficient of coupling \$k\$ quality factor \$Q\$ and high misalignment tolerance [44], [45]. Many researchers have proposed different coil structures to improve the coefficient of coupling and to maintain a high quality factor [49], [46], [56]–[71]. To increase the coupling coefficient, ferrite bars, or ferrite plates are used including an insulating material between ferrite and the coil conductors. The increase in ferrite bars can improve self-inductance, quality factor, and mutual inductance of the coupling pad. However, the addition of ferrite bar increases both, the core losses in a system as well as copper losses due to field modification in the conductors [50].

Efficiency of coupled inductors in a WPT system is affected by the product \$kQ\$, the product of magnetic coefficients of coupling, and the quality factor of the inductors [44], [45], [49], [50]. The geometry, core material, and the distance between the inductors determine these factors. The inductor quality factor, \$Q\$, is the geometric mean of primary and secondary quality factor, which is given by

$$Q = \sqrt{Q_1Q_2}, \quad \text{where} \quad Q_1 = \frac{\omega L_1}{R_1} \quad \text{and} \quad Q_2 = \frac{\omega L_2}{R_2}. \quad (10)$$

To attain a high Q , inductors must be designed to have high self-inductance and low series resistance at high operating frequency. However, the maximum operating frequency is limited to approximately 85 ± 3.7 kHz considering SAE J2594/1 [42], [45]. Therefore, to increase the Q , resistance of the coil must be decreased. Self-inductance of the coil is proportional to the square of the number of turns, the permeability of the used magnetic material, and geometry of the magnetic flux path having cross-sectional area A and mean path length of l

$$L = \frac{\mu N^2 A}{l} \quad (11)$$

where μ is the magnetic permeability of the flux path, N is the number of turns, A is the area of the conductor, and l is the length.

Inductance of a coil is proportional to the square of the number of turns whereas, effective series resistance (ESR) is directly proportional to the number of turns. Therefore, an increase in the number of turns will increase inductance greater than ESR. One should consider the spatial distribution of current (i.e., proximity effect) within neighboring wires at high frequencies as well. Hence, overall Q of the coil increases with increase in a number of turns [49], [50]. Thus, a balance must be found between wire diameter and number of turns to yield an optimum self-inductance. Another option is to add ferrite bars on the coil to increase self-inductance. The purpose of ferrite bars is to guide the flux so that leakage flux can be reduced and high coefficient of coupling can be realized. ESR of the coil consists of dc resistance and ac resistance. The dc resistance of a coil is reduced by increasing the area of the conductor. To reduce ac resistance, litz wire is adopted, which is suitable for the operating frequency range [46].

Different coupler designs are reported in the literature. Traditionally lumped WPT uses a coupler design based on magnetic core topologies such as Pot-, U-, and E-cores [59], [60]. Problems associated with the conventional coupler are: large size for higher power rating and lower efficiency during misalignment [65].

A. Circular Pad

Most commonly reported coil structure is a circular pad as shown in Fig. 9(a). Circular coils are well reported and optimized in [46], [49], [50], [57], [58]. A η -Pareto optimization and guidelines for designing circular coil with respect to efficiency and area-related power density are reported in [49] and [50]. With η -Pareto optimization, Bosshard *et al.* [49], [50] demonstrated dc-dc efficiency of 96.5% with a 210-mm coil diameter and 52-mm air gap. The circular coil coefficient of coupling is of the order of 0.2 when the distance between the coils is a quarter of the diameter. For example, to keep coefficient of coupling in the range 0.15–0.2 when the distance between coils is 150–200 mm the diameter of the coils should be 600–800 mm [59]. In [46], it was reported that WPT coils should operate at current densities less than 3–5 A/mm² in the litz wire or similar cable to achieve acceptable thermal performance. Miller and Daga [46]

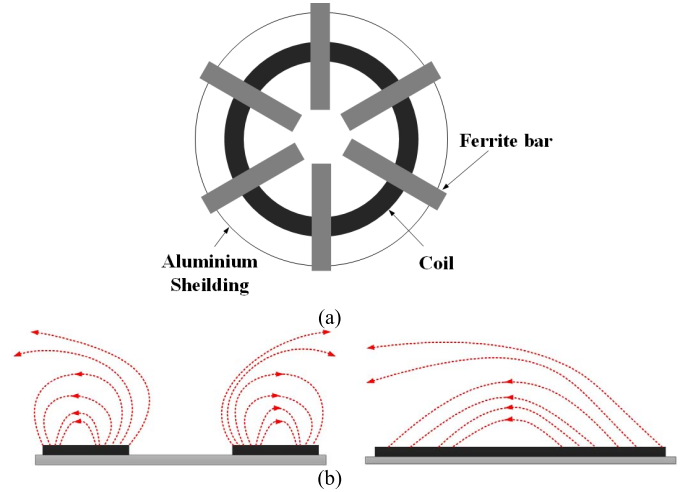


Fig. 9. (a) Circular pad. (b) Flux lines of circular pad side view and front view [59].

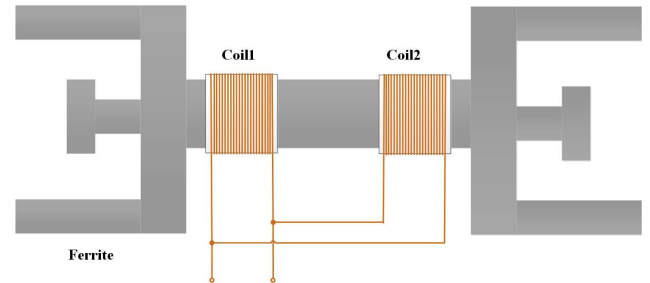


Fig. 10. Flux pipe [60].

gave a very good assessment of WPT for automotive applications, and Covic and Boys [56] provided an excellent treatment of circular pad sizing and the main performance factors for EV chargers. The circular coil and its close variants (i.e., square and rectangular designs) are commonly used in WPT because of the single-sided magnetic field that enters and leaves the coil from the front of the coil, as shown in Fig. 9 [59]. The magnetic field is single sided, and fountain field shaped like the coil sits above the ferrite and the later channels most of the flux beneath the coil and away from rebar and pipes in floor concrete. The single-sided nature of flux pattern helps in reducing leakage flux. Also, aluminum shielding helps to minimize the leakage flux when it is properly designed so that efficiency of the system is not affected [58].

B. Flux Pipe

To improve the coupling, different coil shapes are proposed in the literature, including the rectangular ferrite bar with a coil wounded along its length shown in Fig. 10 [59], [60]. This solenoidal field design exhibits good lateral misalignment tolerance plus the fact that it increases the flux path in ferrite to localize it at the ends of the coils [59], [60]. The benefit of flux pipe design is that the fundamental flux path height is half of the length of receiver pad. Moreover, horizontal (lateral) misalignment tolerance is high, and coefficient of coupling is comparable to a circular pad [59]. The shortcoming of this

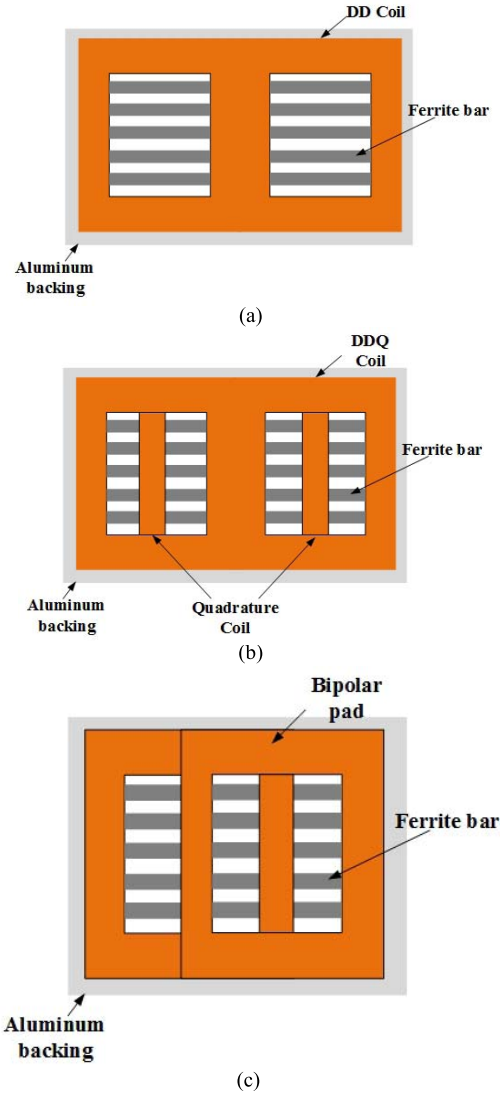


Fig. 11. Different coil structures [62], [63]. (a) DD coil. (b) DDQ coil. (c) BP.

coil design is that it is solenoidal, therefore, when aluminum shielding is used, its proximity to one side of the coil winding will result in intercepting flux and hence reducing the quality factor. This loss of quality factor lowers the efficiency of EV charging [59], [60].

C. DD Coil

Budhia *et al.* [59] proposed a polarized single-sided flux coupler that combines the advantage of both flux pipe and circular pad design, as shown in Fig. 11(a). The middle portion of the double D (DD) coil is similar to flux pipe as the coils are connected in series magnetically [59], [60]. The coils are placed on the top of ferrite; this allows aluminum shielding to be placed under the ferrite without loss in quality factor. The main features of DD coil are single-sided flux paths, flux path height that is proportional to half of the length of the pad, resulting in a higher coefficient of coupling, lower losses in the aluminum shielding, and low leakage flux from the back of the coil. In addition, the no-load quality factor Q is improved [61], [62].

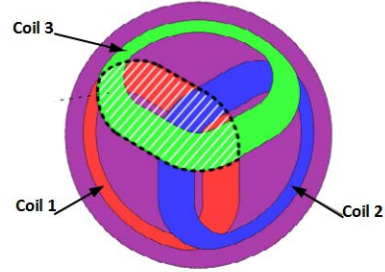


Fig. 12. Tripolar pad [67], [68].

D. Multicoil Polarized Coupler

Multiple coil couplers with different coils either on the primary side or on the secondary side are reported in [59]–[65]. Multicoil polarised couplers are derived from DD coil and circular coil. These coils have the advantage of capturing sinusoidal flux components and therefore the quadrature component of the flux [59]. The main advantages are tolerance to misalignment and small variation in air gap spacing.

1) *DDQ Coil*: double D quadrature (DDQ) coil is derived from DD coil by adding the quadrature coil as shown in Fig. 11(b) [59]. The position of the coil is at the center of DD coil. The coils are placed such that DD coils capture the d -axis flux, and Q coil captures the q -axis flux. Therefore, this coil structure compensates the misalignment to a great extent. However, the size of the coils increases approximately three times with respect to the circular pad or the square coils [59].

2) *Bipolar Pad*: The bipolar pad (BP) is a multicoil coupler with two coils placed on the ferrite bar with an overlap as shown in Fig. 11(c) [62], [63]. BP consists of two identical, partially overlapped, and mutually decoupled coils as shown in Fig. 11(c). The BP has high misalignment tolerance and high coefficient of coupling similar to DDQ pad. The main advantage of BP is that it requires 25% to 30% less copper as compared to DDQ pad [63].

3) *Tripolar Pad*: Tripolar pad (TPP) is a three-coil coupler arranged in such a way that they are mutually decoupled as shown in Fig. 12 [67], [68]. This type of assembly permits high rotational misalignment tolerance of a nonpolarized pad [67], [68]. The three mutually decoupled coils are driven independently to achieve highest coupling factor. Kim *et al.* [67], [68] demonstrated an increase in effective coefficient of coupling with bipolar and circular pad as the secondary coil. This was accomplished by controlling voltage magnitude and phase of the transmitter coil currents. The apparent power demand is reduced by 45% compared to the circular pad for an air gap of 150 mm. The leakage magnetic field reported is also less than the one specified in IECNIRP [51]. However, the need for three separate inverters to drive three mutually decoupled coils adds to its cost and increases complexity of control [67], [68].

4) *Miscellaneous Couplers*: Other multiple coil couplers are reported in the literature specifically to improve efficiency and tolerance to variation in load resistance [69]–[75]. In the three-coil coupling pad shown in Fig. 13(a), an additional coil is added to the transmitter or receiver in the same plane

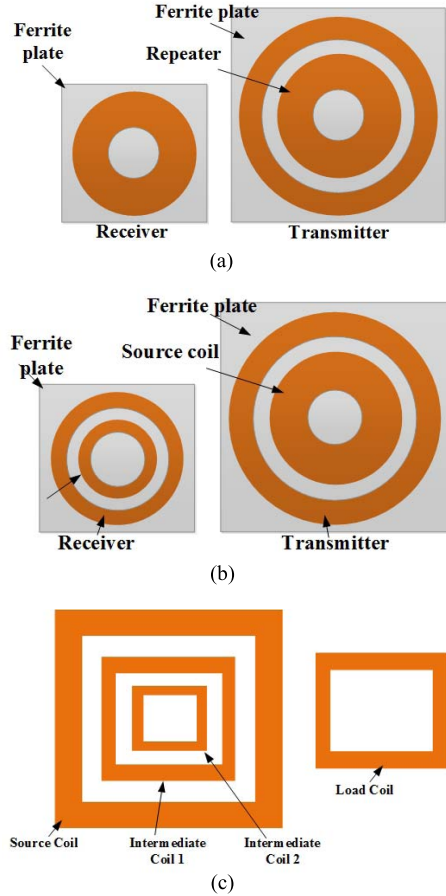


Fig. 13. (a) Three-coil WPT [69], [70]. (b) Four coil [70]. (c) Four-coil WPT Asymmetric four coil WPT [71].

as transmitter or receiver structure. The third coil improves the efficiency of the system, the energy efficiency resilience to load variations, and reduces EMF emissions due to coil misalignments [69]. However, if the source coil is placed close to the transmitter coil, the efficiency of the system degrades slowly when the load resistance diverges from optimal load resistance. Moreover, the coefficient of coupling is improved by the addition of a coil on the receiver side referred to as an intermediate coil. The advantages are an increase in power transfer distance and an overall increase in efficiency. The addition of a coil induces bifurcation phenomenon, therefore a complicated design procedure must be followed to avoid bifurcation. In addition, for a wide variation in load resistance, bifurcation can lead to instability in the system [70]. In [70], the four-coil method as shown in Fig. 13(b), transmitter and receiver each have additional coils referred to as source and load coils. The addition of coils improves the coefficient of coupling compared to three-coil configuration. In [71], two coils are added on the primary-side coil as shown in Fig. 13(c) to boost the coefficient of coupling even further where this double boosting effect improves performance over the conventional four-coil method. Zhang *et al.* [72] proposed an integrated magnetic inductor in DD coil to form magnetic integrated compensation circuit. The proposed structure has the advantage of compactness as the inductor is integrated.

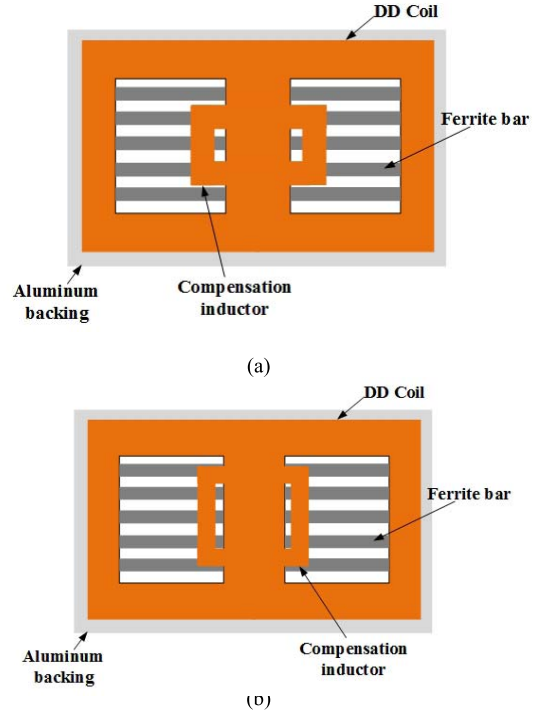


Fig. 14. Integrated inductor DD coil [72]–[74]. (a) Primary coil. (b) Secondary coil [71].

Further, the primary inductor has an angle with respect to secondary inductor as shown in Fig. 14 [72]–[74]. The angle between secondary inductor and primary coil is adjusted to be 90° . In the case of misalignment, the secondary inductor can induce some voltage to compensate for misalignment [74].

E. Performance Comparison of Couplers

Different coil structures shown in Fig. 15 were simulated in ANSYS and compared to assess the relative benefits of the geometry. For a fair comparison among various coil structures, the diameter of circular coil and the diagonal length of the rectangular coil were kept the same. The simulated coils were compared for coefficient of coupling for variation in misalignment, as shown in Fig. 16(a). From the simulation results and the stated coil dimensions in Fig. 16, it can be concluded that BP has the highest coefficient of coupling and misalignment tolerance. However, the coefficient of coupling decreases with the addition of aluminum shielding, as depicted in Fig. 16(b).

From the above comparison of couplers, it can be concluded that circular coil has a better performance with shielding as its coefficient of coupling is not affected much since the flux pattern is single sided. For a double-sided flux pattern such as the BP shielding has adverse effects. Shielding blocks the path of the flux on one side, which leads to losses in shielding. It also results in a subsequent decrease in the coefficient of coupling (Table VIII). Table VIII summarizes the comparisons of magnetic couplers for various parameters. Out of many couplers BP and circular pad are the most popular choices [49], [50]. Circular pad has high coupling coefficient with shielding due to single sided flux and ease

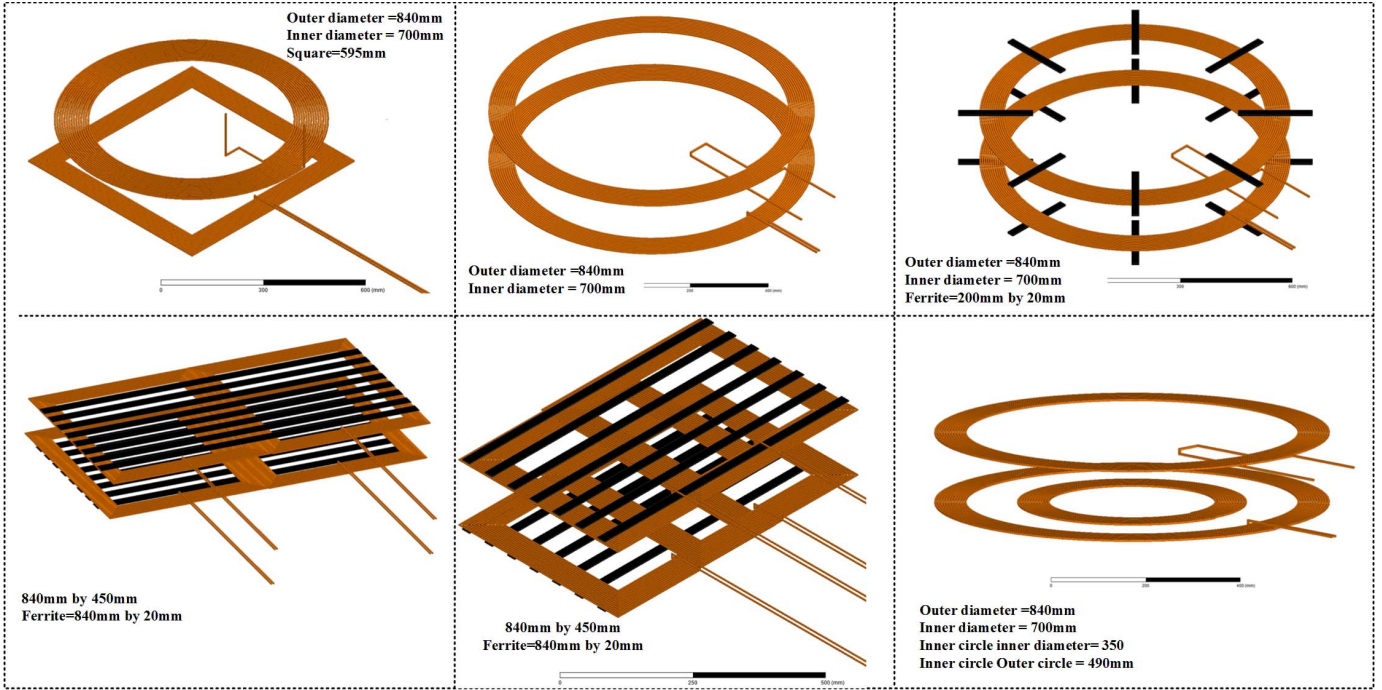


Fig. 15. Simulated coils in ANSYS Maxwell.

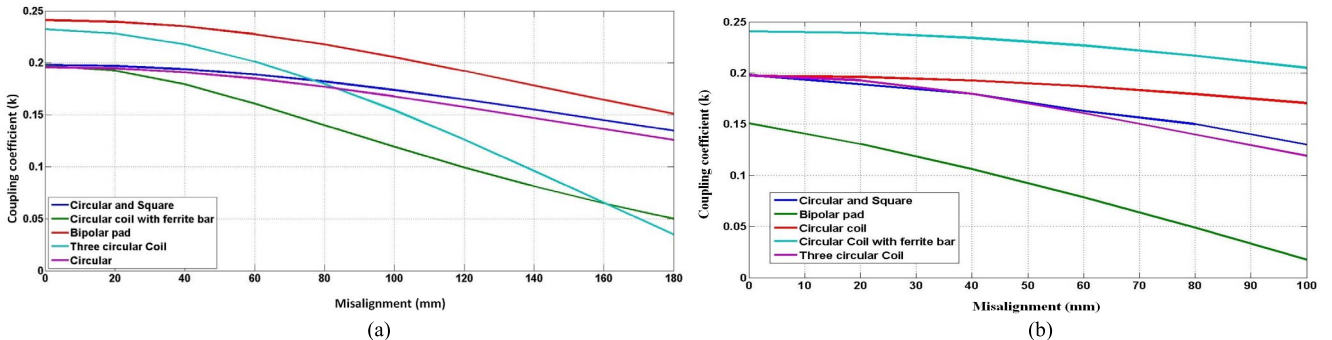


Fig. 16. Comparison of different coils for misalignment. (a) Without shielding. (b) With aluminum shielding.

of implementation. However, BP benefits from high misalignment tolerance as compared to circular with high coupling coefficient. Furthermore, EMF exposure is also less [61].

F. Power Rail and Pickup for DWPT

The charging of EV on the move is referred to variously as DWPT, Road-powered transmitter implementation as segmented IPT tracks or long power rail [34], [35]. The segmented IPT has a short power pad with individual power supply for each pad. These power pads are energized only when a WPT-compliant EV is moving over the top of it [34], [56]. Researchers from Auckland University are working on the segmented IPT system [82]. Multiple ground pads are laid on the road at a specified distance; the particular pad is turned ON as EV is passing over. This method has the advantage of low weight, low EMF and compact structure from an implementation point of view [82]. The magnetic coupler for stationary charging can also be used for dynamic charging.

However, the segmented structure has issues regarding control complexity, complex power supply architecture and high maintenance cost, especially when embedded in a roadway. In 2011, ORNL commenced work on a segmented DWPT that employed many circular coils in a series track having a pitch factor of 0.7 [36]. ORNL integrated their WPT system into different commercial EVs including Chevy Volt, Toyota Prius plug-in, Scion IQ, and Toyota RAV4 with maximum power output of 6.6 kW with 85% efficiency at 162-mm air gap [36]. Further development led to increased system power to 20 kW for the same ground clearance of 162-mm air gap with an efficiency of 92%–93% [36].

Another implementation, and one pioneered by KAIST was to lay a long power supply rail on the roadway [34], [35]. The power rail is energized full time during operation irrespective of the presence of the EV. The basic power rail consisted of two wires without any magnetic material. Due to the absence of magnetic material, the lateral misalignment tolerance of the

TABLE VIII
COMPARISON OF DIFFERENT PAD STRUCTURES [49], [50], [46], [56]–[68]

Coils Structure	Misalignment tolerant	coefficient of coupling	EMF Exposure	Effect of shielding on coefficient of coupling	Magnetic flux
Circular pad	Poor	Low	High	Low	Single sided
Flux pipe	Medium	Medium	Low	High	Double sided
DD Coil	Poor	High	Low	High	Double sided
DD-Q Coil	High	High	Low	High	Double sided
Bipolar pad	Medium	High	Low	High	Double sided
Tripolar pad	High	High	Low	Low	Single sided

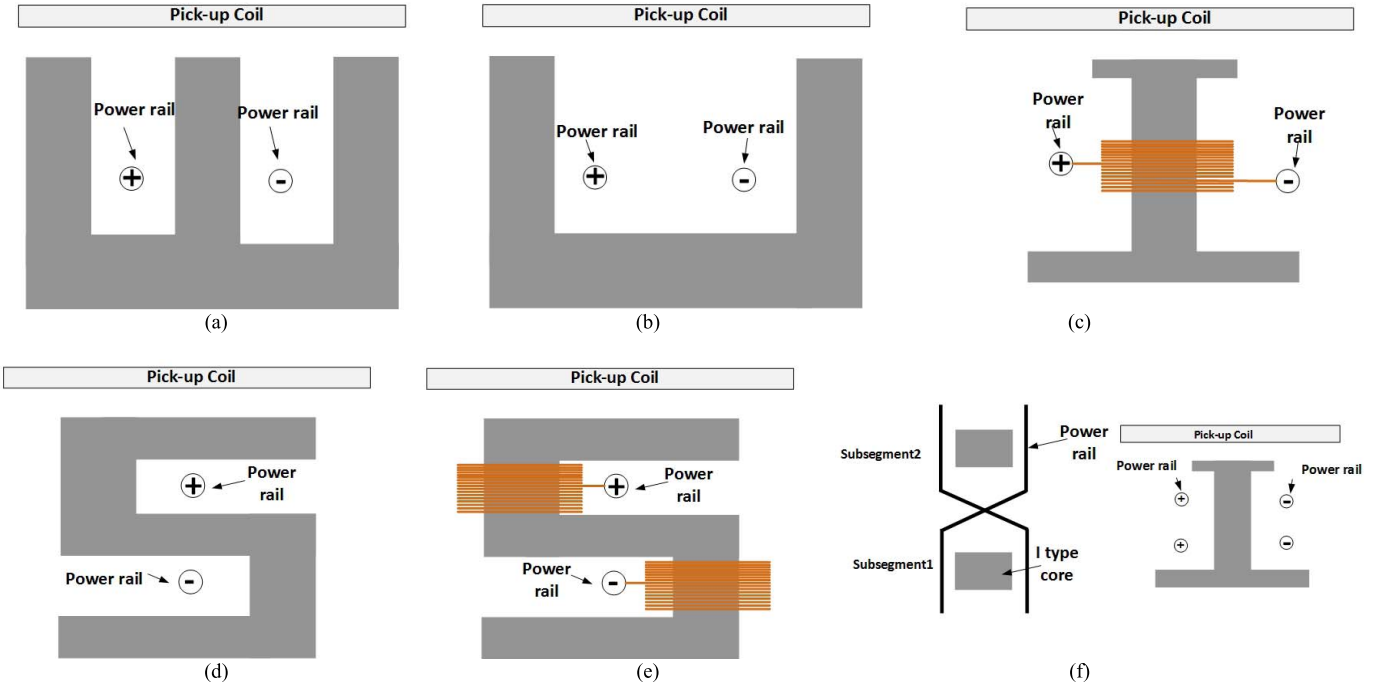


Fig. 17. Different types of power rail. (a) E-type. (b) U-type. (c) I-type. (d) S-type. (e) Ultraslim S-type. (f) Cross-segmented (X-rail) [34], [35], [82]–[84].

system is poor [34], [35]. The performance of the power rail is increased by adding magnetic material with different shapes, i.e., E-type, W-type, U-type, I-type, S-type, ultraslim S-type and cross-segment (X) type [34], [35]. In 2009, KAIST tested its first generation prototype of OLEV with E-shaped magnetic structure with the power rail for a golf cart application, as shown in Fig. 17(a) [35]. The first generation OLEV had mechanically controlled the pickup to align to power supply rail with an air gap of 1 cm. The second generation (2G) OLEV employed U-shaped power rail configuration, as shown in Fig. 17(b). The air gap of 2G OLEV was 17 cm with an efficiency of 72%. The advantages of U-shaped power rail are higher efficiency for larger air gap, lower EMF due to return path for power supply rail being close to the sending rail [34], [35], [83]. The third-generation (3G) OLEV adopted

W-type power rail, and I type pick-up coil. The W-type power supply rail had many W-shaped magnetic core structures arranged at particular intervals. W shape has an advantage compared to U-shape regarding reduced magnetic resistance by a factor of three compared to U-shaped [34], [35]. Therefore, the power output of a system for each pickup is improved from 6 to 15 kW. Other advantages include high coefficient of coupling, no aluminum shielding requirement, and reduced width of the power supply rail to 70 cm. The overall efficiency of the system is improved to 83% at 20-cm air gap. In order to reduce the cost and time of manufacturing for the power supply rail, modular I type magnetic core structure [Fig. 17(c)] for power supply rail is employed [34], [35]. The main advantage of I types structure is reduced the cost of the system by 20% as compared to W-type power rail.

TABLE IX

COMPARISON OF DIFFERENT POWER RAIL CONFIGURATIONS [34], [35], [82]–[84]

Parameters	E-type	U-type	W-type	I-Type	Ultra slim S-type
Rail width	20cm	140cm	80cm	10cm	4cm
Leakage EMF	10mG	51mG	50mG	15mG	<10mG
Air gap	1cm	17cm	20cm	20cm	20cm
Lateral misalignment	0.3cm	20cm	15cm	24cm	30cm
Efficiency	80%	72%	74%	80%	71%
Output power	3kW/pick up	5.2kW/pick up	15kW/pick up	25kW/pick up	22kW/pick up

TABLE X

SUMMARY OF POWER RAIL FOR DWPT [34], [35], [82]–[84]

Power rail	Features
E-type	<ul style="list-style-type: none"> Simple structure and lower manufacturing cost
U-type	<ul style="list-style-type: none"> higher efficiency for larger airgap Lower EMF due to return path near sending power rail
W-type	<ul style="list-style-type: none"> Reduced magnetics resistance by factor of three as compared to W-type Higher power output than W-type and U-type high coefficient of coupling, no aluminum shielding requirement and reduced width of the power supply rail
I-type	<ul style="list-style-type: none"> 20% cost reduction as compared to W-type reduced time of manufacturing lower leakage EMF
S-type	<ul style="list-style-type: none"> Reduction in cost as compared to I-type
Ultra slim S-type	<ul style="list-style-type: none"> reduced width smaller leakage EMF
Cross segment (X) type	<ul style="list-style-type: none"> High efficiency Lower leakage EMF Reduced cost of cable

Furthermore, power rail is arranged to alternate its positions to form alternate magnetic poles along the road to reduce the EMF. Also, the width of the power rail is reduced to 10 cm for an increase in power output per pickup to 25 kW. Further, to reduce the cost, ultra slim S type rail is proposed [34], [35]. The structure of S-type power rail is illustrated in Fig. 17(d). As compared to S-type, the width of the magnetic core is reduced from 10 to 4 cm, and the leakage EMF is also smaller due to reduced width [34], [35]. Ultraslim S-type has multiple turns wound to set the power level by changing a number of turns and current through coil [34], [35].

In an effort to reduce the waste of energy and leakage EMF, the segmented power rail is proposed [34], [35], [82]–[84]. It consists of many sub rails, which can be activated or deactivated through a switch box. However, several power cables are required from the centralized power supply to sub-rails. To reduce the cable harness, the distributed switching power supply rail was proposed [82]. It consists of multiple power supplies distributed along the line. With the distributed switching of the power rail the cable losses are reduced over the entire length. Even so, it requires a common power supply cable which increases the cost of construction. Cross-segmented power supply rail is proposed to eliminate the common power supply cable, as illustrated in Fig. 17(f). It consists of a centralized power supply feeding the segmented power rails, each being separated by a compensation switch box that controls the activation or bypass of each rail. Consequently, the cost of cable is reduced by half compared to a distributed power supply rail [82]. Detailed performance comparisons of different power supply rails are shown in Table IX. As a conclusion to this section, a summary of main characteristics of reviewed power rail is summarized in Table X. It is evident that cross-segmented (X) type power rail has high efficiency and smaller leakage EMF with reduced cost of cabling. Future research in this area is to reduce the cost and leakage EMF further without affecting efficiency.

Fig. 18 illustrates various pick-up systems reported in the literature. The most commonly reported pick-up systems are E- and U-types, which due to the readily available structure of magnetic core are relatively inexpensive to fabricate [85]–[87]. To improve the power density, an S-type pickup is proposed in [86] that the authors claim has two times higher power transfer capability as the U- or E-types for the same ferrite content [86]. Still, the S-type pickup is not yet widely employed due to its complicated magnetic structure and because it requires significant modification in the supporting infrastructure [82]. For the previously mentioned pick-up systems, lateral misalignment can lead to reduced or no power output leading Raabe *et al.* [87] to propose a quadrature pickup. In a quadrature pick-up system, a standard E-type pickup having an additional coil as shown in Fig. 18(e) and (f) is employed [87]. The additional coil is mounted in such a way to capture the flux during misalignment. The output of the additional coil is connected to the rectifier and wired-OR to the main output. The quadrature pickup is more effective for lateral misalignment, however, for longitudinal or for simultaneous lateral and longitudinal misalignment it is not as effective [87].

G. Shielding

The most significant problem in WPT is the leakage field and its adverse effect on the surrounding material and human exposure. The WPT system should be compliant with different electromagnetic interference (EMI) and EMC standards [51]. Also, time-varying magnetic field induces eddy currents in the metal object which is located on or in the vicinity of the transmitter coil, leading to additional losses and possible object heating [88]. Shielding measures that redirect or absorb the magnetic field incur losses and reduce the efficiency of the WPT system. A proven method is to add aluminum shielding to the backside of the ferrite and coil. Fig. 19 shows the circular coil with aluminum shielding (ferrite flux guides

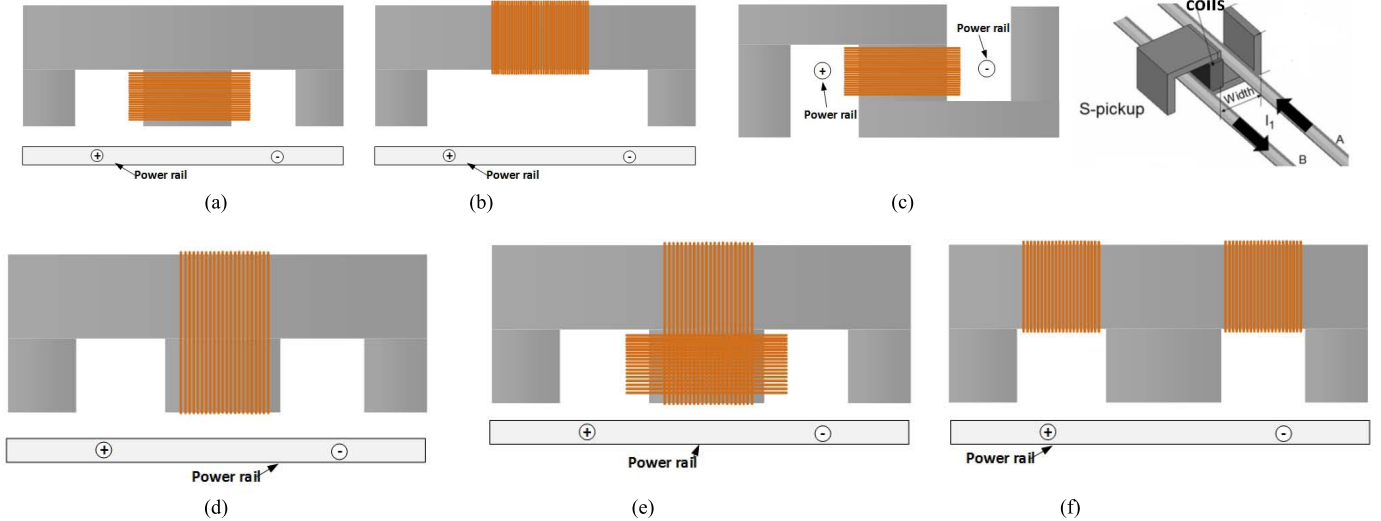


Fig. 18. (a) E-type pickup. (b) U-type pickup. (c) S-type pickup. (d) Flat pickup wound on flat E-core. (e) Quadrature pick-up design 1. (f) Quadrature pick-up design [63], [83], [85], [86].

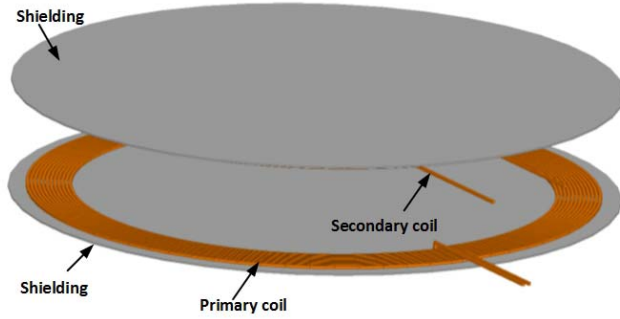


Fig. 19. Circular coil with shielding.

are not illustrated). The presence of shielding affects the performance of the system by reducing coil inductance and increasing losses which requires further capacitance compensation to achieve resonance condition [88]–[90]. Shielding can reduce the efficiency of a system by 1%–2% [88]. Typically, aluminum or copper is employed as a shielding material, as both of the material are highly conductive such that eddy currents induced in the material counteract the incident flux but also lead to losses in the shielding. To reduce losses in the shielding ferrite flux, guides with high permeability and high resistivity are used to divert the magnetic field into the coupling pad active zone, thereby minimizing flux entry into the shield [91], [92]. Passive shielding is necessary in all WPT charging systems including stationary, quasi-stationary, and dynamic WPT for EV charging to take advantage of simplicity, robustness and inexpensive implementation. Kim *et al.* [90] reported resonant reactive shielding method without consuming any additional power. It consists of an additional coil with LC resonant circuit connected to it, as shown in Fig. 20. The reactive shielding induces a canceling magnetic field that attenuates the leakage magnetic field by 64% compared to a conductive shield of the same size. Passive shielding can also be designed to reduce the leakage E -field in proximity to the vehicle undergoing charging [90].

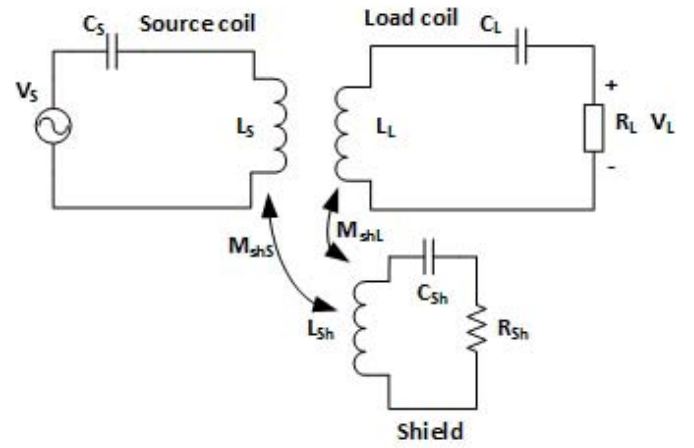


Fig. 20. Reactive power shielding as in [90].

In DWPT applications, the leakage field generated may be considerably higher than a comparable stationary charging system because the power rating will be higher by necessity and because of large k variation due to motion of receiver relative to transmitter coils [89]–[94]. Researchers from KAIST investigated a passive shielding method for DWPT [91]–[94]. KAIST team proposed a metal plate at the bottom of EV to protect the passenger from high EMF [91]. These researchers also included a vertical shielding plate on the side of the transmitting power lines to suppress lateral leakage fields. Furthermore, to decrease EMF, a number of the metallic brushes are mounted on EV in such a way that it makes soft contact with vertical metallic plates. With the increase in the metallic brush volume from 2 to 8, a reduction of 144–35-mG EMF level is achieved [93], [94]. However, passive shielding reduces the system efficiency, especially in DWPT application where the losses can be in kilowatt range. Also, other problems associated are mechanical losses, contact potential, and high initial cost [93], [94].

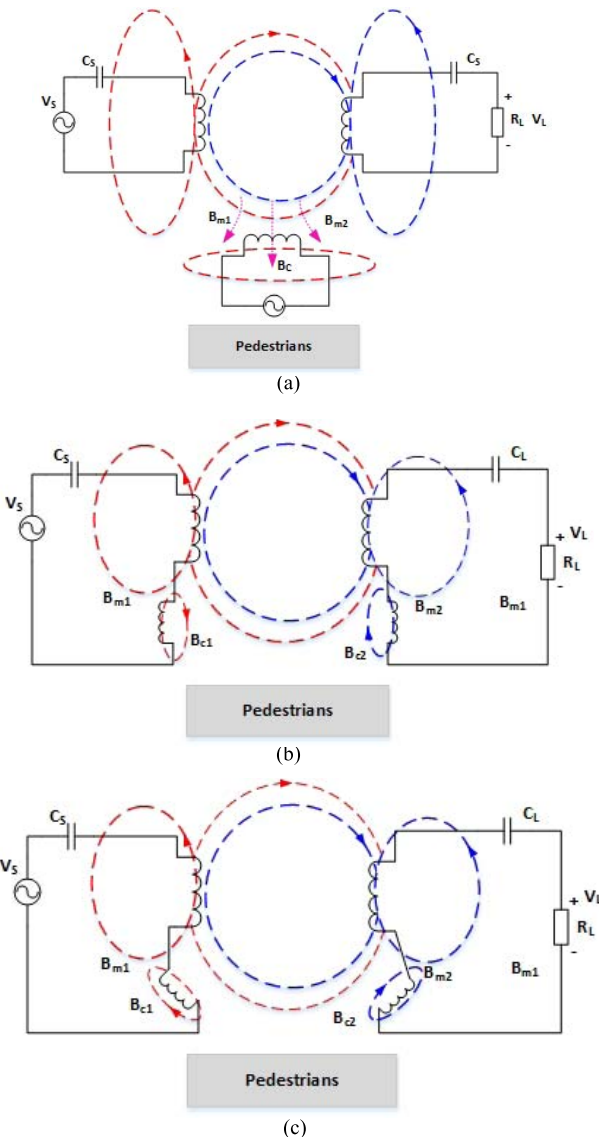


Fig. 21. (a) Principle of active EMF cancellation. (b) ISEC method for EMF cancellation. (c) LFEC method for EMF cancellation [90].

Fig. 21(a) shows the general principle of active shielding. It consists of compensated primary, compensated secondary coil, and EMF cancel coil. Either one or two canceling coils are employed. To cancel leakage EMF, current through the canceling coil should be antiphase with main coil current. Choi *et al.* [34], [94] and Park *et al.* [93] demonstrated the implementation of active shielding for DWPT. Three general design methods and implementation issues for U-type, W-type, and I-type are discussed. Furthermore, Park *et al.* [93] proposed three active EMF cancellation methods: independent self EMF cancel (ISEC) method, 3-dB dominant EMF cancel (3-DEC) method, and Linkage-free EMF cancel (LFEC) method.

In ISEC method, the EMF is reduced by providing the counter magnetic field B_{C1} for primary coil due to canceling coil 1 and B_{C2} for secondary coil from canceling coil 2, as illustrated in Fig. 21(b) [93]. The current for each canceling coil is fed from primary coil and secondary coil. This method

TABLE XI
COMPARISON OF VARIOUS SHIELDING METHODS [34], [35], [88]–[94]

Shielding methods	Metallic material shielding	Magnetic material shielding	Resonant reactive shielding	Active shielding
Shielding effectiveness	Excellent shielding effect scale to power level	Limited shielding effect scalable to power level	High shielding effect suitable for low to medium power	High shielding effect suitable for high power
Eddy current loss	High losses in surrounding metallic material	Low	Low	Low
Active source required	No	No	No	Yes
Effect on Efficiency	1-3% overall reduction	Little effect	Low	High

is simple and effective and can be applied to multiple primary and secondary coils. ISEC method cannot cancel EMF for a wide operation that total magnetic flux, B_t is less than primary magnetic plus cancellation field flux $B_{m1} + B_{C1}$ in 3-DEC method [93].

Fig. 21(c) shows the LFEC method for EMF cancellation. In this method, primary and secondary coils are combined with their canceling coil, respectively. However, the coupling between primary and secondary coil is reduced. Therefore, this method should be avoided [93].

Ahn *et al.* [92] reported active shielding method for DWPT application without affecting the efficiency. In active shielding, a wire is laid in parallel with power rail. The active shield wire carries a current with the same frequency as the primary coil current but out of phase. KAIST team reported 62.5-mG EMF level for 60 kW with 80% efficiency [93]. As a conclusion to this section Table XI compares various shielding methods reported in the literature. For stationary WPT, passive shielding is a most common method to reduce the leakage EMF due to simple, robust and inexpensive implementation [88], [89]. Active shielding method is a most promising method to reduce the leakage EMF for DWPT, as it can actively cancel the leakage EMF and is suitable for high-power applications [90], [94].

IV. COMPENSATION NETWORK FOR WIRELESS POWER TRANSFER

The high leakage inductance and magnetizing inductance of the primary and secondary coils requires a high VA rating of the input source to transfer active power to the load. Also, system losses increase due to high reactive current. To avoid this circulation of high reactive current compensation capacitors are connected either in parallel or series to cancel the leakage inductance [95], [96]. Requirements for compensation network are as follows [95]:

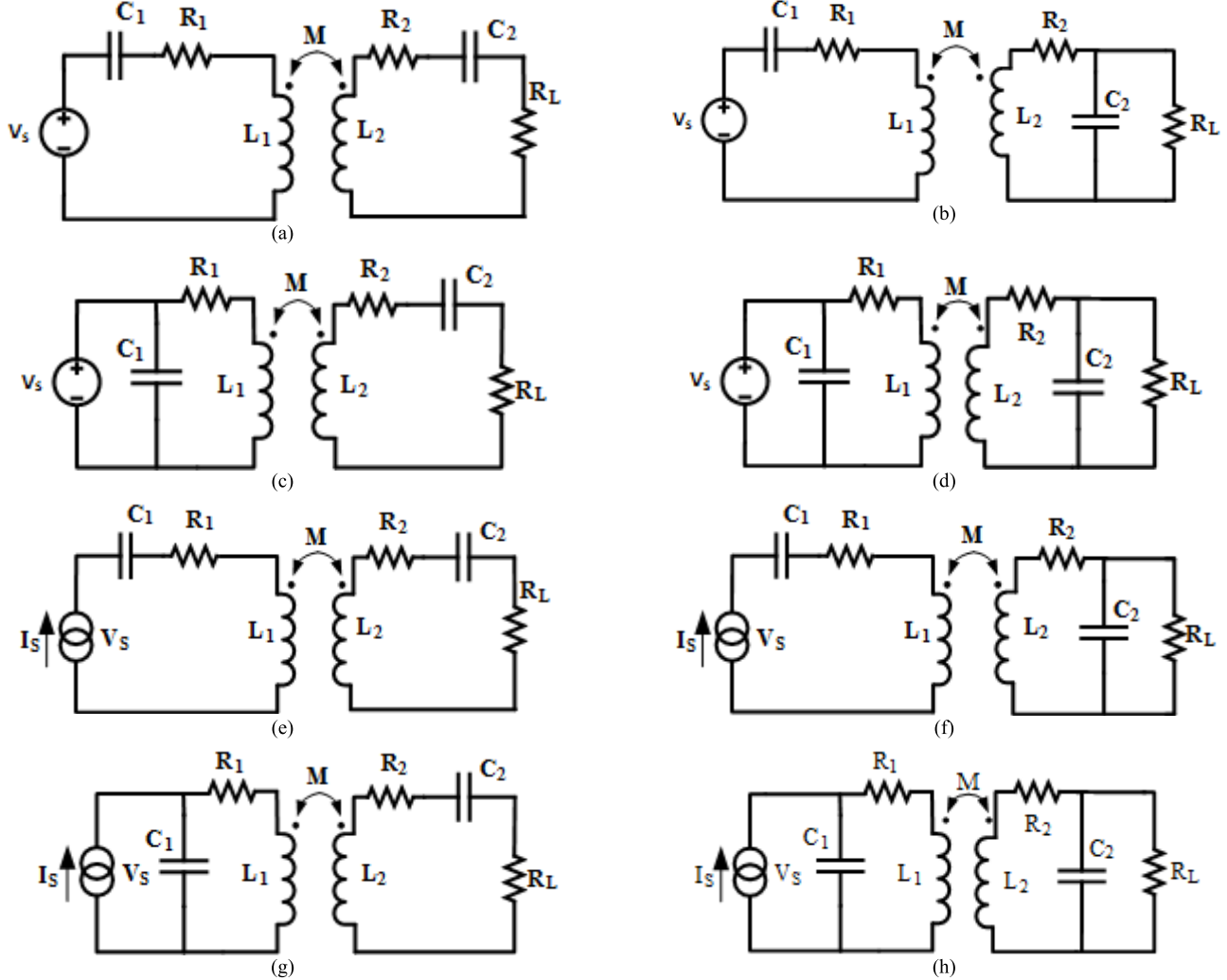


Fig. 22. Basic compensation network. (a) Current source S-S compensation. (b) Current source S-P compensation. (c) Current source P-S compensation. (d) Current source P-P compensation. (e) Voltage source S-S compensation. (f) Voltage source S-P compensation. (g) Voltage source P-S compensation. (h) Voltage source P-P compensation [55], [101].

- 1) maximize the power transfer;
- 2) minimize VA rating of power supply;
- 3) minimize VA rating of power supply;
- 4) constant voltage (CV) or constant current (CC) output, depending on the application;
- 5) high efficiency;
- 6) bifurcation tolerant;
- 7) high misalignment tolerant.

The basic requirement of a compensation network is to minimize the (VA rating of the power supply by providing the reactive power required to establish and sustain the magnetic field [95], [97]. To maximize the power received on the secondary side, leakage inductance is canceled on both primary and secondary sides to attain maximum power transfer [97]–[104]. Typically, compensation components such as metalized film capacitors have very low dissipation and introduce minimal impact on the efficiency of the system. However, inadequate or mistuned compensation results in a higher reactive current that leads to increased VA rating of the power supply [97]–[104]. The flow of reactive current results

in increased semiconductor losses and conduction losses, especially in the inverter diodes. Generally, the primary resonance cancels the primary leakage inductance, thereby increasing PF to near unity, with the secondary coil also operated at or near the same resonant frequency [104].

Wireless charging in EVs is subject to various parameter changes such as those caused by air gap variation, misalignment, and load resistance [55]. To maximize power transfer, different compensation networks are selected to match voltage or current source of the primary to voltage or current source of the secondary loading according to the type of output filter. It is also intended to keep the output voltage constant or output current constant to satisfy battery charging needs [95], [98]. In most cases, the end load for WPT is a battery, which requires charging current to be constant at low states of charge (SOCs) until SOC reaches approximately 85% and then switches to constant voltage charging [99], [102], [103]. Other consideration for choosing compensation network is that it should be bifurcation tolerant. Bifurcation depends on load quality factor,

TABLE XII
DIFFERENT MATHEMATICAL EQUATIONS FOR BASIC COMPENSATION [95], [99], [104]

Compensation topology	Primary capacitance	Theoretical efficiency	Transferred impedance
Series-Series	$\frac{C_2 L_2}{L_1}$	$\frac{\omega^2 M^2 R_L}{((R_2 + R_L)^2) R_1 + (\omega^2 M^2)(R_2 + R_L)}$	$(R_1 + j(\omega L_1 - \frac{1}{\omega C_1})) + \frac{\omega^2 M^2}{R_2 + R_L + j(L_2 \omega - \frac{1}{C_2 \omega})}$
Series-Parallel	$\frac{C_2 L_2^2}{L_1 L_2 - M^2}$	$\frac{\omega^2 L^2 R_L}{R_L \omega^2 + R_2 \omega^2 L_2^2 + R_2 R_L^2 + \frac{R_1 R_2^2 L^2}{M^2} + \frac{R_1 L_2^4 \omega^2}{M^2}}$	$(R_1 + j(\omega L_1 - \frac{1}{\omega C_1})) + \frac{\omega^2 M^2}{R_2 + \frac{R_L}{1 + jR_L C_2 \omega} + jL_2 \omega}$
Parallel-Series	$\frac{C_2 L_2}{\frac{M^4}{L_1 C_2 L_2 R_L} + L_1}$	$\frac{\omega^2 M_{12}^2 R_L}{((R_2 + R_L)^2) R_1 + (\omega^2 M_{12}^2)(R_2 + R_L)}$	$\frac{1}{R_1 + jL_1 \omega + \frac{\omega^2 M^2}{(R_2 + R_L + j(L_2 \omega - \frac{1}{C_2 \omega}))} + jC_1 \omega}$
Parallel-Parallel	$\frac{(L_1 L_2 - M^2) C_2 L_2^2}{\frac{M^4 C_2 R_L}{L_2} + (L_1 L_2 - M^2)^2}$	$\frac{\omega^2 L^2 R_L}{R_L \omega^2 + R_2 \omega^2 L_2^2 + R_2 R_L^2 + \frac{R_1 R_2^2 L^2}{M^2} + \frac{R_1 L_2^4 \omega^2}{M^2}}$	$\frac{1}{R_1 + jL_1 \omega + \frac{1}{\omega^2 M^2 (1 + jR_L C_2 \omega)} + jC_1 \omega}$

compensation network, and the compensation capacitor. Therefore, the compensation network must be designed for single zero phase angle, and ensure system stability for variable frequency control under different loading conditions [95], [96].

Various compensation networks are reported in [95]–[105]. Fig. 22 illustrates that primary series compensation is necessary for voltage source while parallel compensation of primary is required for current source drive. Section IV-A discusses four basic compensation networks.

A. Series-Series (S-S)

Fig. 22 shows the series-series (S-S) compensation network. The main advantage of the S-S configuration is that the value of primary capacitance does not depend on the variation of coupling coefficient [99], [103]. This property of series compensation is especially useful in segmented DWPT applications, where the coupling coefficient varies with movement of the EV. The major drawback occurs at light load condition, and when the receiver is not present and the equivalent impedance seen is zero at the primary resonance frequency with only the parasitic impedance of the capacitor and inductor limiting the current [101], [103], [104]. Therefore, the voltage transferred to the secondary is very high. This makes the terminal voltage across the load very high, leading to an unsafe condition. The desired requirements for a compensation network are high efficiency and high PF. These two variables are of particular importance to study because of the fact that they can potentially fluctuate with the coupling coefficient and load variation [95]. The PF for a compensation network is defined as the ratio of active power to apparent power supplied by a voltage source. The PF is unity (at resonance frequency) for S-S compensation, as shown in Fig. 23(b). The efficiency of S-S is high, even for a low coupling coefficient, as shown in Fig. 23(a).

B. Series-Parallel (S-P)

From the transferred impedance (Table XII), it can be concluded that regardless of the load, there will be some impedance transferred to the primary. If the receiver or load is not present, the primary side will still have a short circuit

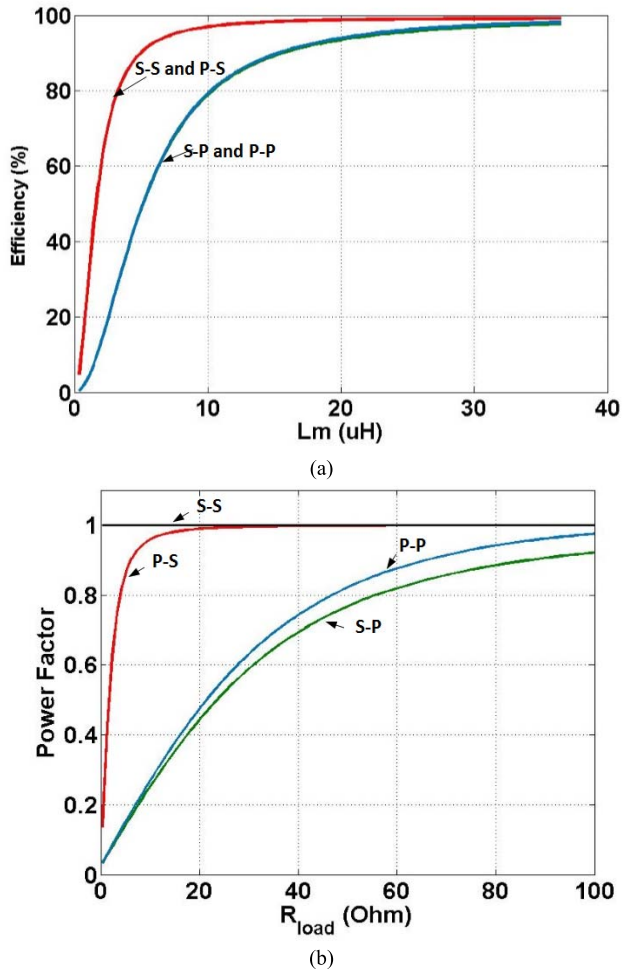


Fig. 23. (a) Effect of misalignment on efficiency. (b) Effect of load resistance on PF.

at the resonance frequency [99], [103]. Therefore, a current limiting control must still be performed on the primary side. In addition, the transferred impedance to the primary is proportional to the square of the mutual inductance. Therefore, with variation in mutual inductance, the PF of the converter and the dynamics of the system will change. This makes

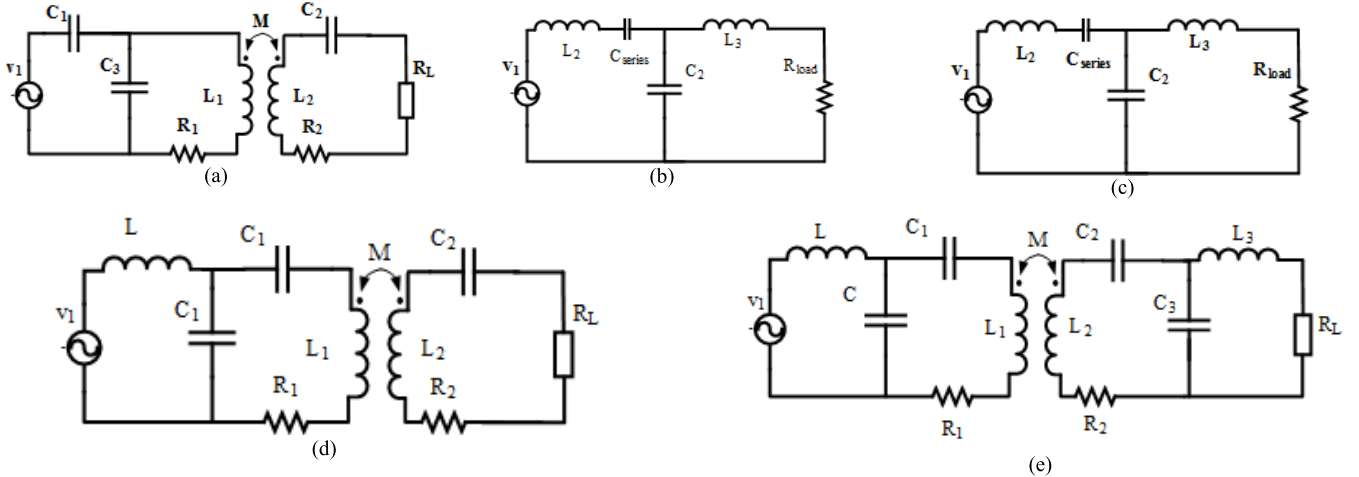


Fig. 24. (a) Series-parallel-series compensation. (b) LCL with partial series compensation. (c) LCL compensation. (d) LCC-series compensation. (e) LCC-LCC compensation [74], [107], [108].

TABLE XIII

COMPARISON OF BASIC COMPENSATION NETWORK FOR 200-kW SYSTEM [97], [103]

Parameters	S-S	S-P	P-S	P-P
Primary turns	6	7	1	1
Secondary turns	4	1	6	1
Primary current(A)	370	370	2412	2400
Secondary current(A)	400	1467	400	2220
Primary inductance (μH)	109	145.5	3	2.99
Copper mass(Kg)	34.6	36.2	45	43
Capacitor loss(W)	2622.7	2758.6	2434.4	2385.2
Primary quality factor	8.5	11	6.1	6.7
Secondary quality factor	4.6	3.6	5.95	5.5
Primary winding section(mm^2)	94	94	600	620
Secondary winding section(mm^2)	100	350	110	575

power transfer DWPT more challenging [99]. For higher load, the efficiency and PF get better as illustrated in Fig. 24(b). In addition, with an increase in the mutual inductance, the efficiency of the system increases as illustrated in Fig. 24(a). From primary capacitance equation (Table XII), it is evident that the value of capacitance changes with mutual inductance, and therefore, the resonant frequency also changes.

C. Parallel-Series (P-S)

The transferred impedance in P-S and S-S configuration is the same [99]. The main advantages are high efficiency and high PF at relatively low mutual inductance and a relatively large range of variation of load and mutual inductance [90], [94], [99]. The PF in P-S is not at unity under low mutual inductance as it appears in Fig. 23(b). One major drawback is it requires current source input to avoid any instantaneous change in voltage [99]. To solve this problem, an inductor is added to create LCL resonant tank. This configuration is called the P-S compensating technique and is the focus of some researchers [99].

D. Parallel-Parallel (P-P)

In a P-P compensation, the transferred impedance to the primary side is the same as in S-P compensation.

TABLE XIV

COMPARISON OF FOUR BASIC COMPENSATION NETWORKS [106]

	Series-Series	Series-Parallel	Parallel-Series	Parallel-Parallel
Dependence on R_L and k	Primary and secondary compensation capacitor are independent of load and coupling factor	Secondary compensation capacitor is dependent on load and coupling factor	Primary compensation capacitor is dependent on load and coupling factor	Primary and secondary compensation capacitor are dependent of load and coupling factor
Inverter device voltage rating	Lower dc link voltage is required (higher than S-P)	Lower dc link voltage	Higher voltage is needed as compared to S-S and S-P	Higher voltage is needed as compared to S-S and S-P
Inverter device current rating	Primary coil current	Primary coil current	Active component of the primary coil current	Active component of the primary coil current

This configuration suffers from the low PF, a high load voltage of the parallel secondary and large current source requirements of the parallel primary [95], [104]. This configuration is not widely studied because of these disadvantages [103], [104].

Sallan *et al.* [97] reported a detailed optimal sizing of 200-kW IPT for different compensation networks. Table XIII summarizes the performance comparison for basic compensation networks. S-S compensation requires the least amount of copper among all [103]. This is a direct saving in cost for the system. S-S and S-P compensations are suitable for high power from an economic point of view. P-S or P-P compensations are typically used for high-power current source driven cables that run over a long distance [105]. Table XIII summarize the comparisons of basic compensation network.

TABLE XV
COMPARISON OF EIGHT BASIC COMPENSATION SCHEMES IN TERMS OF FIVE CRITERIA [55]

Criteria	I-SS		I-SP		I-PS		I-PP	
Maximum efficiency condition	$\frac{\omega_2}{\sqrt{1-1/(2(Q_2//Q_L)^2)}} \sim \omega_2 (*)$		$\frac{\omega_2\sqrt{1+1/(Q_2Q_L)}}{\sqrt{1+k^2Q_1/Q_2}} \sim \omega_2 (**)$		$\frac{\omega_2}{\sqrt{1-1/(2(Q_2//Q_L)^2)}} \sim \omega_2 (*)$		$\frac{\omega_2\sqrt{1+1/(Q_2Q_L)}}{\sqrt{1+k^2Q_1/Q_2}} \sim \omega_2 (**)$	
Maximum load power condition	$\frac{\omega_2}{\sqrt{1-1/2Q_L^2}} \sim \omega_2$		$\sim \omega_2$		$\frac{\omega_1}{\sqrt{1+k^4Q_L^2}} \sim \omega_2$		$\frac{\omega_3}{\sqrt{1+k^4Q_L^2/(1-k^2)^2}} \sim \omega_2$	
Load independent output condition	ω_{VL}	ω_{IL}	ω_{VL}	ω_{IL}	ω_{VL}	ω_{IL}	ω_{VL}	ω_{IL}
	ω_2	Not exist	Not exist	ω_2	ω_5	ω_1	ω_3	ω_5
Coupling coefficient independent condition	Yes		Yes		Yes		No	
Zero coupling allowance	Allowed		Allowed		Not Allowed		Not allowed	

Criteria	V-SS		V-SP		V-PS		V-PP	
Maximum efficiency condition	$\frac{\omega_2}{\sqrt{1-1/(2(Q_2//Q_L)^2)}} \sim \omega_2 (*)$		$\frac{\omega_2\sqrt{1+1/(Q_2Q_L)}}{\sqrt{1+k^2Q_1/Q_2}} \sim \omega_2 (**)$		$\frac{\omega_2}{\sqrt{1-1/(2(Q_2//Q_L)^2)}} \sim \omega_2 (*)$		$\frac{\omega_2\sqrt{1+1/(Q_2Q_L)}}{\sqrt{1+k^2Q_1/Q_2}} \sim \omega_2 (**)$	
Maximum load power condition	$\omega_1 = \omega_2$		$\omega_3 = \omega_2$		ω_4		$\omega_4\sqrt{1 - (1 - k^2)/(2Q_L^2)} \sim \omega_4 (***)$	
Load independent output condition	ω_{VL}	ω_{IL}	ω_{VL}	ω_{IL}	ω_{VL}	ω_{IL}	ω_{VL}	ω_{IL}
	ω_5	ω_1	ω_3	ω_5	ω_4	Not exist	Not exist	ω_4
Coupling coefficient independent condition	Yes		No		No		No	
Zero coupling allowance	Not Allowed		Allowed		Allowed		allowed	

* $1 \ll Q_2$ and $1 \ll Q_L$ ** $1 \ll Q_1$, $1 \ll Q_L$, and $k \ll 1$ *** $1 \ll Q_L$

E. Discussion

In [55], four basic compensations are compared with a constant voltage source and constant current source input for different criteria, as reported in Table XIV. The maximum efficiency condition for all eight compensation is achieved at secondary resonant frequency (ω_2) regardless of the quality factor of the coil [55]. Sohn *et al.* [55] calculated optimum angular frequency to achieve the maximum load power transfer. In case of current source input the angular frequency for maximum efficiency condition is same as maximum load power condition. However, with constant voltage input the maximum efficiency occurs at secondary resonance frequency whereas maximum power condition occurs at different angular frequencies [55]. The angular frequency at which maximum efficiency occurs for series compensation is completely independent of equation in Table XV, whereas for parallel compensation, the maximum efficiency depends on the coupling coefficient. From the comparison in Table XV, it can be concluded that I-SS, I-PS, V-SS, and V-PS are independent of the coupling coefficient [55]. The other criteria are effect

of zero or weak coupling coefficient on the voltage and current stress. The absence of the magnetic coupling happens when there is a misalignment or secondary coil. In this case, the compensation network should guarantee safe operation of WPT system. To allow zero or weak coupling condition, the input impedance of the system should be infinite for current source input and zero for voltage source input [55]. Sohn *et al.* [55] calculated input impedance for I-SS and V-SS to conclude I-SS allows $k = 0$ condition, whereas V-SS does not allow.

F. Additional Compensation Network

1) Series–Parallel Combination: For implementation purposes, series compensation requires higher voltage and current than parallel compensation [107]. Therefore, the S–P combination is required to obtain the required capacitance in order to achieve the desired voltage and current ratings. IPT system requires perfect alignment of coils to transfer power with high efficiency. To tackle the issue of misalignment, a combination of series–parallel–series topology is proposed, as shown in Fig. 24(a) [107]. The benefit of this compensation

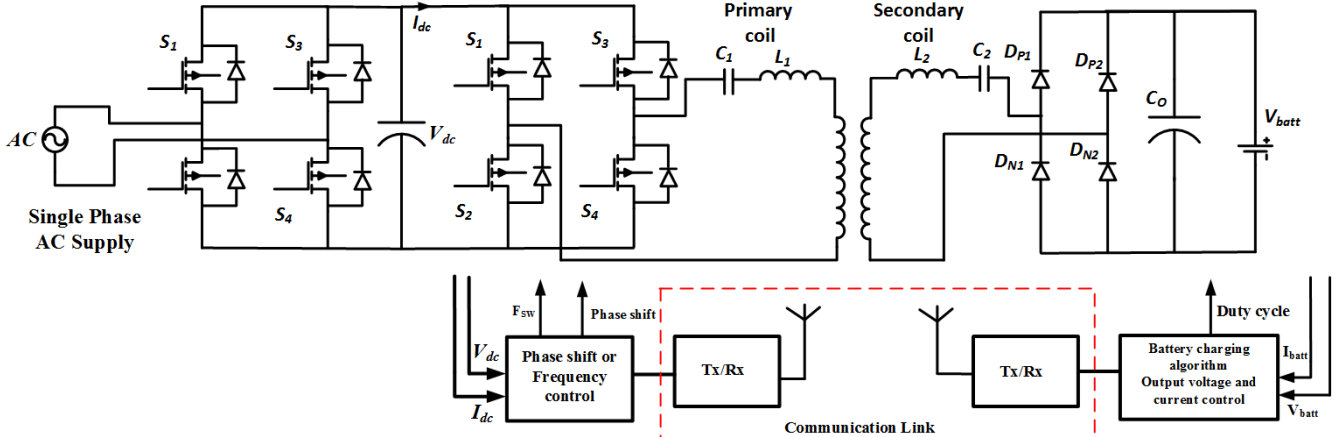


Fig. 25. Power electronics for a WPT system.

scheme is that output power can be maintained constant for high misalignment.

2) *LCL Compensation*: An LCL compensation network with an additional inductor and capacitor is illustrated in Fig. 24(b). This configuration is formed by the addition of inductor to parallel resonance network [102]. This configuration has a current source input, which can be easily controlled by a full-bridge converter for variations in the coupling coefficient and load conditions [102]. Also, the VA rating is reduced. The secondary side of LCL compensation can be either a parallel compensation or series compensation. Parallel compensation is widely used due to its robustness to load variation [74], [108]. The drawback of the parallel tuned system is in the transferred impedance on the primary side which consists of both real and imaginary parts of the load. Due to this, there is some additional current flowthrough primary without contributing to real part of the load. Also, a large dc inductor is required to ensure continuous conduction through the rectifier. This increases the cost and loss in the system [109]. Series-tuned pickup requires large bridge rectifier capacitor to ensure continuous conduction and the pick-up voltage increases to a high value at large power levels [109].

The configuration in Fig. 24(c) is the LCL resonant network, which overcomes the problems associated with S-P compensation [108]. The advantages are lower losses in the rectifier, pickup winding; efficiency of the system is high as compared to parallel pickup. Further, to compensate the nonlinear effect of the rectifier, a series capacitor is added which ensures soft switching of the rectifier diodes.

3) *LCC Compensation*: LCL compensation requires two identical inductors. Therefore, the size of the inductor is large; in order to reduce the size and cost of the system, LCC compensation networks are reported in [74], [108], and [109]. Moreover, by tuning LCC compensation, zero current switching (ZCS) can be achieved. Also, LCC pickup can compensate the reactive power at the secondary side to form a unity PF pickup. Other advantages are: independence of the coupling coefficient and load conditions, with ensured zero voltage switching (ZVS) for MOSFETs [74], [109].

In the literature, double-sided LCC compensation is most popular as it can reduce the current stress in the inverter; it has high misalignment tolerance and load independence characteristics [74], [109].

V. POWER ELECTRONICS FOR WPT

Power electronics plays a critical role in the wireless charging systems for EVs. Performance of the power converter is crucial for maximizing the system efficiency. Fig. 25 illustrates various power electronic stages for a wireless charging of an EV. A typical WPT system includes a front-end ac–dc converter to correct the PF at the utility connection of the system in order to meet low THD as specified by the IEEE-1547, the IEC1000-3-2, and the U.S. National Electric Code 625 and 626 [110], [111]. The second stage is a full-bridge inverter to convert a constant dc voltage into high-frequency bipolar voltage pulses with adjustable duty cycle to the compensation circuit. The secondary side consists of a compensating network and rectifier to convert high-frequency ac voltage into dc voltage. Different compensation networks can be used, depending on the application, to keep either output current or output voltage constant. After rectification an optional dc–dc converter may be employed for additional voltage regulation. The primary function is to charge the battery under CV or CC control and as noted earlier, while the secondary function is to match the load impedance with source impedance for optimum power transfer [114], [115]. The full bridge inverter may be voltage-fed or current-fed depending on the application and the input source. Some researchers are working on current-fed converter for WPT application [116]–[119]. A typical current-fed converter for WPT application is shown in Fig. 26. A parallel resonance is employed for a transmitter with the advantage of lower circulating current from the power electronics circuit, as parallel capacitor forms a low impedance path for the circulating current. However, the voltage stress on the switches increases with power [116]–[119]. The WPT architecture cited in [116] is a current-fed design. A CCL transmitter and LC receiver are employed for compensation. In general, current-fed inverters have advantages such as lower current stress, short circuit protection, and higher reliability [120]. However, a large dc

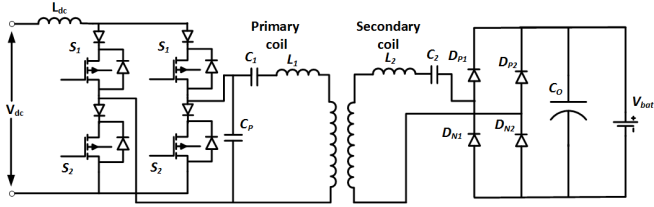


Fig. 26. Current-fed converter as in [116].

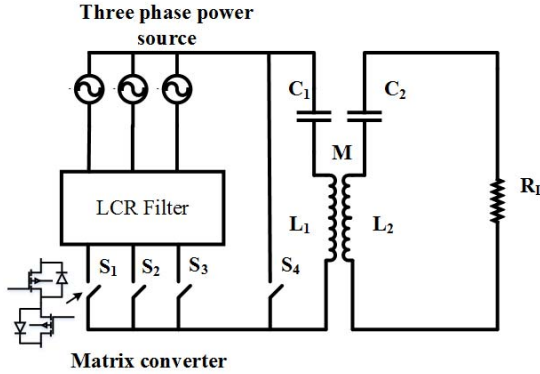


Fig. 27. Matrix converter WPT system [121].

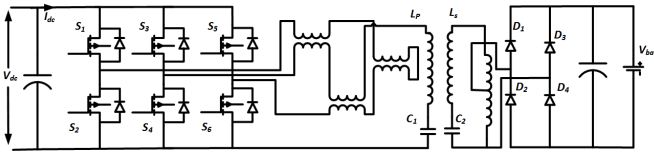


Fig. 28. Multiphase wireless converter [123].

inductor is required, which increases the size and cost of the system. Depending on the power flow direction the charger can be categorized as unidirectional or bidirectional [116], [120].

A. Unidirectional Inductive Charger

The unidirectional charger transfers the power from Grid to Vehicle (G2V). In the literature, different configurations are reported for the unidirectional converter, with basic H-bridge being most common. The matrix converter is reported in the literature to reduce the number of conversion stages without the need for a dc link [121], [122]. Fig. 27 shows a low power matrix converter developed for WPT system [121] that has advantages of a reduced number of semiconductor devices for the facile conversion of direct current to the high-frequency current supplied to the transmitter coil. The system efficiency is high. However, the power rating of the system is low due to high stress across the power semiconductor devices. Therefore, it may not be the best option for high power applications. A multiphase inverter for interfacing the utility to transmitter coil is reported in [123] and [124] to increase the power rating. Fig. 28 illustrates such a three-phase wireless EV battery charger for high-power applications [123], [124]. The charger has three phases wherein each phase is connected to two interphase transformers to share the current between

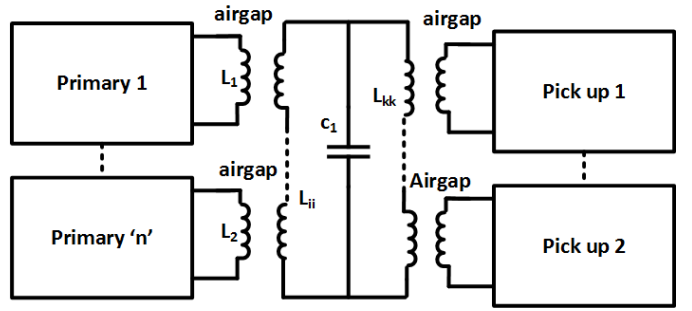


Fig. 29. Modular WPT [125].

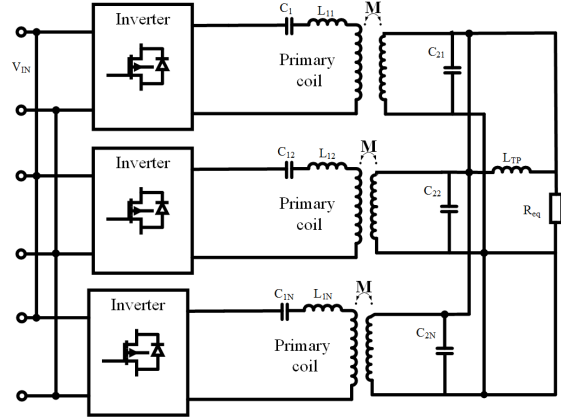


Fig. 30. Parallel LCL-T topology for high-power IPT system as in [129].

parallel inverter legs. The coupling coils on both transmitter and receiver are connected via an S-S compensation. Although the converter can be employed for high power application the need for additional components adds to its cost. A modular high-power IPT system is shown in Fig. 29 [125] that integrates multiple low-power IPT systems, to increase power level [126]. Multiple primary and secondary coils are connected in series with an LCL resonant circuit. Some researchers paralleled various low power modules to increase power, as shown in Fig. 30 [129] in order to realize advantages of low cost, minimization of uneven power-sharing due to components tolerance, and fault-tolerant operation with increased reliability of the system. Multilevel converters can be utilized to increase the power capacity of wireless charging systems. They allow the use of lower rating devices and are suitable for WPT2 and WPT3 levels [41], [121], [124], [126], [128]. The cascaded multilevel converter in Fig. 31 is adopted to increase power capacity in WPT [129]. The phase shift pulsewidth modulation method is employed to control output power and to eliminate selected harmonics. While the cascaded converters are suitable for high power applications, they require multiple power supplies to increase voltage levels resulting in a reduction of efficiency and an increase in the number of switching devices, which increases the cost [129].

B. Bidirectional Inductive Charger (V2G)

A typical bidirectional inductive charger has two stages: the front-end bidirectional ac–dc converter and the bidirectional

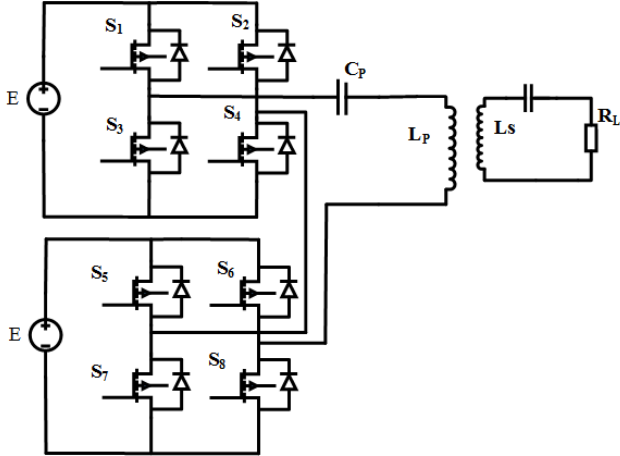


Fig. 31. Cascaded multilevel inverter as in [130].

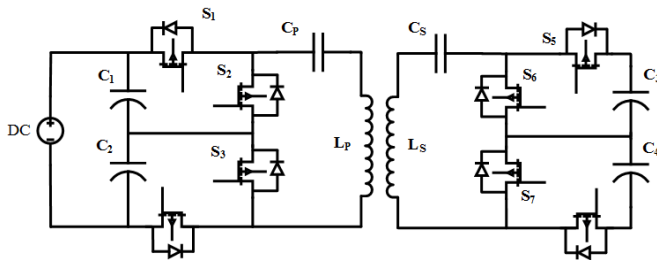


Fig. 32. Bidirectional IPT presented in [131].

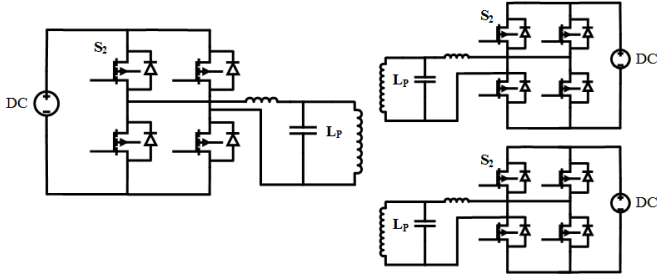


Fig. 33. Multilevel bidirectional IPT as in [132].

dc–dc converter. The ac–dc converter corrects the PF in the G2V case and supplies power to grid in the context of vehicle-to-grid (V2G) dynamic energy resource (DER). Optionally, there is a bidirectional dc–dc converter to regulate the battery current and to minimize over depletion of the battery when used as DER. The architecture is shown in Fig. 32 is a bidirectional WPT system with many EVs connected to a single primary coil [131]. However, the power level of the system is limited due to the full-bridge converter and complicated control as a number of pick-up coil increases. A bidirectional multilevel converter for WPT is presented in Fig. 33 [132] consisting of a multilevel converter at both transmitter and receiver ends that is suitable for high-voltage and high-power application. Furthermore, high efficiency is claimed with optimized phase shift control with the caveat that unbalanced voltage across input capacitor and output capacitor can lead to uneven stress distribution across the

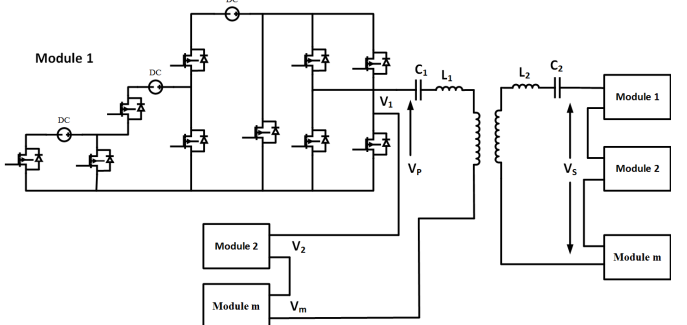


Fig. 34. Bidirectional cascaded modular converter [133].

power switches. Another cascaded multilevel converter suitable for high-power IPT system is shown in Fig. 34 [133]. The output of the converter comprised multiple voltage levels generated by the isolated power supply. Advantages of this system include high-power scalability, lower switching losses, and simple control. The downside of the system is that it requires multiple isolated dc voltage sources and the switch count is high. Table XVI summarizes the advantages and disadvantages of the unidirectional and bidirectional converters for WPT system. Conventional H-bridge inverters are suitable for stationary charging with lower power application for both unidirectional and bidirectional power flow as it has features such as less count of power devices, high system efficiency and simple control [49], [50]. For high power application multilevel converters are more suitable as they reduce the device stress, and a modular structure can be implemented [130].

C. Power Supply Architecture for Dynamic Wireless Charging

DWC or in-motion WPT refers to the ability to charge an electric vehicle while it is moving. DWC enables reduction of battery size, and hence, lowers cost, and increases the overall range of EVs [34], [35]. One challenge of DWC is the short interacting time of an in-motion receiver coil with a sequence of roadway transmitter coils that leads to a need for high-power rating electronics and high misalignment tolerance to facilitate high system efficiency. DWC can be implemented in either of two distinct methods: the first uses a single long track transmitter cable and second a track consisting of multiple, small segmented coils [14], [34]. An implementation challenge of coil segmentation is selecting the proper pitch for the coils, that is, the ratio of coil length to segment span [134]. In general, DWC consists of a large power rating supply with compensation circuit to supply power to a long cable (100s of meters) or segmented track of fractional meter length coils. EV with chassis mounted pickup coil is employed to capture the high-frequency ac signal from the primary coils [134]. The received signal after rectification is smooth dc voltage for the long cable but pulsating dc for a segmented track. In either approach the rectified dc voltage is fed to a dc–dc converter, which controls the charging requirement of the batteries. In a long track system, a single power source drives the complete track while maintaining a constant current, as shown in Fig. 35 [34], [135], [136]. The segmented DWC consists of multiple

TABLE XVI
UNIDIRECTIONAL AND BIDIRECTIONAL WPT SYSTEM AND ITS MAIN FEATURES [102], [116]–[138]

Power flow direction	Converter	Advantages	Disadvantages
Unidirectional converter (G2V)	Matrix converter	<ul style="list-style-type: none"> Reduced number of stages Higher system efficiency 	<ul style="list-style-type: none"> Lower power application
	Multiphase inverter	<ul style="list-style-type: none"> High power application 	<ul style="list-style-type: none"> Higher cost due to additional components
	Modular high power IPT system	<ul style="list-style-type: none"> Modular structure to increase power level Lower switch stress 	<ul style="list-style-type: none"> Multiple primary and secondary coils
	Cascaded Multilevel converter	<ul style="list-style-type: none"> High power application Phase shift modulation to eliminate selected harmonics 	<ul style="list-style-type: none"> Multiple power supply required Increase in power electronics devices
	Parallel LCT IPT system	<ul style="list-style-type: none"> Modular structure High power application Fault tolerant operation 	<ul style="list-style-type: none"> Multiple primary and secondary coils
Bidirectional converter(V2G)	Multilevel bidirectional IPT	<ul style="list-style-type: none"> High power and high voltage application High efficiency with phase shift control 	<ul style="list-style-type: none"> Unbalanced switch voltage stress and capacitor voltage stress
	Multi-port bidirectional IPT	<ul style="list-style-type: none"> Bidirectional power capability Multiport configuration to interface multiple EV 	<ul style="list-style-type: none"> Limited power handling capacity Complicated control due to multiple pick up
	Bidirectional cascaded modular converter	<ul style="list-style-type: none"> High power scalability Lower switching losses Simple control 	<ul style="list-style-type: none"> Multiple isolated dc voltage required Higher switch count

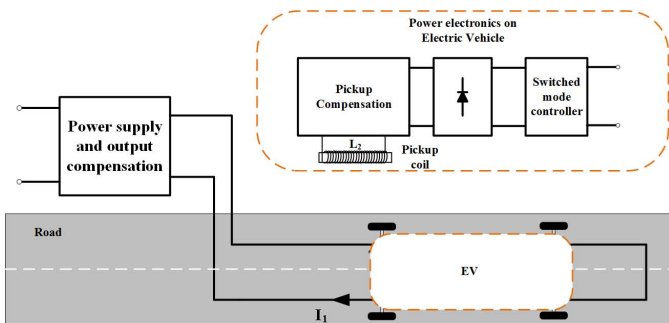


Fig. 35. Long track supplied by centralized power supply [136].

ground pads supplied by the full bridge inverter. The ground pad can be connected through individual H-bridge converter for each ground pad. Another approach is to connect a single high-power inverter supplying multiple ground pad, and each coil is turned ON and OFF through a switch box, as shown in Fig. 36 [135], [136].

The centralized power supply system approach has the problem of requiring high power rating components; the entire rail is activated, and that incurs large power loss, diminishes reliability and efficiency [81], [136]. Furthermore, it will be sensitive to parameter variation and requires a motion-inclusive control scheme. In the segmented rail, different segments are turned ON at different times as the vehicle to be charged passes over. Therefore, power loss is reduced, and the converter can be of lower power ratings. Reliability is improved because even if one segment breaks down, another segment can supply power, and it has lower sensitivity to

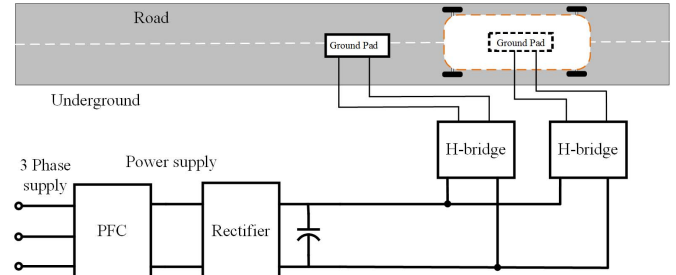


Fig. 36. Central power supply with extended connections to ground pads [136].

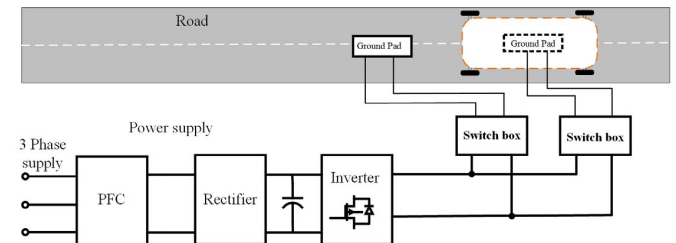


Fig. 37. Segmented WPT as presented in [136].

parameter variation. Problems associated with this scheme are higher maintenance, high initial cost, and complex control. A combination of segmented rail and centralized power supply scheme is shown in Fig. 37 [83], [136]. The scheme has a central power supply feeding a power rail, and the ground pads are turned ON and OFF through a switch box. This scheme has the advantage of fewer power electronics components, reduced

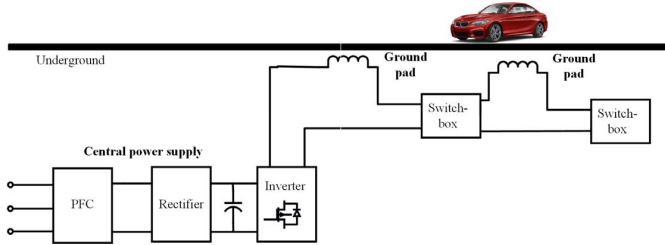


Fig. 38. Series connected to ground pads with switch boxes as in [136].

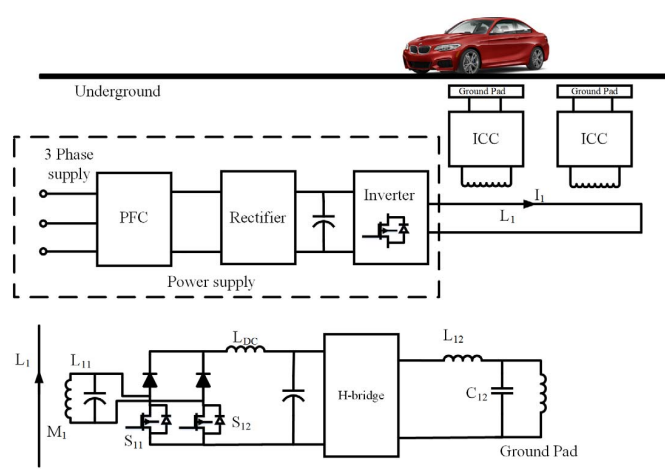


Fig. 39. Double-coupled system as presented in [136].

cost of installation and low power loss as each segment is turned on at different times [136]. This scheme has the disadvantage of lower reliability and high loss in the power cable connecting the segments. A variation of centralized power supply with series connected ground pad with switch box is illustrated in Fig. 38. Fig. 39 shows the double-couple scheme capable of reducing the losses in the power rail [136]. It consists of a high-frequency power rail embedded under the road to supply power to the intermediate coupler at a selected location. The output of the intermediate coupler is connected to a controlled rectifier to convert high-frequency ac voltage into dc voltage. The rectified dc voltage is fed to an H-bridge which controls the ground pad. The individual charging controller controls selected ground pads according to vehicle presence. This system resolves the limitation of the abovementioned power supply architecture [83], [136]. The advantages are isolation between ground pad and power supply, power supply rail is operated at a lower frequency, and the ground pad operates at a higher frequency to improve the efficiency of the system. However, the problems include the high cost of power electronics and lower reliability due to central power supply unit for the entire system [136].

Conventional single phase IPT systems employ a single transmitter coil, which is energized with a constant current. Repetitive misalignment due to vehicle motion reduces efficiency and requires a larger pick-up coil. An alternative reported by some researchers is the use of a multiphase long track system that permits multiple vehicles to charge simulta-

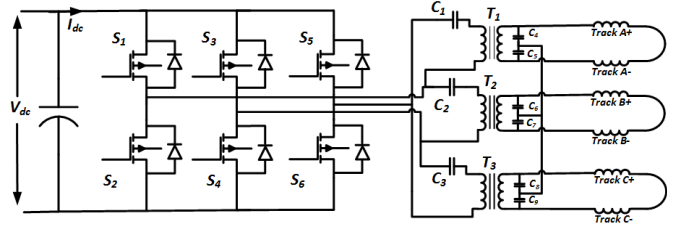


Fig. 40. Three-phase inductive power transfer system for roadway-powered vehicles [137].

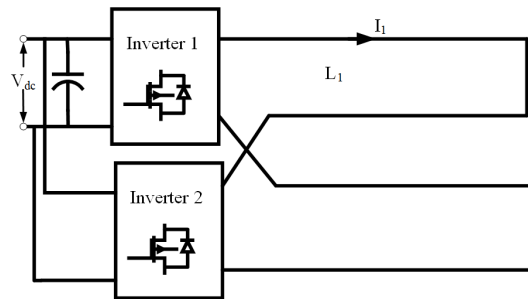


Fig. 41. Two-phase IPT system [138].

neously while on the move and to also provide high misalignment tolerance [102], [138]. Fig. 40 shows a representative three-phase IPT system having multiple vehicles charging side by side while on the move [102]. Other advantages include short power boost that can be given to charging vehicles during steep slopes and high misalignment tolerance. Two-phase IPT system shown in Fig. 41 was reported to reduce the cost without affecting misalignment tolerance [138]. As a conclusion to this section Table XVII summarizes the various power supply architectures for DWPT. Work on power supply scheme for DWPT is still in progress, and the further research focus would be handling power pulsation, reducing the cost of implementation and improving the reliability of the system [82], [102], [135]–[138].

VI. MISALIGNMENT TOLERANCE

Typically, WPT transmitter coils are placed flush or beneath the ground and in some installations, depending on regulations may be surface mounted, provided a strict height limit is maintained [42]. To charge the battery at high transfer efficiency requires good alignment of the transmitter and receiver coils. Typically in stationary or dynamic charging of EV, it is difficult to align transmitter and receiver as it depends on the driver, the vehicle, and the environment. SAE J2594/1 mandates an overall efficiency of no less than 80% during misalignment [42]. According to SAE J2594/1, a WPT system must be misalignment tolerant in x - and y -directions, and also capable of z -direction variability due to vehicle ground clearance and loading. In addition, it also specifies tolerance in tilt and rotation misalignment (yaw) the detailed requirements of which are given in Tables IV and V. Various researchers have discussed and proposed solutions for the aforementioned problems [102], [136]–[144].

Some solutions focus on the coil design to improve the misalignment tolerance [59], [61], [143], [144], whereas

TABLE XVII
COMPARISON OF VARIOUS DWPT POWER SUPPLY ARCHITECTURES [81], [102], [135]–[138]

Power Supply Scheme	Merits	Demerits
Centralized power supply scheme	<ul style="list-style-type: none"> Simple in construction, lower cost of installation and maintenance Centralized power station better utilizes local energy storage to minimize load pulsation on the utility connection 	<ul style="list-style-type: none"> Large power rating of components the whole rail is activated which causes power losses low reliability low efficiency and sensitivity to variation in parameters
Segmented rail power supply	<ul style="list-style-type: none"> Selected segments can be turned on or off which reduces power losses smaller size power converter high reliability and lower sensitivity to parameter variation. Also benefits from local energy storage. 	<ul style="list-style-type: none"> High maintenance and construction cost difficult to control automatic detection system required to turn the selected ground pad
High frequency segmented rail	<ul style="list-style-type: none"> Distributed power electronics converters Selected ground pad can be switched on to reduce the power losses Easy to maintain 	<ul style="list-style-type: none"> Lower reliability high power loss in high-frequency power rail
Combination scheme	<ul style="list-style-type: none"> High efficiency as selected segments can be switched Suitable for large power dynamic charging system 	<ul style="list-style-type: none"> Complex system, high installation cost, and high maintenance cost Lower reliability

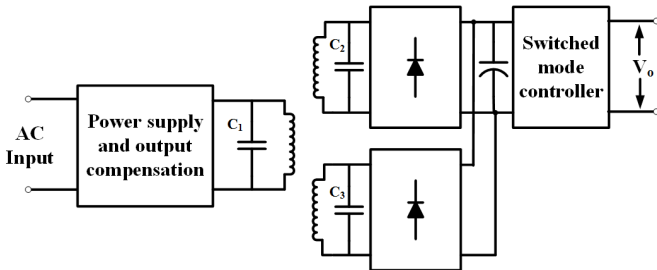


Fig. 42. Power electronics implementation of DDQ as in [64].

some favor control techniques such as changing the resonant frequency, to improve the efficiency of the system [115]. Other researchers have focused on higher order compensation techniques such as LCC and LCL resonant compensation networks [103].

As a general rule, the primary coil diameter should be equal to or only slightly larger than that of the secondary for good coefficient of coupling when the magnetic gaps are equal to half of the transmitter coil diameter. The size of the coils becomes very large if we follow this guideline [143], [144], which led many researchers to employ the modular approach discussed in Section V-A. A polarized flux pipe was reported in [59] that has better misalignment tolerance than a circular coil. A DDQ coil was proposed in [64] to improve the misalignment tolerance of the system. It contains three coils, two of which are mounted along the *d*-axis direction and the third coil is mounted along the quadrature *q*-axis. In the case of misalignment, the quadrature axis coils pick up the flux along the *q*-axis and compensates for misalignment to a greater extent. The output of the *q*-axis coil is added to the *d*-axis, as shown in Fig. 42. A BP with reduced copper requirements was reported in [64]. It has the same misalignment characteristics as the DDQ coil.

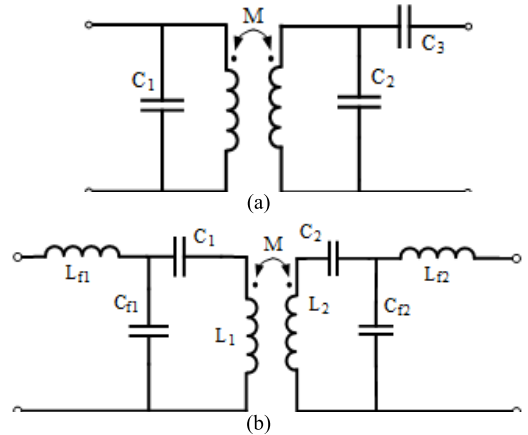


Fig. 43. (a) PPS compensation [144]. (b) LCC compensation [147].

Performance comparison of S-S, S-P, P-S, and P-P for misalignment was reported in [103] and discussed in Section IV. S-S and P-S circuit compensation technique have very low sensitivity to misalignment. It is well understood that efficiency of a network degrades with misalignment. To improve the misalignment performance, Fotopoulos and Flynn [144] proposed a compensation circuit that adds a series capacitor to parallel resonant circuit, as shown in Fig. 43(a). Kissin *et al.* [140] claimed to achieve increases in power transfer efficiency of 15% for horizontal misalignment of 100 mm compared to P-P network. The PF was also improved from PF = 0.3 to 0.4. The designed system includes the variation of coefficient of coupling to ensure minimum frequency and phase shift. An alternate approach to improve efficiency in misalignment is to optimize the compensation capacitor. An efficiency improvement of 38.3% is reported for a four coil WPT system [147]. The scheme in Fig. 43(b) is a double-sided LCC compensation network. Zhu *et al.* [147] and Li *et al.* [108] report a high misalignment

TABLE XVIII
COMPARISON OF DIFFERENT CONTROL TECHNIQUES FOR DWPT [85], [148]–[161]

Control strategy	Merits	Demerits
Primary side control	<ul style="list-style-type: none"> Constant current control for transmitter control is independent of load no need of communication link between primary and secondary 	Efficiency of the system is low as it is independent of load
Secondary side control	<ul style="list-style-type: none"> Constant current control maximum efficiency control can be implemented 	Controlled power electronics on secondary side
Dual side control with close loop communication	<ul style="list-style-type: none"> Desired power control and maximum efficiency control can be achieved Bidirectional power flow can be achieved 	<ul style="list-style-type: none"> Require secure wireless communication between primary and secondary the delay in communication should be minimum
Dual side control without close loop communication	<ul style="list-style-type: none"> Independent control of primary and secondary desired power with maximum efficiency control can be implemented 	<ul style="list-style-type: none"> Conflict between primary secondary control can cause stability issues

tolerance of up to 310 mm at a coefficient of coupling of 0.18 with just $\sim 1\%$ drop in efficiency. In addition to misalignment tolerance, the ZVS of the full bridge is ensured by tuning the parameters of compensation network. A control technique to improve the efficiency of the WPT system by 5%–7% via searching for the optimal value of switching frequency and phase shift was reported in [115]. Overall for high-power application, double-sided LCC compensation network is reported to have tolerance to misalignment. Also it does not require additional power electronics or auxiliary coils [147], [108]. For somewhat lower power application, misalignment compensation by changing frequency and phase shift is very effective method, as it does not require any additional components [115].

VII. CONTROL OF WPT

Different techniques are reported in the literature to control the power flow and to maintain the SOC of the battery [148]–[150]. These techniques can be classified as primary-side control, secondary-side control or dual-sided control [45]. In primary-side control, the battery SOC information is transmitted from the secondary side to the primary side by a communication link [45]. Secondary-side control requires active rectification and is used in an application where multiple pick-up coils are connected. In dual-sided control, full-bridge and active rectifiers are both controlled simultaneously to control the power flow to the load [148]. A phasor modeling concept was developed in [45] to have a resemblance of a power transmission line. The control technique was able to control reactive power using a voltage control method. This control method does not require any active control on the secondary side. However, control is complicated and needs a lookup table to implement [45]. Typically, primary-side control has the advantage of minimum interaction with secondary-side electronics. Therefore, a vehicle will only have lower power electronics, which has cost benefits. Miller *et al.* [151] investigated a grid side power regulation method to reduce the complexity of control on the primary and secondary sides power electronics. However, at no-load and in the absence of the secondary coil, the current in the primary coil increases to a very large value.

The basic control strategies to control the H-bridge inverter are phase shift control and frequency control. In phase shift control, the phase shift of the leg of full-bridge converter is controlled to vary the voltage applied to the coupling coil with a constant frequency. However, inductive operation of the circuit requires judicious selection of switching frequency relative to the loaded resonant point due to pole splitting [85], [152], [153]. Soft switching remains an option but may have additional concerns [85]. A 6-kW WPT system with phase controlled full bridge is reported in [45]. The control provides flexibility for the selection of operating frequency and benefits from its resemblance to a power transmission network. However, control is complicated and the conduction angle must be calculated offline and stored in the controller for operation at different power levels. In frequency control, the switching frequency of the full-bridge converter is varied above the resonance frequency, in the inductive region of operation. If the switching frequency is increased, the input impedance of the compensating circuit increases [152], [153]. This leads to a decrease in the input current and output power. The problem with variable frequency controller is uncertainty in behavior self-sustained oscillating control, the switching frequency and over bifurcation region when present [108], [148]–[152]. In phase shift of the full-bridge converter are changed simultaneously to control the output power [108], [148], [153]. In this control, zero crossing of primary coil current is sensed to trigger the gating signal for a full-bridge converter. The advantages of dual control are its ZCS turn-ON and ZVS turn-OFF. Inductive operation is ensured for all operating frequencies [108], [148]. Phase shift control can be categorized into symmetric voltage cancellation (SVC), asymmetric duty cycle (ADC), and asymmetric voltage cancellation (AVC) [157]. An ADC method was proposed to improve the ZVS range for a wide load range. The problem with ADC is that it generates higher THD in the primary track current and higher EMI, as compared to SVC. AVC methods, which have the advantages of wide ZVS range for load and reduced EMI, are reported in [157]–[161]. The detailed comparison of the various control techniques is compiled in Table XVIII. For stationary WPT, dual-side control with closed-loop communication is the most popular control method. However, some

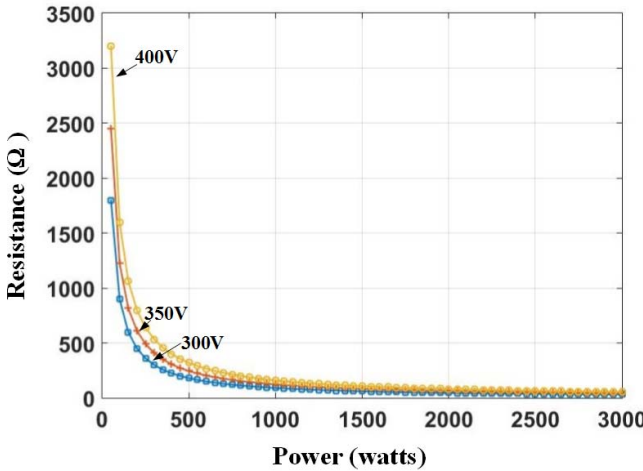


Fig. 44. Variation in terminal resistance with output for different battery voltages.

of issues such as wireless communication security and delay in communication are the bottlenecks which require further research [85], [148]–[161]. For DWPT, ideally independent control of primary and secondary is the most suitable form of control. However, conflict between primary and secondary control can cause stability. Dual-side control with closed-loop communication is most stable control method but for DWPT the communication latency can cause delay in control and stability issue. Overall communication methods require more research to reduce the latency [85], [148]–[161].

VIII. IMPEDANCE MATCHING FOR MAXIMUM EFFICIENCY TRACKING

In the literature, it is well reported that the optimal value of load resistance depends on the operating frequency and the mutual inductance between the coils, and other constant parameters [135]. Miller *et al.* [135] reported variation in efficiency with variation in operating frequency for various load resistance and mutual inductance. Typically, for the EV applications, battery is connected as a load; hence, the equivalent resistance seen by a wireless system is $R_{ac} = 8R_B/\pi^2$, where $R_B = V_B/I_B$, V_B is the battery terminal voltage, and I_B is the charging current. The optimal resistance varies over a wide range for the variation in coupling factor. Generally, for EVs, the battery voltage ranges from 300 to 400 V [36], [158], [159].

Because of this high battery voltage, the variation in load resistance seen from the terminal is very high for lower power rating as compared to a higher power as shown in Fig. 44.

To achieve high efficiency, optimal load resistance has to be connected to load [163]. That is, the load resistance has to match with the input impedance of WPT, which is also referred to as an optimal matching condition in [163]. In order to achieve optimal matching in WPT, four approaches are reported in [114], [163]–[166] and are depicted in Fig. 45. The first approach for optimal matching depicted in Fig. 45(a) consists of secondary-side active rectifier whose phase shift is controlled to obtain optimal impedance [163] given that secondary-side diodes are replaced with controlled switches.

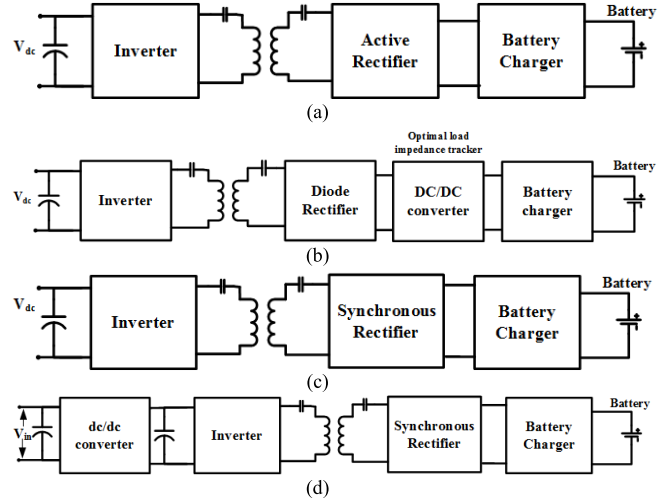


Fig. 45. (a) First approach, (b) second approach, (c) third approach, (d) preregulation approach.

TABLE XIX
INPUT RESISTANCE OF DIFFERENT CONVERTERS [114]

Converter	Input resistance
Buck	$\frac{R_L}{D^2}$
Boost	$R_L(1-D)^2$
Buck-Boost	$\frac{R_L(1-D)^2}{D^2}$
Tristate boost	$\frac{R_LD_0^2}{(1-D_f)\cos^4\left(\frac{D_f\pi}{2}\right)}$

Note that the phase shift of secondary switches must be calculated offline to match the optimal value of the impedance. Fig. 45(b) shows the second approach in which dc–dc converter is inserted after the rectifier. The input resistance of the dc–dc converter is modulated by changing the duty cycle of the converter [164]. Table XIX gives the relationship of input resistance with duty cycle for various converters [114]. The third approach consisting of a full-bridge inverter and a battery charger is shown in Fig. 45(c). The full-bridge inverter having switching frequency and phase shift control is used to maximize the efficiency of the system. An online efficiency optimization algorithm, which increases the efficiency of the system by 5%–7% for alignment and misalignment, is reported in [110]. Pantic *et al.* [114] proposed a parallel-compensated WPT with a tristate boost converter presented in Fig. 46. The tristate boost converter has an additional degree of freedom to shape the discontinuous input current such that the input impedance can be varied in order to obtain the optimal impedance. Last, a preregulation-based approach to achieve optimal impedance is shown in Fig. 45(d) [114]. In this method, dc–dc converter is connected to the full-bridge inverter to vary the input voltage of the inverter and hence the input impedance of the system.

IX. FOREIGN OBJECT DETECTION AND VEHICLE DETECTION

An essential necessity for commercialization of WPT in stationary and DWC is FOD and vehicle detection [42], [167], [169]. In the absence of a vehicle, the primary

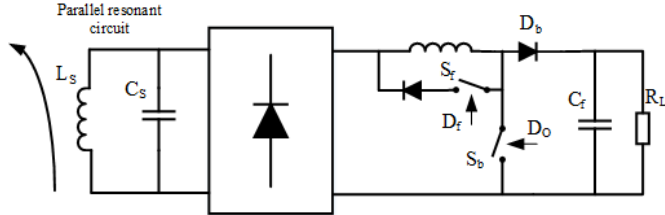


Fig. 46. Tristate boost converter with parallel-compensated pickup as in [114].

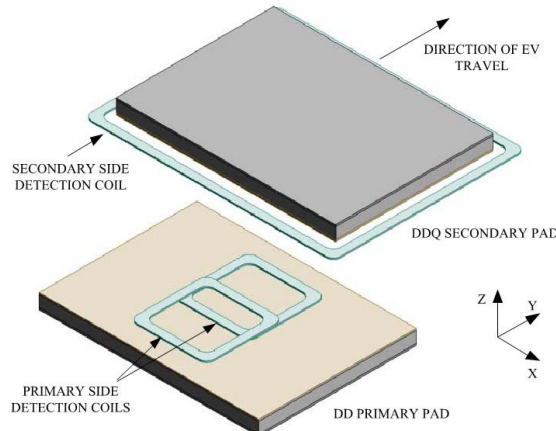


Fig. 47. Three-coil detection system as in [175].

coils should automatically turn-OFF and prevent conductive object heating due to eddy current losses. To prevent the heating of metallic object, several FOD methods have been reported in [168]. WiTricity has developed an overlapped coil structure to detect the FOD. It has coils mounted in a particular manner on the transmitter; FOD is detected by measuring the voltage, current, phase, power, and frequency of the resonator with and without conductive objects [168]. In [169], power loss with and without a conductive object is compared to find the foreign object. This method is easy to implement, simple in operation and does not require any additional hardware. However, for high power, the power loss in the conductive object is small compared to the power transferred. Jeong *et al.* [170] report an FOD method based on the measurement of quality factor (Q), metallic object tends to decrease in Q . This method is easy to implement, however, in the case of misalignment or if the pick-up coil moves, the quality factor of the coil also changes.

In the literature, several papers have reported vehicle detection system [171]–[177]. Communications is the key method to detect a vehicle. However, for DWPT, high-speed communications with minimum latency is essential [176]. Other method to detect the position of EV is the use of sensors. However, the overall cost of the system increases due to sensors and are difficult to implement in a multilane highway [175]. Jang *et al.* [171] reported a detection method which uses multiple coils mounted on the primary and secondary sides to detect the position of an EV, as shown in Fig. 47. The coil mounted on the secondary is energized by high-frequency current which induces a voltage in secondary when EV travels

TABLE XX
ECONOMIC DATA FOR WIRELESS CHARGING [167], [179], [180]

Vehicle	Charging	Cost	Note	Location
Car	Dynamic	\$2.8million/lane-mile	Hardware cost including labor cost	Ann Arbor
Car	Dynamic	\$2.4million/lane-mile	Power electronics cost and power delivery cost	Atlanta, GA
Bus	Dynamic	\$0.85-1.07million/km	Power electronics and construction	Korea
Bus	Dynamic	\$15,000 (fixed) + \$200/m (variable) per station	Fixed cost for power electronics and variable cost for length of power transmitter	Korea

over it. This voltage is processed to detect the presence of EV and accordingly turns-ON and turns-OFF the primary coil. However, the detection system electronics and coils structure is difficult to implement, and have issues with detuning and magnetic interference. In addition, it cannot detect EV coming from side lane instead of same lane [176]. Deng *et al.* [177] reported a sensorless alternative to detect the position of an EV by measuring the phase angle between current and voltage which reflects the edge position of the vehicle. Hasan *et al.* reported a sensorless position method based on the control algorithm [178]. The control algorithm regulates the power transfer by measuring the input dc power in standby case, and if this input power is above a certain value, the primary coil starts delivering the full power to the load. However, the primary coil has to be always energized which increases the standby losses in this system.

X. CHALLENGES

A. Economics

The economics aspect of WPT depends on charging infrastructure and battery storage. In stationary WPT charging, the cost of the magnetic coupler and power electronics are additional compared to a wired charging. However, the increased cost is acceptable considering the gains in terms of convenience, battery size reduction and leveled cost reduction over the lifetime of the system [167], [179]. Wireless charging for the electric bus can sustainably reduce the fuel cost by as much as 80% when as compared to diesel bus [180]. Despite the low dependence on battery storage system, lack of charging infrastructure is currently the main impediment to DWPT. It requires efforts from the private sector and also from the government. DWPT can mitigate the high cost of EVs by substantially reducing the onboard battery size [96]. Some of the reported cost data for wireless charging from the literature are summarized in Table XX [167], [179], [180]. In [34], economic feasibility of the OLEV with conventional electric vehicles, PHEV, internal combustion engine (ICE), and BEV for Seoul, South Korea, was analyzed as reported in Table XXI. The traveled distance of a vehicle is assumed to be 20000 km/year. The initial cost of infrastructure for OLEV is about U.S. \$0.48B, which is much lower than other options.

TABLE XXI
COMPARISON OF COST FOR DIFFERENT VEHICLES [34]

Costs	BEV	PHEV	ICE	OLEV
One vehicle	50k\$	35k\$	20k\$	20-25k\$
Energy(for 10 years)	3.6k\$	7.8k\$	20k\$	4k\$
Home charger	5k\$	5k\$	0	0-5k\$
Unit vehicle price	58.6k\$	47.8k\$	40.0k\$	24-34k\$
Infra (charger)	3500 EA	700 EA	700 EA	600 km
Price/infra	5 M\$	5M\$	5M\$	0.8M\$/km
Total infra cost	17.5 B\$	3.5B\$	3.5B\$	0.48B\$

Cost (B\$) vs. No. of vehicles (10k)

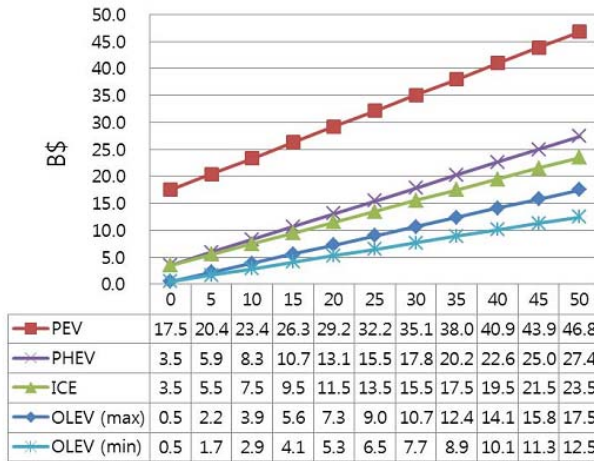


Fig. 48. Total cost versus number of cars deployed in Seoul [34].

Further, the authors compared the overall cost of vehicles, including operation and infrastructure cost for 10 years as shown in Fig. 48. OLEV is about 4–24 times cheaper compared to other vehicles. This is due to the relatively lower cost of operation [34].

B. Communication

Communication plays an important role in DWPT to ensure a timely power transfer to battery charging system otherwise the charging system is likely to fail. Therefore, the data exchange between the transmitter and EV has to be done in real time [181]. Ideally, a real-time control system is designed for the execution of the control loop of a battery charging system. However, successful performance of this control in a DWPT system strongly depends on the delay introduced by wireless communications. The main criteria to select communications method are: 1) low latency; 2) ability to support multiple vehicles simultaneously; and 3) medium range coverage [180]. Table XXII gives a comparison of different wireless communication methods for DWPT. DSRC offers the lowest latency. However, its range is less. Future research direction would have to focus on finding communication architectures with minimum latency and longer range [182].

C. Health and Safety Concern

Extensive research has been conducted to investigate the impact of EMF on humans, i.e., the human electromagnetic exposure limits [42]. Biological response caused by exposure

TABLE XXII
COMPARISON OF WIRELESS TECHNOLOGIES FOR DYNAMIC WPT [181]

	FM radio	Cellular	WiMax	DSRC	Satellite
Range	~100km	~10km	<50km	<1km	~1000km
Data rate	>10kbps	100kbps	70kbps	3-27Mbps	100Mbps>
Latency	High	Low	High	Very low	Very high
Mobile connectivity	low	Very high	High	low	Very high

to electric and magnetic fields below 100 kHz, surface electric discharge, induction in the retina of phosphenes, heating in human tissue, heating in implanted medical devices and metals are discussed in [51] and [167]. The human body is a decent conductor of electricity. An external electric field surrounding it induces an electric field inside the body. ICNIRP has set a limit to the electric field and magnetic field for human tissues. The set internal electric field limit is $1.35 \times 10^{-4} f$, where f is the frequency of the electric field and the limit for general public is 83 V/m. A similar ICNIRP limit for the magnetic field is 27 μT [42], [51], [167]. Shielding can efficiently block the EMF exposure from the affecting passengers by utilizing aluminum plates in the back of the charging pad [167]. However, further research is required to ensure health and safety of dynamic charging systems in open space on the road. Also, research with various conditions such as varying speed of vehicle, accidental leakage exposure, and people with implanted medical device, LOD, FOD need to be investigated thoroughly [167], [180]–[183].

XI. CONCLUSION

WPT applications for EVs can reduce national reliance on fossil fuels and minimize emission of greenhouse gases. A major hurdle in mass deployment of EVs is the limited battery capacity and its high cost. This problem can be mitigated to a great extent with an electrified road for in-motion charging. Consequently, the range of EVs can be increased and the fear of “range anxiety” alleviated. This paper presented a review of current status of wireless charging for EV applications. The development history of WPT and necessary components were discussed along with a comprehensive review of the design of coupling pads, power electronics, various compensation circuits, misalignment tolerance, control techniques, and impedance matching circuits. Further, recent standards governing the WPT system for an EV were explored. The major limiting factors in the implementation of DWPT are the absence of adequate communication network, the human exposure (EMF), and the cost of implementation.

REFERENCES

- [1] Use of Energy in the United States Explained. Accessed: Jan. 20, 2016. [Online]. Available: http://www.eia.gov/EnergyExplained/?page=us_energy_transportation
- [2] M. Ehsani, Y. Gao, and A. Emadi, *Modern Electric, Hybrid Electric, and Fuel Cell Vehicles: Fundamentals, Theory, and Design*. Boca Raton, FL, USA: CRC Press, 2009.

- [3] A. Emadi, M. Ehsani, and J. M. Miller, Eds., *Vehicular Electric Power Systems: Land, Sea, Air, and Space Vehicles*. Boca Raton, FL, USA: CRC Press, 2003.
- [4] J. Larminie and J. Lowry, *Electric Vehicle Technology Explained*. New York, NY, USA: Wiley, 2003.
- [5] A. Y. Saber and G. K. Venayagamoorthy, "One million plug-in electric vehicles on the road by 2015," in *Proc. 12th Int. IEEE Conf. Intell. Transp. Syst.*, St. Louis, MO, USA, Oct. 2009, pp. 1–7.
- [6] *Understanding the Electric Vehicle Landscape to 2020*. Accessed: Feb. 22, 2016. [Online]. Available: https://www.iea.org/publications/freepublications/publication/GlobalEVOutlook_2013.pdf
- [7] M. Chinthavali and O. C. Onar, "Tutorial on wireless power transfer systems," in *Proc. IEEE Transp. Electric. Conf. Expo (ITEC)*, Dearborn, MI, USA, Jun. 2016, pp. 1–142.
- [8] M. Yilmaz and P. T. Krein, "Review of battery charger topologies, charging power levels, and infrastructure for plug-in electric and hybrid vehicles," *IEEE Trans. Power Electron.*, vol. 28, no. 5, pp. 2151–2169, May 2013.
- [9] *Lithium-Ion Costs to Fall by Up to 50% Within Five Years*. Accessed: Feb. 23, 2016. [Online]. Available: <http://analysis.energystorageupdate.com/lithium-ion-costs-fall-50-within-five-years>
- [10] H.-Y. Mak, Y. Rong, and Z.-J. M. Shen, "Infrastructure planning for electric vehicles with battery swapping," *Manage. Sci.*, vol. 59, no. 7, pp. 1557–1575, 2013.
- [11] *Electric-Car Maker Touts 10-Minute Fill-Up*. Accessed: Feb. 24, 2016. [Online]. Available: <http://spectrum.ieee.org/transportation/advancedcars/electriccar-maker-touts-10minute-fillup>
- [12] *Inductive Power Transfer IPT-Charge*. Accessed: Feb. 25, 2016. [Online]. Available: http://www.conductix.us/en/products/inductive-powertransfeript/inductive-powertransfer-ipt-charge?parent_id=5798
- [13] (Jul. 2013). *Charging Electric Buses Quickly and Efficiently: Bus Stops Fitted With Modular Components Make 'Charge & Go' Simple to Implement*. Accessed: Feb. 28, 2016. [Online]. Available: <http://www.conductix.us/en/news/2013-05-29/chargingelectric-buses-quickly-and-efficiently-busstops-fittedmodular-components-make-charge-go>
- [14] J. M. Miller, M. B. Scudiere, J. W. McKeever, and C. White, "Wireless power transfer, in Oak Ridge National Laboratory's," in *Proc. Power Electron. Symp.*, 2011.
- [15] (Jul. 2013). *WiTricityCorp: WiT 3300 Electric Vehicle Charging Kit*. Accessed: Mar. 1, 2016. [Online]. Available: <http://www.witricity.com/pages/ev-charging-system.html>
- [16] (Mar. 2013). *Primove*. Accessed: Mar. 5, 2016. [Online]. Available: <http://primove.bombardier.com/>
- [17] (Jun. 2013). *Momentum Dynamics*. Accessed: Mar. 8, 2016. [Online]. Available: <http://www.momentumdynamics.com/>
- [18] J. Cobb. *Momentum Dynamics Promises Fast and Easy Wireless EV*. Accessed: Apr. 6, 2016. [Online]. Available: <http://www.hybricars.com/momentum-dynamics-promises-fast-and-easy-wireless-ev-charging-4717/>
- [19] *Momentum Dynamics Says It Will Deliver a 200 kW Wireless Charging Systems by the End of the Year*. Accessed: Apr. 10, 2016. [Online]. Available: <https://electrek.co/2016/04/15/momentum-dynamics-200-kw-wireless-charging/>
- [20] *Heinrich Hertz's Wireless Experiment*. Accessed: Apr. 15, 2016. [Online]. Available: http://people.seas.harvard.edu/~jones/cscie129/nu_lectures/lecture6/hertz/Hertz_exp.html
- [21] *The Lost Journal of Nikola Tesla*. Accessed: Apr. 18, 2016. [Online]. Available: http://www.bibliotecapleyades.net/tesla/esp_tesla_10.htm
- [22] J. I. Agbinya, Ed., *Wireless Power Transfer*, vol. 45. Gistrup, Denmark: River Publishers, 2015.
- [23] A. El Oualkadi, A. El Oualkadi, and J. Zbitou, *Handbook of Research on Advanced Trends in Microwave and Communication Engineering*, 1st ed. Hershey, PA, USA: IGI Global, 2016.
- [24] P. Glaser, "Method and apparatus for converting solar radiation to electrical power," U.S. Patent 3 781 647, Dec. 25, 1973.
- [25] M. Kesler, "Highly resonant wireless power transfer: Safe, efficient, and over distance," WiTricity Corp., Watertown, MA, USA, White Paper 20161218, 2013. Accessed: Apr. 20, 2016. [Online]. Available: http://witricity.com/wpcontent/uploads/2016/12/White_Paper_20161218.pdf
- [26] T. M. Fisher, K. B. Farley, Y. Gao, H. Bai, and Z. T. H. Tse, "Electric vehicle wireless charging technology: A state-of-the-art review of magnetic coupling systems," *Wireless Power Transf.*, vol. 1, no. 2, pp. 87–96, 2014.
- [27] *DRIVE: Electric Vehicles*. Accessed: May 2, 2016. [Online]. Available: <http://witricity.com/products/automotive/>
- [28] J. T. Boys and G. A. Covic. (Jul. 2016). *IPT Fact Sheet Series: No. 1—Basic Concepts*. [Online]. Available: <https://www.qualcomm.com/media/documents/files/ipt-fact-sheet-1-uoa-2012.pdf>
- [29] QualcommHalo. (2011). *First Electric Vehicle Wireless Charging Trial Announced for London*. Accessed: Jul. 2013. [Online]. Available: <http://www.qualcomm.com/media/releases/2011/11/10/first-electric-vehicle-wireless-charging-trial-announced-london>
- [30] Conductix-Wampfler. (2013). *Charging Electric Buses Quickly and Efficiently: Bus Stops Fitted With Modular Components Make 'Charge & Go' Simple to Implement*. [Online]. Available: <http://www.conductix.us/en/news/2013-05-29/charging-electric-buses>
- [31] *Review and Evaluation of Wireless Power Transfer (WPT) for Electric Transit Applications*. Accessed: Jun. 5, 2016. [Online]. Available: https://www.transit.dot.gov/sites/fta.dot.gov/files/FTA_Report_No._0060.pdf
- [32] S. E. Shladover, "Systems engineering of the roadway powered electric vehicle technology," in *Proc. 9th Int. Electr. Veh. Symp.*, 1988.
- [33] Systems Control Technology, Inc., "California PATH Program. Roadway powered electric vehicle project track construction and testing program phase 3D," Univ. California, Berkeley, Berkeley, CA, USA, Tech. Rep., Mar. 1994. [Online]. Available: <http://www.path.berkeley.edu/sites/default/files/publications/PRR-94-07.pdf>
- [34] S. Y. Choi, B. W. Gu, S. Y. Jeong, and C. T. Rim, "Advances in wireless power transfer systems for roadway-powered electric vehicles," *IEEE J. Emerg. Sel. Topics Power Electron.*, vol. 3, no. 1, pp. 18–36, Mar. 2015.
- [35] C. C. Mi, G. Buja, S. Y. Choi, and C. T. Rim, "Modern advances in wireless power transfer systems for roadway powered electric vehicles," *IEEE Trans. Ind. Electron.*, vol. 63, no. 10, pp. 6533–6545, Oct. 2016.
- [36] O. C. Onar, S. L. Campbell, L. E. Seiber, C. P. White, and M. Chinthavali, "A high-power wireless charging system development and integration for a Toyota RAV4 electric vehicle," in *Proc. IEEE Transp. Electric. Conf. Expo (ITEC)*, Dearborn, MI, USA, Jun. 2016, pp. 1–8.
- [37] *WAVE: Wireless Advanced Vehicle Electrification*. Accessed: Jun. 8, 2016. [Online]. Available: <http://www.waveipt.com/about/>
- [38] R. Tavakoli and Z. Pantic, "Analysis, design and demonstration of a 25-kW dynamic wireless charging system for roadway electric vehicles," *IEEE J. Emerg. Sel. Topics Power Electron.*, to be published.
- [39] S. Li and C. C. Mi, "Wireless power transfer for electric vehicle applications," *IEEE J. Emerg. Sel. Topics Power Electron.*, vol. 3, no. 1, pp. 4–17, Mar. 2015.
- [40] F. Musavi and W. Eberle, "Overview of wireless power transfer technologies for electric vehicle battery charging," *IET Power Electron.*, vol. 7, no. 1, pp. 60–66, Jan. 2014.
- [41] J. D. Jackson, *Classical Electrodynamics*. Hoboken, NJ, USA: Wiley, 1999.
- [42] *Wireless Power Transfer for Light-Duty Plug-In/Electric Vehicles and Alignment Methodology*, Standard SAEJ2954, May 2016. [Online]. Available: http://standards.sae.org/j2954_201605/
- [43] SAE Taskforce J2954 on Wireless Charging and Positioning Standards Looking to Have Final Draft of Guideline This Year; Significant Industry Involvement. Accessed: Jun. 10, 2016. [Online]. Available: <http://www.greencarcongress.com/2012/01/j2954-2012022.html>
- [44] C.-S. Wang, O. H. Stielau, and G. A. Covic, "Design considerations for a contactless electric vehicle battery charger," *IEEE Trans. Ind. Electron.*, vol. 52, no. 5, pp. 1308–1314, Oct. 2005.
- [45] J. M. Miller, O. C. Onar, and M. Chinthavali, "Primary-side power flow control of wireless power transfer for electric vehicle charging," *IEEE J. Emerg. Sel. Topics Power Electron.*, vol. 3, no. 1, pp. 147–162, Mar. 2015.
- [46] J. M. Miller and A. Daga, "Elements of wireless power transfer essential to high power charging of heavy duty vehicles," *IEEE Trans. Transport. Electric.*, vol. 1, no. 1, pp. 26–39, Jun. 2015.
- [47] *IEEE Standard for Military Workplaces—Force Health Protection Regarding Personnel Exposure to Electric, Magnetic, and Electromagnetic Fields, 0 Hz to 300 GHz*, IEEE Standard C95.1-2345, 2014.
- [48] L. Tang, M. Chinthavali, O. C. Onar, S. Campbell, and J. M. Miller, "SiC MOSFET based single phase active boost rectifier with power factor correction for wireless power transfer applications," in *Proc. IEEE Appl. Power Electron. Conf. Expo.*, Fort Worth, TX, USA, Mar. 2014, pp. 1669–1675.

- [49] R. Bosshard, J. W. Kolar, J. Mühlthaler, I. Stevanović, B. Wunsch, and F. Canales, "Modeling and η - a -Pareto optimization of inductive power transfer coils for electric vehicles," *IEEE J. Emerg. Sel. Topics Power Electron.*, vol. 3, no. 1, pp. 50–64, Mar. 2015.
- [50] R. Bosshard, "Multi-objective optimization of inductive power transfer systems for EV charging," Ph.D. dissertation, Dept. Inf. Technol. Elect. Eng., ETH Zurich, Zürich, Switzerland, 2015.
- [51] International Commission on Non-Ionizing Radiation Protection, "Guidelines for limiting exposure to time-varying electric and magnetic fields (1 Hz to 100 kHz)," *Health Phys.*, vol. 99, no. 6, pp. 818–836, 2010.
- [52] *Electrically Propelled Road Vehicles—Magnetic Field Wireless Power Transfer—Safety and Interoperability Requirements*, document ISO/PAS 19363:2017, 2017. [Online]. Available: <https://www.iso.org/standard/64700.html>
- [53] *Road Vehicles—Vehicle to Grid Communication Interface—Part 1: General Information and Use-Case Definition*. Accessed: Jul. 10, 2016. [Online]. Available: <https://www.iso.org/standard/55365.html>
- [54] *Road Vehicles—Vehicle to Grid Communication Interface—Part 8: Physical Layer and Data Link Layer Requirements for Wireless Communication*. Accessed: Jul. 15, 2016. [Online]. Available: <https://www.iso.org/standard/62984.html>
- [55] Y. H. Sohn, B. H. Choi, E. S. Lee, G. C. Lim, G. H. Cho, and C. T. Rim, "General unified analyses of two-capacitor inductive power transfer systems: Equivalence of current-source SS and SP compensations," *IEEE Trans. Power Electron.*, vol. 30, no. 11, pp. 6030–6045, Nov. 2015.
- [56] G. A. Covic and J. T. Boys, "Modern trends in inductive power transfer for transportation applications," *IEEE J. Emerg. Sel. Topics Power Electron.*, vol. 1, no. 1, pp. 28–41, Mar. 2013.
- [57] R. Bosshard and J. W. Kolar, "Inductive power transfer for electric vehicle charging: Technical challenges and tradeoffs," *IEEE Power Electron. Mag.*, vol. 3, no. 3, pp. 22–30, Sep. 2016.
- [58] B. R. Long, J. M. Miller, A. Daga, P. C. Schrafel, and J. Wolgemuth, "Which way for wireless power: High Q or high k ?" in *Proc. IEEE PEELS*, Oct. 2016, pp. 6–10.
- [59] M. Budhia, G. A. Covic, and J. T. Boys, "Design and optimization of circular magnetic structures for lumped inductive power transfer systems," *IEEE Trans. Power Electron.*, vol. 26, no. 11, pp. 3096–3108, Nov. 2011.
- [60] M. Budhia, J. T. Boys, G. A. Covic, and C.-Y. Huang, "Development of a single-sided flux magnetic coupler for electric vehicle IPT charging systems," *IEEE Trans. Ind. Electron.*, vol. 60, no. 1, pp. 318–328, Jan. 2013.
- [61] M. Budhia, G. Covic, and J. Boys, "A new IPT magnetic coupler for electric vehicle charging systems," in *Proc. 36th Annu. Conf. IEEE Ind. Electron. Soc. (IECON)*, Glendale, AZ, USA, Nov. 2010, pp. 2487–2492.
- [62] A. Zaheer, G. A. Covic, and D. Kacprzak, "A bipolar pad in a 10-kHz 300-W distributed IPT system for AGV applications," *IEEE Trans. Ind. Electron.*, vol. 61, no. 7, pp. 3288–3301, Jul. 2014.
- [63] G. A. Covic, M. L. G. Kissin, D. Kacprzak, N. Clausen, and H. Hao, "A bipolar primary pad topology for EV stationary charging and highway power by inductive coupling," in *Proc. IEEE Energy Convers. Congr. Expo.*, Phoenix, AZ, USA, Sep. 2011, pp. 1832–1838.
- [64] G. A. J. Elliott, S. Raabe, G. A. Covic, and J. T. Boys, "Multiphase pickups for large lateral tolerance contactless power-transfer systems," *IEEE Trans. Ind. Electron.*, vol. 57, no. 5, pp. 1590–1598, May 2010.
- [65] D. Patil, M. Ditsworth, J. Pacheco, and W. Cai, "A magnetically enhanced wireless power transfer system for compensation of misalignment in mobile charging platforms," in *Proc. IEEE Energy Convers. Congr. Expo. (ECCE)*, Montreal, QC, Canada, Sep. 2015, pp. 1286–1293.
- [66] J. T. Boys and G. A. Covic, "IPT fact sheet series: No. 2: Magnetic circuits for powering electric vehicles," Dept. Elect. Comput. Eng., Univ. Auckland, Auckland, New Zealand, Tech. Rep., 2014, p. 2.
- [67] S. Kim, G. A. Covic, and J. T. Boys, "Tripolar pad for inductive power transfer systems for EV charging," *IEEE Trans. Power Electron.*, vol. 32, no. 7, pp. 5045–5057, Jul. 2017.
- [68] S. Kim, A. Zaheer, G. Covic, and J. Boys, "Tripolar pad for inductive power transfer systems," in *Proc. 40th Annu. Conf. IEEE Ind. Electron. Soc. (IECON)*, Dallas, TX, USA, Oct./Nov. 2014, pp. 3066–3072.
- [69] M. Kiani, U.-M. Jow, and M. Ghovanloo, "Design and optimization of a 3-coil inductive link for efficient wireless power transmission," *IEEE Trans. Biomed. Circuits Syst.*, vol. 5, no. 6, pp. 579–591, Dec. 2011.
- [70] S. Moon, B.-C. Kim, S.-Y. Cho, C.-H. Ahn, and G.-W. Moon, "Analysis and design of a wireless power transfer system with an intermediate coil for high efficiency," *IEEE Trans. Ind. Electron.*, vol. 61, no. 11, pp. 5861–5870, Nov. 2014.
- [71] S. Moon and G.-W. Moon, "Wireless power transfer system with an asymmetric four-coil resonator for electric vehicle battery chargers," *IEEE Trans. Power Electron.*, vol. 31, no. 10, pp. 6844–6854, Oct. 2016.
- [72] J. Zhang, X. Yuan, C. Wang, and Y. He, "Comparative analysis of two-coil and three-coil structures for wireless power transfer," *IEEE Trans. Power Electron.*, vol. 32, no. 1, pp. 341–352, Jan. 2017.
- [73] J. Deng, J. Deng, W. Li, S. Li, and C. Mi, "Magnetic integration of LCC compensated resonant converter for inductive power transfer applications," in *Proc. IEEE Energy Convers. Congr. Expo. (ECCE)*, Pittsburgh, PA, USA, Sep. 2014, pp. 660–667.
- [74] W. Li, H. Zhao, S. Li, J. Deng, T. Kan, and C. C. Mi, "Integrated LCC compensation topology for wireless charger in electric and plug-in electric vehicles," *IEEE Trans. Ind. Electron.*, vol. 62, no. 7, pp. 4215–4225, Jul. 2015.
- [75] T. Kan, T.-D. Nguyen, J. C. White, R. K. Malhan, and C. C. Mi, "A new integration method for an electric vehicle wireless charging system using LCC compensation topology: Analysis and design," *IEEE Trans. Power Electron.*, vol. 32, no. 2, pp. 1638–1650, Feb. 2017.
- [76] A. Roßkopf, E. Bär, C. Joffe, and C. Bonse, "Calculation of power losses in Litz wire systems by coupling FEM and PEEC method," *IEEE Trans. Power Electron.*, vol. 31, no. 9, pp. 6442–6449, Sep. 2016.
- [77] R. Laouamer, M. Brunello, J. P. Ferrieux, O. Normand, and N. Buchheit, "A multi-resonant converter for non-contact charging with electromagnetic coupling," in *Proc. 23rd Int. Conf. Ind. Electron., Control Instrum. (IECON)*, vol. 2. New Orleans, LA, USA, Nov. 1997, pp. 792–797.
- [78] F. Nakao, Y. Matsuo, M. Kitaoka, and H. Sakamoto, "Ferrite core couplers for inductive chargers," in *Proc. Power Convers. Conf.-Osaka*, vol. 2. Osaka, Japan, Apr. 2002, pp. 850–854.
- [79] C.-G. Kim, D.-H. Seo, J.-S. You, J.-H. Park, and B. H. Cho, "Design of a contactless battery charger for cellular phone," *IEEE Trans. Ind. Electron.*, vol. 48, no. 6, pp. 1238–1247, Dec. 2001.
- [80] S. Valtchev, B. Borges, K. Brandisky, and J. B. Klaassens, "Resonant contactless energy transfer with improved efficiency," *IEEE Trans. Power Electron.*, vol. 24, no. 3, pp. 685–699, Mar. 2009.
- [81] S. Lee, J. Huh, C. Park, N.-S. Choi, G.-H. Cho, and C.-T. Rim, "On-line electric vehicle using inductive power transfer system," in *Proc. IEEE Energy Convers. Congr. Expo.*, Atlanta, GA, USA, Sep. 2010, pp. 1598–1601.
- [82] A. Gil and J. Taiber, "A literature review in dynamic wireless power transfer for electric vehicles: Technology and infrastructure integration challenges," in *Sustainable Automotive Technologies 2013*. Ingolstadt, Germany: Springer, 2013, pp. 289–298.
- [83] S. Choi, J. Huh, W. Y. Lee, S. W. Lee, and C. T. Rim, "New cross-segmented power supply rails for roadway-powered electric vehicles," *IEEE Trans. Power Electron.*, vol. 28, no. 12, pp. 5832–5841, Dec. 2013.
- [84] J. Huh, S. W. Lee, W. Y. Lee, G. H. Cho, and C. T. Rim, "Narrow-width inductive power transfer system for online electrical vehicles," *IEEE Trans. Power Electron.*, vol. 26, no. 12, pp. 3666–3679, Dec. 2011.
- [85] J. T. Boys, G. A. Covic, and A. W. Green, "Stability and control of inductively coupled power transfer systems," *IEEE Proc.-Electr. Power Appl.*, vol. 147, no. 1, pp. 37–43, Jan. 2000.
- [86] G. A. Covic and J. T. Boys, "Inductive power transfer," *Proc. IEEE*, vol. 101, no. 6, pp. 1276–1289, Jun. 2013.
- [87] S. Raabe, G. A. J. Elliott, G. A. Covic, and J. T. Boys, "A quadrature pickup for inductive power transfer systems," in *Proc. IEEE Conf. Ind. Electron. Appl.*, Harbin, China, May 2007, pp. 68–73.
- [88] T. Campi, S. Cruciani, and M. Feliziani, "Magnetic shielding of wireless power transfer systems," in *Proc. Int. Symp. Electromagn. Compat.*, Tokyo, Japan, May 2014, pp. 422–425.
- [89] J. Kim *et al.*, "Coil design and shielding methods for a magnetic resonant wireless power transfer system," *Proc. IEEE*, vol. 101, no. 6, pp. 1332–1342, Jun. 2013.
- [90] S. Kim, H.-H. Park, J. Kim, J. Kim, and S. Ahn, "Design and analysis of a resonant reactive shield for a wireless power electric vehicle," *IEEE Trans. Microw. Theory Techn.*, vol. 62, no. 4, pp. 1057–1066, Apr. 2014.
- [91] S. Ahn and J. Kim, "Magnetic field design for high efficient and low EMF wireless power transfer in on-line electric vehicle," in *Proc. 5th Eur. Conf. Antennas Propag.*, Rome, Italy, 2011, pp. 3979–3982.

- [92] S. Ahn *et al.*, "Low frequency electromagnetic field reduction techniques for the on-line electric vehicle (OLEV)," in *Proc. IEEE Int. Symp. Electromagn. Compat.*, Jul. 2010, pp. 625–630.
- [93] H. H. Park, J. H. Kwon, S. I. Kwak, and S. Ahn, "Effect of air-gap between a ferrite plate and metal strips on magnetic shielding," *IEEE Trans. Magn.*, vol. 51, no. 11, Nov. 2015, Art. no. 9401504.
- [94] S. Y. Choi, B. W. Gu, S. W. Lee, W. Y. Lee, J. Huh, and C. T. Rim, "Generalized active EMF cancel methods for wireless electric vehicles," *IEEE Trans. Power Electron.*, vol. 29, no. 11, pp. 5770–5783, Nov. 2014.
- [95] W. Zhang and C. C. Mi, "Compensation topologies of high-power wireless power transfer systems," *IEEE Trans. Veh. Technol.*, vol. 65, no. 6, pp. 4768–4778, Jun. 2016.
- [96] M. T. Outeiro, G. Buja, and D. Czarkowski, "Resonant power converters: An overview with multiple elements in the resonant tank network," *IEEE Ind. Electron. Mag.*, vol. 10, no. 2, pp. 21–45, Jun. 2016.
- [97] J. Sallan, J. L. Villa, A. Llombart, and J. F. Sanz, "Optimal design of ICPT systems applied to electric vehicle battery charge," *IEEE Trans. Ind. Electron.*, vol. 56, no. 6, pp. 2140–2149, Jun. 2009.
- [98] P. Knaup and K. Hasse, "Zero voltage switching converter for magnetic transfer of energy to movable systems," in *Proc. Eur. Conf. Power Electron. Appl.*, vol. 2, 1997, pp. 168–173.
- [99] W. Zhang, S.-C. Wong, C. K. Tse, and Q. Chen, "An optimized track length in roadway inductive power transfer systems," *IEEE J. Emerg. Sel. Topics Power Electron.*, vol. 2, no. 3, pp. 598–608, Sep. 2014.
- [100] C.-S. Wang, G. A. Covic, and O. H. Stielau, "General stability criterions for zero phase angle controlled loosely coupled inductive power transfer systems," in *Proc. 27th Annu. Conf. IEEE Ind. Electron. Soc. (IECON)*, vol. 2. Denver, CO, USA, Nov./Dec. 2001, pp. 1049–1054.
- [101] M. K. McDonough, "A multi-port power electronics interface for battery powered electric vehicles: Application of inductively coupled wireless power transfer and hybrid energy storage system," Ph.D. dissertation, Erik Jonsson School Eng. Comput. Sci., Univ. Texas Dallas, Dallas, TX, USA, 2014.
- [102] N. A. Keeling, G. A. Covic, and J. T. Boys, "A unity-power-factor IPT pickup for high-power applications," *IEEE Trans. Ind. Electron.*, vol. 57, no. 2, pp. 744–751, Feb. 2010.
- [103] A. Khaligh and S. Dusmez, "Comprehensive topological analysis of conductive and inductive charging solutions for plug-in electric vehicles," *IEEE Trans. Veh. Technol.*, vol. 61, no. 8, pp. 3475–3489, Oct. 2012.
- [104] K. Aditya and S. S. Williamson, "Design considerations for loosely coupled inductive power transfer (IPT) system for electric vehicle battery charging—A comprehensive review," in *Proc. IEEE Transp. Electricif. Conf. Expo. (ITEC)*, Dearborn, MI, USA, Jun. 2014, pp. 1–6.
- [105] J. M. Miller and B. R. Long, "What all technology adopters should know about WPT for high power charging," presented at the IEEE PEŁs Workshop Emerg. Technol., Wireless Power (WOW), Knoxville, TN, USA, Oct. 2016.
- [106] O. Onar and P. T. Jones, *Technology Requirements and Evaluations for High Power Applications of Wireless Power Transfer*. Accessed: Jul. 25, 2016. [Online]. Available: https://energy.gov/sites/prod/files/2015/07/f24/vss152_onar_2015_o.pdf
- [107] J. L. Villa, J. Sallan, J. F. S. Osorio, and A. Llombart, "High-misalignment tolerant compensation topology for ICPT systems," *IEEE Trans. Ind. Electron.*, vol. 59, no. 2, pp. 945–951, Feb. 2012.
- [108] S. Li, W. Li, J. Deng, T. D. Nguyen, and C. C. Mi, "A double-sided LCC compensation network and its tuning method for wireless power transfer," *IEEE Trans. Veh. Technol.*, vol. 64, no. 6, pp. 2261–2273, Jun. 2015.
- [109] P. Si and A. P. Hu, "Analyses of DC inductance used in ICPT power pick-ups for maximum power transfer," in *Proc. IEEE/PES Transmiss. Distrib. Conf. Expo., Asia-Pacific*, Dalian, China, Aug. 2005, pp. 1–6.
- [110] *IEEE Standard for Interconnecting Distributed Resources With Electric Power Systems*, IEEE Standard 1547, 2003.
- [111] *Power Quality Requirements for Plug-In Vehicle Chargers—Part 1: Requirements*, SAE International Standard J2894, 2011.
- [112] *Electromagnetic Compatibility (EMC)—Part 3: Limits—Section 2: Limits for Harmonic Current Emissions*, document IEC1000-3-2, 1995.
- [113] *National Electric Code*, Nat. Fire Protection Assoc., Inc., Quincy, MA, USA, 2002.
- [114] Z. Pantic and S. M. Lukic, "Framework and topology for active tuning of parallel compensated receivers in power transfer systems," *IEEE Trans. Power Electron.*, vol. 27, no. 11, pp. 4503–4513, Nov. 2012.
- [115] D. Patil, M. Sirico, L. Gu, and B. Fahimi, "Maximum efficiency tracking in wireless power transfer for battery charger: Phase shift and frequency control," in *Proc. IEEE Energy Convers. Congr. Expo. (ECCE)*, Milwaukee, WI, USA, Sep. 2016, pp. 1–8.
- [116] S. Samanta and A. K. Rathore, "Analysis and design of current-fed (L)(C) (LC) converter for inductive wireless power transfer (IWPT)," in *Proc. IEEE Energy Convers. Congr. Expo. (ECCE)*, Montreal, QC, Canada, Sep. 2015, pp. 5724–5731.
- [117] S. Samanta and A. K. Rathore, "A new current-fed CLC transmitter and LC receiver topology for inductive wireless power transfer application: Analysis, design, and experimental results," *IEEE Trans. Transport. Electricif.*, vol. 1, no. 4, pp. 357–368, Dec. 2015.
- [118] S. Samanta and A. K. Rathore, "Wireless power transfer technology using full-bridge current-fed topology for medium power applications," *IET Power Electron.*, vol. 9, no. 9, pp. 1903–1913, Jul. 2016, doi: [10.1049/iet-pel.2015.0775](https://doi.org/10.1049/iet-pel.2015.0775).
- [119] A. P. Hu, J. T. Boys, and G. A. Covic, "Frequency analysis and computation of a current-fed resonant converter for ICPT power supplies," in *Proc. Int. Conf. Power Syst. Technol.*, vol. 1, 2000, pp. 327–332.
- [120] A. VanderMeulen and J. Maurin, *Current Source Inverter vs. Voltage Source Inverter Topology, Technical Data TD02004004E*, Eaton, Dublin, Ireland, 2010.
- [121] N. X. Bac, D. M. Vilathgamuwa, and U. K. Madawala, "A SiC-based matrix converter topology for inductive power transfer system," *IEEE Trans. Power Electron.*, vol. 29, no. 8, pp. 4029–4038, Aug. 2014.
- [122] H. L. Li, A. P. Hu, and G. A. Covic, "A direct AC–AC converter for inductive power-transfer systems," *IEEE Trans. Power Electron.*, vol. 27, no. 2, pp. 661–668, Feb. 2012.
- [123] M. Bojarski, E. Asa, K. Colak, and D. Czarkowski, "Analysis and control of multiphase inductively coupled resonant converter for wireless electric vehicle charger applications," *IEEE Trans. Transport. Electricif.*, vol. 3, no. 2, pp. 312–320, Jun. 2017.
- [124] M. Bojarski, E. Asa, K. Colak, and D. Czarkowski, "A 25 kW industrial prototype wireless electric vehicle charger," in *Proc. IEEE Appl. Power Electron. Conf. Expo. (APEC)*, Long Beach, CA, USA, Mar. 2016, pp. 1756–1761.
- [125] B. X. Nguyen, D. M. Vilathgamuwa, G. Foo, A. Ong, P. K. Sampath, and U. K. Madawala, "Cascaded multilevel converter based bidirectional inductive power transfer (BIPT) system," in *Proc. Int. Power Electron. Conf.*, 2014, pp. 2722–2728.
- [126] A. Daga, J. M. Miller, B. R. Long, R. Kacergis, P. Schrafel and J. Wolgemuth, "Electric fuel pumps for wireless power transfer: Enabling rapid growth in the electric vehicle market," *IEEE Power Electron. Mag.*, vol. 4, no. 2, pp. 24–35, Jun. 2017.
- [127] E. Babaei and S. H. Hosseini, "New cascaded multilevel inverter topology with minimum number of switches," *Energy Convers. Manage.*, vol. 50, no. 11, pp. 2761–2767, Nov. 2009.
- [128] H. R. Rahnamaei, U. K. Madawala, and D. J. Thrimawithana, "A modified hybrid multi-level converter for high-power high-frequency IPT systems," in *Proc. Electron. Appl. Int. Conf. Expo.*, 2014, pp. 624–629.
- [129] H. Hao, G. A. Covic, and J. T. Boys, "A parallel topology for inductive power transfer power supplies," *IEEE Trans. Power Electron.*, vol. 29, no. 3, pp. 1140–1151, Mar. 2014.
- [130] Y. Li, R. Mai, M. Yang, and Z. He, "Cascaded multi-level inverter based IPT systems for high power applications," *J. Power Electron.*, vol. 15, no. 6, pp. 1508–1516, 2015.
- [131] U. K. Madawala and D. J. Thrimawithana, "A bidirectional inductive power interface for electric vehicles in V2G systems," *IEEE Trans. Ind. Electron.*, vol. 58, no. 10, pp. 4789–4796, Oct. 2011.
- [132] K. Colak, E. Asa, D. Czarkowski, and H. Komurcugil, "A novel multi-level bi-directional DC/DC converter for inductive power transfer applications," in *Proc. IEEE Ind. Electron. Soc.*, Yokohama, Japan, Nov. 2015, pp. 003827–003831.
- [133] B. X. Nguyen, D. M. Vilathgamuwa, G. Foo, P. Wang, and A. Ong, "A modified cascaded multilevel converter topology for high power bidirectional inductive power transfer systems with the reduction of switching devices and power losses," in *Proc. Int. Conf. Power Electron. Drive Syst.*, Sydney, NSW, Australia, 2015, pp. 93–97.
- [134] J. M. Miller and O. Onar, "ORNL's in-motion WPT system," in *Proc. Conf. Electr. Roads Vehicles (CERV)*, Park City, UT, USA, Feb. 2012.

- [135] J. M. Miller *et al.*, "Demonstrating dynamic wireless charging of an electric vehicle: The benefit of electrochemical capacitor smoothing," *IEEE Power Electron. Mag.*, vol. 1, no. 1, pp. 12–24, Mar. 2014.
- [136] L. Chen, G. R. Nagendra, J. T. Boys, and G. A. Covic, "Double-coupled systems for IPT roadway applications," *IEEE J. Emerg. Sel. Topics Power Electron.*, vol. 3, no. 1, pp. 37–49, Mar. 2015.
- [137] G. A. Covic, J. T. Boys, M. L. G. Kissin, and H. G. Lu, "A three-phase inductive power transfer system for roadway-powered vehicles," *IEEE Trans. Ind. Electron.*, vol. 54, no. 6, pp. 3370–3378, Dec. 2007.
- [138] M. L. G. Kissin, J. T. Boys, and G. A. Covic, "Interphase mutual inductance in polyphase inductive power transfer systems," *IEEE Trans. Ind. Electron.*, vol. 56, no. 7, pp. 2393–2400, Jul. 2009.
- [139] M. L. G. Kissin, H. Hao, and G. A. Covic, "A practical multiphase IPT system for AGV and roadway applications," in *Proc. IEEE Energy Convers. Congr. Expo.*, Atlanta, GA, USA, Sep. 2010, pp. 1844–1850.
- [140] M. L. G. Kissin, G. A. Covic, and J. T. Boys, "Steady-state flat-pickup loading effects in polyphase inductive power transfer systems," *IEEE Trans. Ind. Electron.*, vol. 58, no. 6, pp. 2274–2282, Jun. 2011.
- [141] Z. Dang and J. A. A. Qahouq, "Modeling and investigation of magnetic resonance coupled wireless power transfer system with lateral misalignment," in *Proc. IEEE Appl. Power Electron. Conf. Expo. (APEC)*, Fort Worth, TX, USA, Mar. 2014, pp. 1317–1322.
- [142] Z. Dang and J. A. A. Qahouq, "Elimination method for the transmission efficiency valley of death in laterally misaligned wireless power transfer systems," in *Proc. IEEE Appl. Power Electron. Conf. Expo. (APEC)*, Charlotte, NC, USA, Mar. 2015, pp. 1644–1649.
- [143] S. G. Lee, H. Hoang, Y. H. Choi, and F. Bien, "Efficiency improvement for magnetic resonance based wireless power transfer with axial-misalignment," *Electron. Lett.*, vol. 48, no. 6, pp. 339–340, Mar. 2012.
- [144] K. Fotopoulos and B. W. Flynn, "Wireless power transfer in loosely coupled links: Coil misalignment model," *IEEE Trans. Magn.*, vol. 47, no. 2, pp. 416–430, Feb. 2011.
- [145] A. P. Sample, D. T. Meyer, and J. R. Smith, "Analysis, experimental results, and range adaptation of magnetically coupled resonators for wireless power transfer," *IEEE Trans. Ind. Electron.*, vol. 58, no. 2, pp. 544–554, Feb. 2011.
- [146] K. Throngnumchai, T. Kai, and Y. Minagawa, "A study on receiver circuit topology of a cordless battery charger for electric vehicles," in *Proc. IEEE Energy Convers. Congr. Expo.*, Phoenix, AZ, USA, Sep. 2011, pp. 843–850.
- [147] Q. Zhu, Y. Guo, L. Wang, C. Liao, and F. Li, "Improving the misalignment tolerance of wireless charging system by optimizing the compensate capacitor," *IEEE Trans. Ind. Electron.*, vol. 62, no. 8, pp. 4832–4836, Aug. 2015.
- [148] H. H. Wu, A. Gilchrist, K. D. Sealy, and D. Bronson, "A high efficiency 5 kW inductive charger for EVs using dual side control," *IEEE Trans. Ind. Informat.*, vol. 8, no. 3, pp. 585–595, Aug. 2012.
- [149] R. Bosshard, U. Badstüber, J. W. Kolar, and I. Stevanović, "Comparative evaluation of control methods for inductive power transfer," in *Proc. Int. Conf. Renew. Energy Res. Appl. (ICRERA)*, Nagasaki, Japan, 2012, pp. 1–6.
- [150] R. Bosshard, J. W. Kolar, and B. Wunsch, "Control method for inductive power transfer with high partial-load efficiency and resonance tracking," in *Proc. Int. Power Electron. Conf.*, Hiroshima, Japan, 2014, pp. 2167–2174.
- [151] J. M. Miller, C. P. White, O. C. Onar, and P. M. Ryan, "Grid side regulation of wireless power charging of plug-in electric vehicles," in *Proc. IEEE Energy Convers. Congr. Expo. (ECCE)*, Raleigh, NC, USA, Sep. 2012, pp. 261–268.
- [152] C. Y. Huang, J. T. Boys, and G. A. Covic, "LCL pickup circulating current controller for inductive power transfer systems," *IEEE Trans. Power Electron.*, vol. 28, no. 4, pp. 2081–2093, Apr. 2013.
- [153] C.-S. Wang, G. A. Covic, and O. H. Stielau, "Power transfer capability and bifurcation phenomena of loosely coupled inductive power transfer systems," *IEEE Trans. Ind. Electron.*, vol. 51, no. 1, pp. 148–157, Feb. 2004.
- [154] J. A. Sabate, M. M. Jovanovic, F. C. Lee, and R. T. Gean, "Analysis and design-optimization of LCC resonant inverter for high-frequency AC distributed power system," *IEEE Trans. Ind. Electron.*, vol. 42, no. 1, pp. 63–71, Feb. 1995.
- [155] H. Pinheiro, P. Jain, and G. Joos, "Self-sustained oscillating resonant converters operating above the resonant frequency," in *Proc. Appl. Power Electron. Conf. (APEC)*, vol. 2, Atlanta, GA, USA, 1997, pp. 993–999.
- [156] F. da Silveira Cavalcante, "High output voltage series-parallel resonant DC-DC converter for medical X-ray imaging applications," Ph.D. dissertation, Dept. Inf. Technol. Elect. Eng., ETH Zurich, Zürich, Switzerland, 2006.
- [157] B. Sharp and H. Wu, "Asymmetrical voltage-cancellation control for LCL resonant converters in inductive power transfer systems," in *Proc. 27th Annu. IEEE Appl. Power Electron. Conf. Expo. (APEC)*, Orlando, FL, USA, Feb. 2012, pp. 661–666.
- [158] L. A. Barragan, J. M. Burdío, J. I. Artigas, D. Navarro, J. Acero, and D. Puyal, "Efficiency optimization in ZVS series resonant inverters with asymmetrical voltage-cancellation control," *IEEE Trans. Power Electron.*, vol. 20, no. 5, pp. 1036–1044, Sep. 2005.
- [159] J. M. Burdío, L. A. Barragan, F. Monterde, D. Navarro, and J. Acero, "Asymmetrical voltage-cancellation control for full-bridge series resonant inverters," *IEEE Trans. Power Electron.*, vol. 19, no. 2, pp. 461–469, Mar. 2004.
- [160] M. Chinthalivali, O. C. Onar, S. L. Campbell, and L. M. Tolbert, "Integrated charger with wireless charging and boost functions for PHEV and EV applications," in *Proc. IEEE Transp. Electricif. Conf. (ITEC)*, Dearborn, MI, USA, Jun. 2015, pp. 1–8.
- [161] M. Chinthalivali, O. C. Onar, S. L. Campbell, and L. M. Tolbert, "Isolated wired and wireless battery charger with integrated boost converter for PEV applications," in *Proc. IEEE Energy Convers. Congr. Expo. (ECCE)*, Montreal, QC, Canada, Sep. 2015, pp. 607–614.
- [162] A. Berger, M. Agostinelli, S. Vesti, J. A. Oliver, J. A. Cobos, and M. Huemer, "A wireless charging system applying phase-shift and amplitude control to maximize efficiency and extractable power," *IEEE Trans. Power Electron.*, vol. 30, no. 11, pp. 6338–6348, Nov. 2015.
- [163] W. X. Zhong and S. Y. R. Hui, "Maximum energy efficiency tracking for wireless power transfer systems," *IEEE Trans. Power Electron.*, vol. 30, no. 7, pp. 4025–4034, Jul. 2015.
- [164] H. Li, J. Li, K. Wang, W. Chen, and X. Yang, "A maximum efficiency point tracking control scheme for wireless power transfer systems using magnetic resonant coupling," *IEEE Trans. Power Electron.*, vol. 30, no. 7, pp. 3998–4008, Jul. 2015.
- [165] M. Fu, H. Yin, X. Zhu, and C. Ma, "Analysis and tracking of optimal load in wireless power transfer systems," *IEEE Trans. Power Electron.*, vol. 30, no. 7, pp. 3952–3963, Jul. 2015.
- [166] Y. Moriwaki, T. Imura, and Y. Hori, "Basic study on reduction of reflected power using DC/DC converters in wireless power transfer system via magnetic resonant coupling," in *Proc. IEEE Int. Telecommun. Energy Conf.*, Amsterdam, The Netherlands, Oct. 2011, pp. 1–5.
- [167] Z. Bi, T. Kan, C. C. Mi, Y. Zhang, Z. Zhao, and G. A. Keoleian, "A review of wireless power transfer for electric vehicles: Prospects to enhance sustainable mobility," *Appl. Energy*, vol. 179, pp. 413–425, Oct. 2016.
- [168] *Highly Resonant Wireless Power Transfer: Safe, Efficient, and Over Distance*. Accessed: Jul. 26, 2016. [Online]. Available: http://willtricity.com/wp-content/uploads/2016/12/White_Paper_20161218.pdf
- [169] M. R. Sonapreetha, S. Y. Jeong, S. Y. Choi, and C. T. Rim, "Dual-purpose non-overlapped coil sets as foreign object and vehicle location detections for wireless stationary EV chargers," in *Proc. IEEE PEELS Workshop Emerg. Technol., Wireless Power (WoW)*, Daejeon, South Korea, Jun. 2015, pp. 1–7.
- [170] S. Y. Jeong, H. G. Kwak, G. C. Jang, and C. T. Rim, "Living object detection system based on comb pattern capacitive sensor for wireless EV chargers," in *Proc. IEEE 2nd Annu. Southern Power Electron. Conf. (SPEC)*, Auckland, New Zealand, Dec. 2016, pp. 1–6.
- [171] G. C. Jang, S. Y. Jeong, H. G. Kwak, and C. T. Rim, "Metal object detection circuit with non-overlapped coils for wireless EV chargers," in *Proc. IEEE 2nd Annu. Southern Power Electron. Conf. (SPEC)*, Auckland, New Zealand, Dec. 2016, pp. 1–6.
- [172] S. Fukuda, H. Nakano, Y. Murayama, T. Murakami, O. Kozakai, and K. Fujimaki, "A novel metal detector using the quality factor of the secondary coil for wireless power transfer systems," in *Proc. IEEE MTT-S Int. Microw. Workshop Ser. Innov. Wireless Power Transmiss., Technol., Syst., Appl.*, Kyoto, Japan, May 2012, pp. 241–244.
- [173] H. Kudo, K. Ogawa, N. Oodachi, N. Deguchi, and H. Shoki, "Detection of a metal obstacle in wireless power transfer via magnetic resonance," in *Proc. IEEE 33rd Int. Telecommun. Energy Conf. (INTELEC)*, Amsterdam, The Netherlands, Oct. 2011, pp. 1–6.

- [174] N. Kuyvenhoven, C. Dean, J. Melton, J. Schwannecke, and A. E. Umenei, "Development of a foreign object detection and analysis method for wireless power systems," in *Proc. IEEE Symp. Product Compliance Eng.*, San Diego, CA, USA, Oct. 2011, pp. 1–6.
- [175] G. R. Nagendra, L. Chen, G. A. Covic, and J. T. Boys, "Detection of EVs on IPT highways," *IEEE J. Emerg. Sel. Topics Power Electron.*, vol. 2, no. 3, pp. 584–597, Sep. 2014.
- [176] A. Kamineni, M. J. Neath, A. Zaheer, G. A. Covic, and J. T. Boys, "Interoperable EV detection for dynamic wireless charging with existing hardware and free resonance," *IEEE Trans. Transport. Electricific.*, vol. 3, no. 2, pp. 370–379, Jun. 2017.
- [177] Q. Deng *et al.*, "Edge position detection of on-line charged vehicles with segmental wireless power supply," *IEEE Trans. Veh. Technol.*, vol. 66, no. 5, pp. 3610–3621, May 2017.
- [178] N. Hasan, H. Wang, T. Saha, and Z. Pantic, "A novel position sensorless power transfer control of lumped coil-based in-motion wireless power transfer systems," in *Proc. IEEE Energy Convers. Congr. Expo. (ECCE)*, Montreal, QC, Canada, Sep. 2015, pp. 586–593.
- [179] J. R. Bailey and M. E. Hairr, "Wayside charging and hydrogen hybrid bus: Extending the range of electric shuttle buses," Dept. Transp., Federal Transit Admin., Washington, DC, USA, FTA Rep. 0028, 2012. [Online]. Available: https://www.transit.dot.gov/sites/fta.dot.gov/files/FTA0028_Research_Report_Summary.pdf
- [180] P. T. Jones and O. Onar, "Impact of wireless power transfer in transportation: Future transportation enabler, or near term distraction," in *Proc. IEEE Int. Electr. Vehicle Conf. (IEVC)*, Florence, Italy, Dec. 2014, pp. 1–7.
- [181] A. Gil, P. Sauras-Perez, and J. Taiber, "Communication requirements for dynamic wireless power transfer for battery electric vehicles," in *Proc. IEEE Int. Electr. Vehicle Conf. (IEVC)*, Florence, Italy, Dec. 2014, pp. 1–7.
- [182] A. Echols, S. Mukherjee, M. Mickelsen, and Z. Pantic, "Communication infrastructure for dynamic wireless charging of electric vehicles," in *Proc. IEEE Wireless Commun. Netw. Conf. (WCNC)*, San Francisco, CA, USA, Mar. 2017, pp. 1–6.
- [183] S. Y. R. Hui, W. Zhong, and C. K. Lee, "A critical review of recent progress in mid-range wireless power transfer," *IEEE Trans. Power Electron.*, vol. 29, no. 9, pp. 4500–4511, Sep. 2014.



Devendra Patil (S'10) received the bachelor's degree in electrical engineering from Mumbai University, Mumbai, India, in 2009, and the master's degree in power electronics and power system from IIT Bombay, Mumbai, in 2013. He is currently pursuing the Ph.D. degree in electrical engineering at the Department of Electrical Engineering, The University of Texas at Dallas, Richardson, TX, USA, with a focus on power electronics.

From 2009 to 2010, he was a Design Engineer with Tata Power SED, Mumbai. From 2013 to 2014, he was a Research Engineer with the National University of Singapore, Singapore. He joined Apple Inc., Cupertino, CA, USA, as an intern in 2017. His current research interests include soft-switched converters, renewable energy sources, wireless power transfer, and electric machine design and drive.

Mr. Patil was a recipient of the first prize in the IEEE IAS 2015 Master graduate thesis award.



Matthew K. McDonough (S'10–M'15) received the B.Sc. degree in electrical engineering from the University of Texas at Arlington, Arlington, TX, USA, in 2010, and the Ph.D. degree from the University of Texas at Dallas, Richardson, TX, USA, in 2014 with a dissertation focusing on multiport power electronics and wireless power transfer.

He joined the Renewable Energy and Vehicular Technology Laboratory, The University of Texas at Dallas, in 2010. He is currently a Senior Member of Technical Staff with the Sandia National Laboratories, Albuquerque, NM, USA. His current research interests include the application of renewable energy resources, specifically microgrids, dc–dc converters, integration of wide band-gap devices, dc–ac and ac–dc converters, multiport converters, and transportation technology.



John M. Miller (S'82–M'83–SM'94–F'99–LF'16) received the B.S.E.E. degree from the University of Arkansas, Fayetteville, AR, USA, the M.S.E.E. degree from Southern Methodist University, Dallas, TX, USA, and the Ph.D. degree from Michigan State University, East Lansing, MI, USA.

He has more than 41 years of experience in electrical engineering across various industries that include automotive, aerospace, white goods, and electrical practice. He held various senior management and engineering positions at Maxwell Technologies, San Diego, CA, USA, Ford Motor Company, Dearborn, MI, USA, and Texas Instruments, Dallas, TX, USA. He was a Distinguished Research and Development Scientist at the Oak Ridge National Laboratory, Oak Ridge, TN, USA, where he held positions as the Director of the Power Electronics and Electric Power Systems Research Center, and served as the Program Manager of the DOE Vehicular Technologies subprogram APEEM. He is the Owner and the Founder of J-N-J Miller Design Services PLLC, Longview, TX, USA, which was established in 2002 to provide professional consulting to industry. He joined Momentum Dynamics Technical Advisory Board in 2014 as a Senior Scientist, focusing on wireless power transfer for heavy-duty vehicles. He is an Industry Consultant on electric traction drive and energy storage systems for an electric vehicle manufacturer. He has authored or co-authored several books related to wireless charging, ultracapacitor applications (translated to Chinese in 2015), propulsion systems for hybrid vehicles (translated to Chinese in 2016), automotive power electronics, and vehicular electric power systems.

Dr. Miller is a fellow of the SAE, and was a Registered Professional Engineer in Michigan in 1980 and in Texas in 2014.



Babak Fahimi (S'96–M'99–SM'03–F'15) received the B.S. and M.S. degrees in electrical engineering with the highest distinction from the University of Tehran, Tehran, Iran, in 1991 and 1993, respectively, and the Ph.D. degree in electrical engineering from Texas A&M University, College Station, TX, USA, in 1999.

He is currently a Distinguished Chair in engineering and the Director of the Renewable Energy and Vehicular Technology with the University of Texas at Dallas, Richardson, TX, USA. He has co-authored more than 300 scientific articles, 15 book chapters, and several technical reports in the general area of adjustable speed motor drives and power electronics. He holds 18 U.S. patents and has six more pending.

Dr. Fahimi was a recipient of the DAAD scholarship from 1993 to 1995, the IEEE R.M. Bass Power Electronics Young Investigator Award in 2003, the SAE Ralph Teetor Educational Award in 2008, the Fulbright scholarship in 2010, and the IEEE Cyril Veinott Electromechanical Energy Conversion Award in 2015. He has supervised 26 Ph.D. (four tenured/tenure-track professors) and 20 M.S. students.



Poras T. Balsara (F'14) received the L.E.E. Diploma degree in electronics from The Victoria Jubilee Technical Institute, Mumbai, India, in 1980, the B.E. (electrical) degree from the University of Bombay, Mumbai, India, in 1983, and the M.S. and Ph.D. degrees from the Penn State University, State College, PA, USA, in 1985 and 1989, respectively.

In 1989, he joined the faculty of the Erik Jonsson School of Engineering and Computer Science, The University of Texas at Dallas, Richardson, TX, USA, where he is currently a Professor of electrical engineering and the Associate Dean for Academic Affairs. He has authored several journal and conference publications and has coauthored a book in the following research areas. His current research interests include very large scale integration design, power electronics, design of energy efficient digital circuits and systems, and digitally assisted mixed-signal design.